2007

Accuracy of cranial coplanar beam therapy with BrainLAB ExacTrac image guidance

Justin Vinci
Louisiana State University and Agricultural and Mechanical College

ACCURACY OF CRANIAL COPLANAR BEAM THERAPY WITH BRAINLAB EXACTRAC IMAGE GUIDANCE

A THESIS

Submitted to the Graduate Faculty of the
Louisiana State University and
Agricultural and Mechanical College
in partial fulfillment of the
requirements for the degree of
Master of Science

in

The Department of Physics and Astronomy

By
Justin Vinci
B.S. University of Connecticut, 2004
December, 2007

Acknowledgements

I would like to extend my thanks to my committee chair, Dr. Kenneth Hogstrom for all his advice and help in research and preparation of this thesis and to all of the members of my supervisory committee: Dr. Isaac Rosen, Dr. Maurice King, Dr. Gabriele Gonzales, and Daniel Neck for their assistance and taking time to serve on this research committee. I would also like to thank Connel Chu for his contributions to this work. All those around me were extremely helpful in matters pertaining to this research, as well as matters above and beyond it.

I would also like to thank Mary Bird Perkins Cancer Center and the staff for their assistance and equipment access and for the excellent patient care which they provide, as well as the way they treat their medical physics students. Additionally, I would like to thank BrainLAB for their financial support. Finally, I would like to thank my family and friends for their continued support.

Table of Contents

Abstract

Purpose: To develop a system for measuring 2D dose distributions in the cranium and to use this system to evaluate the accuracy of coplanar conformal therapy using ExacTrac image guidance.

Methods: Techniques were developed to measure dose distributions in each principal plane using a CIRS anthropomorphic head phantom with a custom internal film cassette. Sections of EDR2 film were cut, processed, and digitized using custom templates. Spatial and dosimetric accuracy and precision of the film system was assessed. BrainScan was used to plan a coplanar-beam treatment conforming to irradiate a 2-cm ϕ x 2-cm cylindrical target. Prior to delivery phantom misalignments were imposed in combinations of ±8-mm offsets in each of the principal directions. ExacTrac X-ray correction was applied until the phantom was within an acceptance criteria of 1mm-1° (first two measurement sessions) or 0.4mm-0.4º (last two measurement sessions). Measured dose distributions on film were registered to the treatment plan and compared.

Results: Alignment errors(displacement between midpoints of planned and measured 70% isodose contours), were 0.48±0.40, -0.20±0.44 and 0.45±0.43mm along the Posterior-Anterior, Right-Left and Superior-Inferior directions, respectively, using acceptance criteria of 1mm-1°, and 0.72±0.18, 0.12±0.18 and -0.14±0.34mm, respectively, using acceptance criteria, 0.4mm-0.4°. Positional errors of the 80% isodose line were -0.36±0.43, 0.38±0.38, and 0.03±0.44mm, on the Posterior, Right, and Inferior edges of each profile, respectively, and 0.68 ±0.40, -0.14 ±0.38, and 0.88±0.40mm for the Anterior, Left, and Superior edges, respectively for the 1mm-1° criteria. Using the 0.4mm-0.4° criteria, errors were -0.35±0.23, 0.31± 0.18, and 0.72±0.27mm on the Posterior, Left and Inferior portion of each profile respectively and 1.12±0.18, 0.22±0.23,

and 0.35±0.33mm for the Anterior, Left and Superior portions, respectively. Data ranged approximately two standard deviations about the mean. Winston-Lutz tests with errors of approximately 0.5mm correlated with increased Anterior error in three measurement sessions.

Conclusions: The ExacTrac system is capable of achieving sub-mm(2σ) accuracy given the alignment errors were small(<0.3mm) when Winston-Lutz results were small(<0.2mm), indicating pre-treatment corrections could be made.

Chapter 1 Introduction

1.1 Stereotactic Radiosurgery and Stereotactic Radiation Therapy

Stereotactic Radiosurgery (SRS) and Stereotactic Radiotherapy (SRT) are radiation techniques using multiple focused beams to treat stereotactically localized lesions, usually in the brain. External beam SRS/SRT employs multiple therapeutic radiation beams with small field sizes focused on a small target. High accuracy patient imaging and registration techniques are required to localize the target in the stereotactic frame, align the target to the treatment machine isocenter within sub-mm accuracy. The AAPM Task Group 42 requirements for SRS acceptance tests are a positional accuracy of ±1mm and numerical dose delivery of ± 5%(Schell *et al* 1995).

The basis of SRS/SRT is accurate localization of the target within a well-defined coordinate system during the treatment planning phase. This is accomplished by fixing a stereotactic localization box to the patient prior to imaging, as shown in figure 1a. The localization box mounts to the stereotactic head ring (c.f. Figure 1b) in a rigid and reproducible way. The head ring, or head frame, is a device rigidly fixed to the patient's head, which (1) mounts to the treatment couch and (2) allows the localization box to be mounted to it.

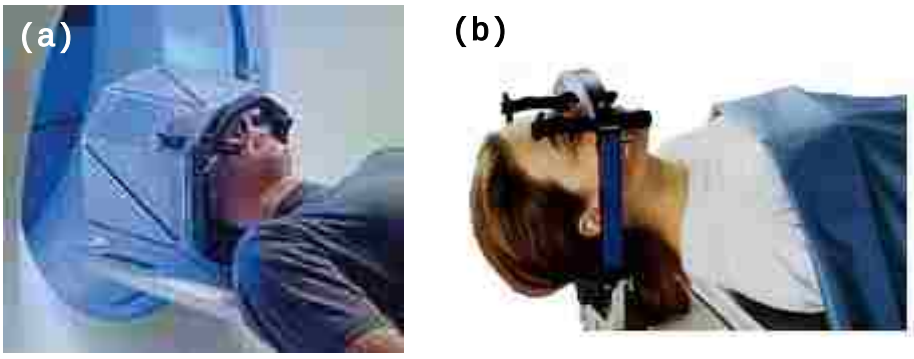

Figure 1. (a) CT stereotactic localization box mounted to stereotactic head ring. Fiducial rods along the localization box define the stereotactic coordinate system in the treatment planning system. (b) Stereotactic Head Ring. The head ring bolts rigidly secure to patient's forehead and mounts to treatment couch. (from www.nebraskamed.com)

Radio-opaque rods along the localization box describe a reference coordinate system to which the target volume can be mapped. By imaging the patient within a fixed stereotactic frame the target position can be known at treatment time relative to the stereotactic reference frame. The stereotactic head ring locks into the stereotactic couch mount with mounts to the treatment couch. The position of the head ring can be adjusted with fine adjustment knobs on the stereotactic couch mount to achieve an accurate setup, i.e. to match localized target coordinates to machine isocenter.

SRS/SRT is used for treatment of primary brain tumors such as anaplastic astrocytoma and giloblastoma multiforma, as well as brain metastases. SRS/SRT is also used to treat functional disorders such as acoustic neuromas and trigeminal neuralgia and vascular lesions such as arteriovenous malformations.

The distinction between SRS and SRT is that SRS is a single radiation treatment (fraction), while SRT involves fractionation, which spreads the treatment over the course of multiple deliveries (fractions). Historically fractionated SRT treatments have been used for malignant tumors, while SRS has been used for treatment of benign diseases, functional disorders, vascular malformations and metastatic disease. Recently, however, SRT has gained interest even for conditions traditionally treated with SRS, e.g. acoustic neuromas, as technological advancements have allowed for improved immobilization and positioning accuracy (Solberg *et al* 1998). While SRS is the more precise treatment option in that it is not subject to daily setup uncertainty, it lacks in that the patient does not get the biological benefit of fractionation. Fractionation allows for increased sparing of normal tissue due to repair of sublethal damage, as well as reduction of acute reactions.(Solberg *et al* 1998) Traditionally, SRS is less desirable in terms of patient comfort, as it requires a semi-permanent, semi-invasive

immobilization device (c.f. Figure 1b), a stereotactic head ring bolted to the patients skull palliated by local anesthetic.

SRT on the other hand makes use of the same procedure as SRS with the use of a removable, non-invasive immobilizing frame (e.g. thermo-plastic mask or occipital pad with bite-block). Because the frame must be repositioned at each treatment this procedure lends itself to additional inter-fraction setup uncertainty due to the combination of head position change inside the mask between treatments and daily setup error. Alheit, *et al* 2001, who demonstrated the accuracy of the position of a patient's head within the BrainLAB relocatable mask system can be as much as 2 mm (without image guidance), recommended safety margins of 3-4 mm to cover the PTV for 95.5 % of all clinical treatments due to the uncertainty in target position at delivery. One viable solution to improving setup accuracy for stereotactic treatments is image guidance. This is especially true when performing fractionated SRT with a non-invasive immobilization system because of the inherent setup uncertainties.

1.2 Traditional Procedure for Stereotactic Treatments

For stereotactic treatments the patient is first imaged using a conventional CT scan and/or MRI in treatment position with a stereotactic localization box affixed to a rigid immobilization frame (head ring), which is holding the patient in place. In the treatment planning phase the stereotactic frame must be defined in the treatment planning system to establish the stereotactic coordinate system. To do this the relative locations of the localization fiducial rods are automatically located by the treatment planning computer and used to establish the stereotactic coordinate system. Treatment planning consists of contouring targets and critical structures and then determining a set of beam parameters suitable for treatment. Treatment options available using the stereotactic radiosurgery treatment planning system (BrainScan version 5.3) at Mary

Bird Perkins Cancer Center (MBPCC) include multiple coplanar circular arced beams, conformal beams, conformal arced beams, dynamic conformal arced beams and IMRS treatments ().

The patient, immobilized in the stereotactic head ring, is setup on the treatment couch, and the head ring is mounted to the treatment couch and adjusted so that the localized (planned) isocenter is coincident with the linac isocenter. Using extensive pre-treatment quality assurance, medical physics staff and a radiation oncologist verify that (1) the location of the patient's head within the stereotactic head ring has not changed since treatment planning and (2) the head ring is accurately positioned to the machine isocenter based on the target's stereotactic coordinates. This "stereotactic" alignment method can be replaced by implementing image guidance. In such cases the 3D patient anatomy localized with respect to the treatment machine replaces the stereotactic head ring as the means to align the patient to the treatment device. This bypasses the need for the extensive patient-specific pretreatment quality assurance (QA) and potentially accounts for the inherent uncertainty in non-invasive immobilization systems e.g. mask or bite-block systems used for frameless stereotactic and fractionated radiotherapy treatments.

The shift from invasive immobilization within stereotactic coordinates to noninvasive immobilization with image guidance represents a relatively new paradigm in the treatment of small cranial targets. The latter case, (i.e. without use of a stereotactic reference frame) is referred to as "frameless radiosurgery/radiotherapy." This modality uses anatomical images to align the patient to achieve high spatial accuracy treatments.

1.3 Image Guided Radiation Therapy

The prevalence of image guided radiation therapy (IGRT) has increased in recent years. IGRT utilizes various imaging techniques, which are employed immediately prior to treatment to verify the patient's position. Commonly used IGRT systems can be divided into two groups,

CT-based IGRT and planar-image-based IGRT. CT-based IGRT systems include megavoltage CT (MVCT) and kilovoltage CT (kVCT) systems which generate a 3D image of the patient on the treatment couch. Each of these can be incorporated as either gantry mounted, e.g. cone-beam MVCT (Siemens), serial MVCT (TomoTherapy), or conebeam kVCT (Varian or Elekta) or as a separate entity, e.g. CT on rails (Siemens). Planar imaging techniques employ X-rays directed at the patient immediately prior to treatment. These techniques include megavoltage (MV) portal images or kilovoltage (kV) radiographs. Both systems can also be gantry mounted as with MV electronic portal imaging devices (EPIDs) and gantry mounted kV X-ray tubes (same setup as is used for kVCT), or positioned independent of the gantry (i.e. kV X-ray tubes mounted elsewhere in the treatment room).

The images taken prior to treatment are compared to some form of reference image(s) from the treatment planning system, such as a 3D CT representation of the patient, digitally reconstructed radiograph (DRR) projections, or a set of fiducial marker locations. Through this comparison translations and rotations of the patient, which are necessary to locate the patient with respect to the treatment device as planned, are determined. By realigning the patient and verifying final positioning, IGRT should effectively reduce setup error. Disadvantages of IGRT include an increased overall treatment time and increased patient dose; however, these are usually considered minor.

1.4 Brainlab Novalis ExacTrac IGRT

This work focused on IGRT by means of the BrainLAB ExacTrac, which employs a room-based orthogonal kV X-ray imaging system. This IGRT system supports the use of the Novalis BrainLAB 6MV radiotherapy accelerator. This treatment machine has an “in-line” 6 MeV accelerating structure, and its gantry, head, and couch are designed to meet the treatment

accuracy required for stereotactic radiosurgical treatments. The Novalis uses circular cones of varying diameter (4 mm to 15 mm) for radiosurgical circular beams or circular arc treatments, or it uses the BrainLAB m3 mico-multileaf collimator (mMLC) for conformal beam shaping and IMRT. Cones can be used for radiosurgery of small spherical lesions; however, more commonly at MBPCC, the mMLC is used for radiosurgery and radiotherapy treatments using either multiple static fields, arced beams, or IMRT/IMRS. Images of the treatment room, ExacTrac components, and coordinate system (IEC convention 61217 as defined in Novalis Bocy/ ExacTrac Clinical Users Guide version 5.0) are shown in Figure 2.

The BrainLAB m3 mMLC is mounted to the gantry head and features 26 leaf pairs capable or creating variable field shapes up to 9.8 x 9.8 cm^2. Leaf widths are 3 mm, 4.4 mm and 5.5 mm at isocenter, gradually increasing from the central axis outward. Leaf positions are controlled by the BrainLAB MLC controller and MLC workstation software interface. The mMLC leaf ends (in the direction of leaf travel) are considered 'rounded' through they are actually comprised of 3 connected line segments. These segments are designed to match the beam divergence at leaf positions of + 5 cm (fully retracted), 0, and -5 cm (fully extended) (Cosgrove *et al* 1998). The opposing edges (perpendicular to leaf travel direction) are also divergent and have a tongue and groove design to reduce interleaf leakage. A drawing of an mMLC leaf is shown in Figure 3.

The Novalis ExacTrac X-ray system consists of two floor mounted X-ray tubes and two ceiling mounted amorphous silicon (aSi) flat panel detectors. The X-ray tubes have variable energy (40 kV-150 kV), current (10 mA-320 mA), and time (2 ms-6300 ms) settings for a range of contrast and brightness. The flat panel detectors are 512 x 512 pixels with an active area of

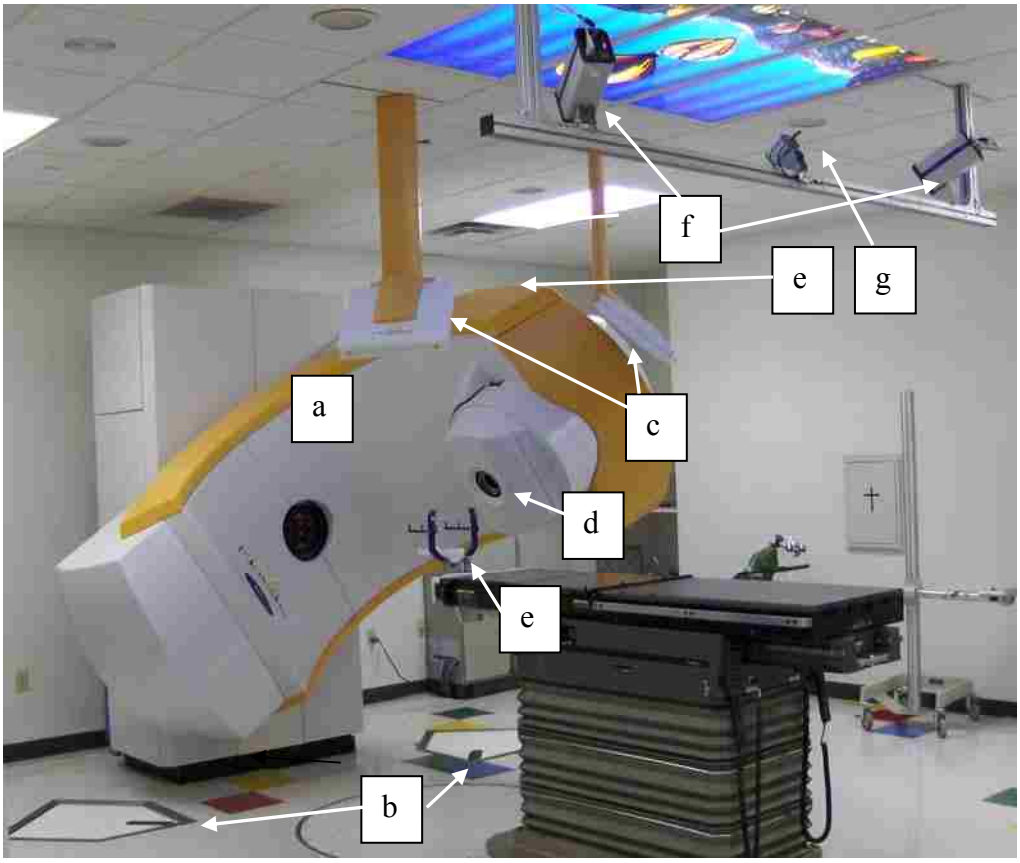

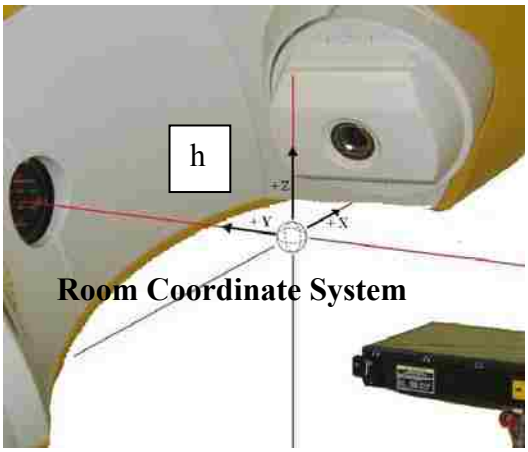

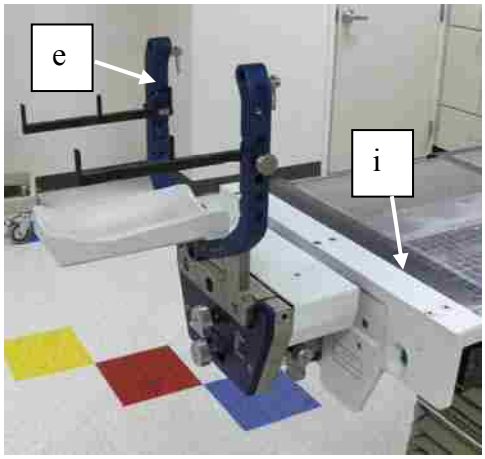

Figure 2. BrainLAB Treatment Room: (a) BrainLAB Novalis 6MV Linac; (b) X-ray Tubes; (c) aSi Flat Panel Detectors; d) BrainLAB m3 MicroMLC; (e) SRT U-frame: supports BrainLAB mask immobilization system; (f) Infrared Camera System; (g) Video Camera System; (h) Room Coordinate System (IEC convention 61217); (i) BrainLAB Couch Mount.

20 cm x 20 cm, which provides a field of view of view of ≈ 13 cm x 13 cm at isocenter with an image pixel size of 0.4 mm x 0.4 mm.

This system is designed to generate orthogonal X-ray images directly thorough isocenter for verification with the planned setup prior to treatment. The flat panel detectors (c.f. Figure 2c) record the projected images from the X-ray tubes in the floor (c.f. Figure 2b) at angles of 45º vertically from the floor and 45º longitudinally towards isocenter. Figure 4 is a pictorial representation of the ExacTrac X-ray projections.

Infrared (IR) cameras (c.f. Figure 2f), also mounted to the ceiling, track the locations of infrared reflective markers placed on the patient or on immobilization devices. IR tracking provides position feedback used for adjustments to the patient's position to be made and tracked outside the treatment room.

X-ray images generated with the ExacTrac system are two orthogonal X-ray projections through isocenter (i.e. from the floor mounted X-ray tube, through isocenter to the detector), which can be viewed at the user console. The ExacTrac software then uses the treatment planning CT data to create a digitally reconstructed radiograph (DRR) of the patient according to the projection angle of the X-ray tubes (Novalis Bocy/ ExacTrac Clinical Users Guide version 5.0). A DRR is a simulated radiograph reconstructed from the CT data as a planar image. After X-rays are taken the ExacTrac user console displays both X-ray images and their corresponding DRR projections, examples of which are shown in Figure 5. Note that the DRR image does not have the same web pattern as the X-ray image (c.f. Figure 5). This is a consequence of the look-up-table (LUT) settings on ExacTrac which are set to visualize cranial bones in the DRR.

If there is "exact" alignment, the two images should be identical in terms of the location of bony anatomy, air cavities, and any internal markers. To achieve this case of optimal alignment the user can select the Automatic 6D Image Fusion feature which employs a mutual information image fusion algorithm to determine the optimal match of the bony anatomy

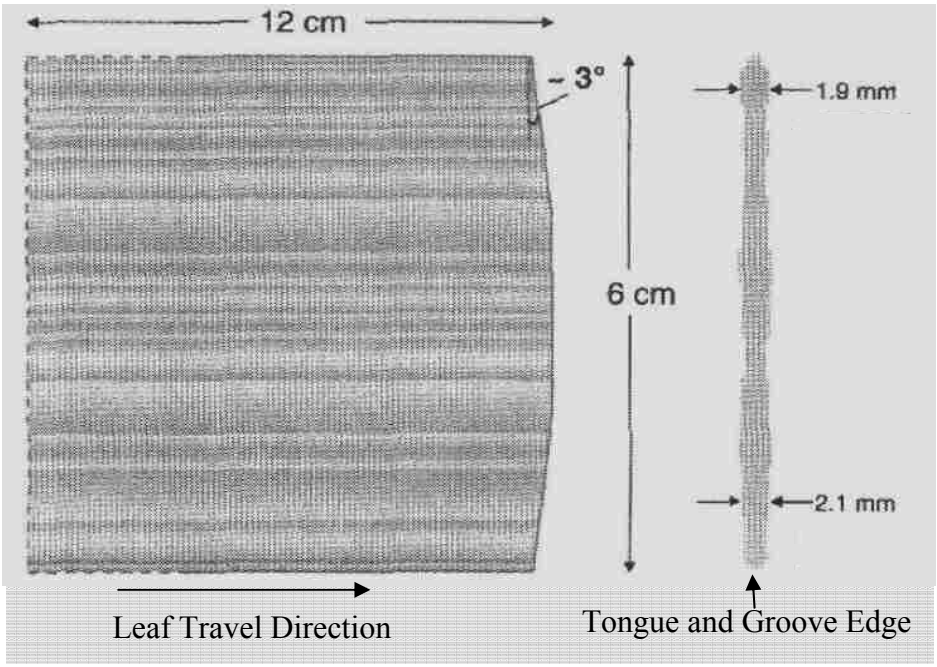

Figure 3. BrainLAB m3 mMLC leaf design showing the angled leaf edge in the direction of leaf travel and the tongue and groove edge in the cross section. (from Cosgrove *et al* 1999)

Figure 4. ExacTrac X-ray beams. X-rays are directed through isocenter to the flat panel detectors. X-ray tubes shown here with covers removed.

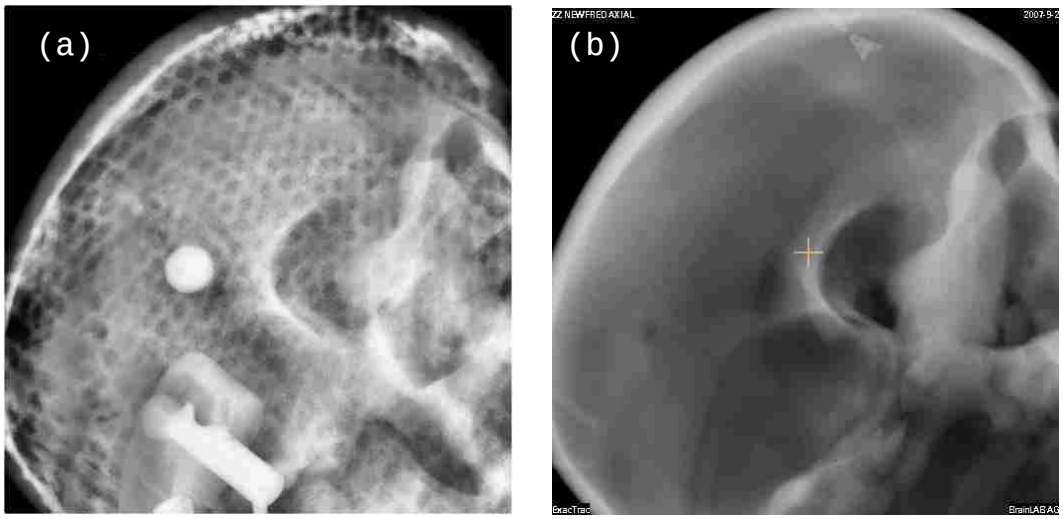

Figure 5. (a) ExacTrac X-ray Image. The white circle is created by an IR marker on the phantom surface and the web pattern is a result of the immobilization mask. (b) BrainScan DRR image. The crosshair mark denotes the location of planned isocenter.

between each X-ray image and its corresponding DRR projection over the set of possible translations and rotations from true isocenter, thus indicating the current patient alignment error. Manipulating the CT data through varying projections (i.e. translations from isocenter and rotations about isocenter) and converging on the best match is found by iteration and maximization of a similarity measure (detection of edges). Robar *et al* (2004) demonstrated that this type of image fusion is capable of providing 3D registration with an accuracy less that the CT voxel size.

The BrainLAB ExacTrac Clinical User's Guide version 5.0 states that ExacTrac can reliably correct setup errors less than 10 mm. The BrainLAB software (1) suggests shifts that would place the patient at the calculated match and (2) transfers new destination coordinates to the IR system. The IR tracking ensures that the suggested shifts are made correctly by the therapist. A set of verification X-rays using the ExacTrac system can be taken after the shift and

prior to treatment as a final check for patient alignment. Additional ExacTrac iterations can be performed as needed.

1.4.1 Calibration of IGRT System

Each day prior to use, the ExacTrac IR system is calibrated using the room lasers to define the IR isocenter. The IR system then is used to position the X-ray calibration phantom, which is then used to calibrate the ExacTrac X-ray system. Clearly the accuracy of the laser definition of isocenter is paramount the accuracy of the system, as is the frequency and quality of the ExacTrac X-ray system calibration. System performance is reliant upon proper calibration of each module of the image guidance system, which are detailed below.

1.4.1.1 Determination of Isocenter

A Winston-Lutz test (Lutz *et al* 1988) is routinely performed to verify radiation – laser isocenter coincidence. For this test (specific to the BrainLAB Stereotactic system) a 3 mm tungsten ball is setup at isocenter according to the treatment room wall lasers (c.f. Figure 10a). Fine adjustments can be made to align the Lutz pointer to the lasers using knobs on the couch mount. Then, a 10 mm radiosurgery cone is attached to the treatment head, and film exposures are recorded downstream from the ball at varying gantry and couch angles. The ball creates a circular region (of lower dose) on film corresponding to blocked radiation, which is surrounded by a circular high dose region defined by the cone (c.f. Figure 6b).

The deviation of the centers of both circles is a measure of the deviation between radiation and laser isocenter, with concentric circles indicating perfect alignment. Laser adjustments are made based on results of the Winston-Lutz test, where the laser intersection is positioned at the location of intersection of radiation beams from a set of gantry and couch angles.

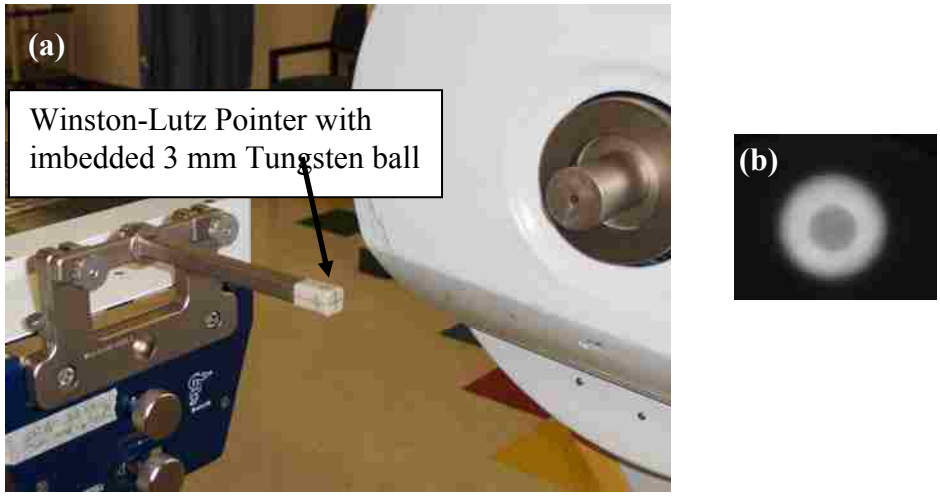

Figure 6. (a) Winston Lutz pointer attached to the couch mount. (b) Winston Lutz film result for a single gantry/couch combination.

1.4.1.2 Calibration of Infrared Cameras

The first of a series of ExacTrac calibrations, as outlined in the Novalis Bocy/ ExacTrac Clinical Users Guide version 5.0, is the infrared camera calibration. This is accomplished using the infrared calibration grid (c.f. Figure 7a), which is a frame comprised of 25 infrared markers at known relative locations from one another. The calibration grid is positioned near isocenter, and each marker is detected by both IR cameras establishing the spatial relationship between the two cameras. This calibrates the system for relative movements.

The next step is to register the position of isocenter in the ExacTrac IR system using the isocenter phantom shown in Figure 7b, a block with 5 infrared markers attached. This phantom is visually aligned to the lasers using crosshair marks on the surface of the block. This procedure sets the laser isocenter as origin of the infrared coordinate system and provides the basis for the subsequent X-ray calibration.

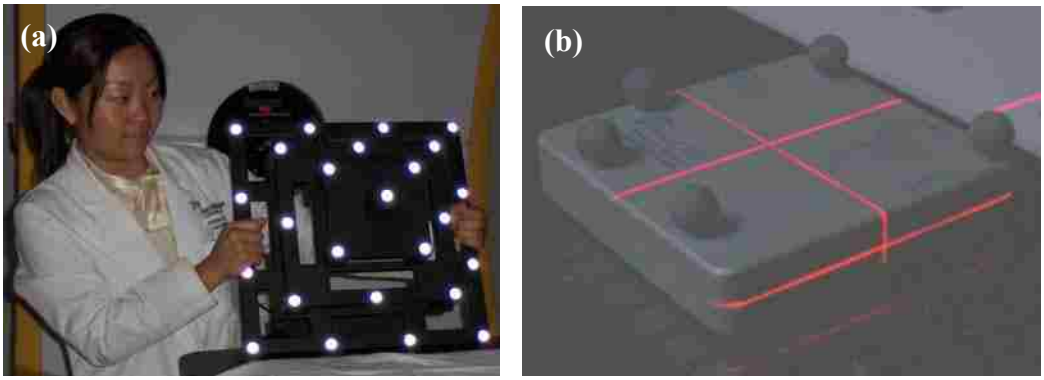

Figure 7. (a) IR Calibration grid positioned near isocenter (b) Isocenter Phantom. Marks on the outside of the phantom guide placement according to room lasers. 5 IR balls on the phantom are detected for IR isocenter calibration.

1.4.1.3 Calibration of X-ray System

Based on the calibrated IR coordinate system the X-ray calibration phantom (c.f. Figure 8) is aligned to IR isocenter. IR markers on the outside of the X-ray calibration phantom guide the user to correctly position the phantom such that the phantom is aligned to the previously calibrated isocenter. Inside this phantom are radio-opaque disks. Images from the two orthogonal X-rays are taken, and a marker detection algorithm is used to locate the markers on the resulting images. The locations of these markers are used to solve for projection parameters in the pinhole camera model mapping the 3D space to the 2D projection space. At this point the IR and X-ray system are fully calibrated. Daily calibration removes the system's sensitivity to small shifts in position of the ceiling mounted, flat panel detectors or IR cameras.

1.4.2 Image Guidance for SRT

There is potential for a small, but significant amount of inter-fraction PTV movement due to head position and inter-fraction setup error, even though a custom immobilization device is fit to each patient before the planning CT scan is performed. The immobilization system used for Novalis BrainLAB SRT is a non-invasive custom mask that is formed around the patients head. The patients head is enclosed within two heated sheets of thermo-plastic, which creates a rigid

mold upon cooling that is custom fit to the patient's face. This mask system does not place the head at the exact same position every fraction because it allows for a small degree of motion due to shifting of skin and facial tissues. Alheit *et al* (2001) reported that treatments using the BrainLAB mask system typically require an additional setup margin of 2-4mm for such uncertainty. While ensuring adequate tumor coverage, large margins place more normal tissue inside the PTV.

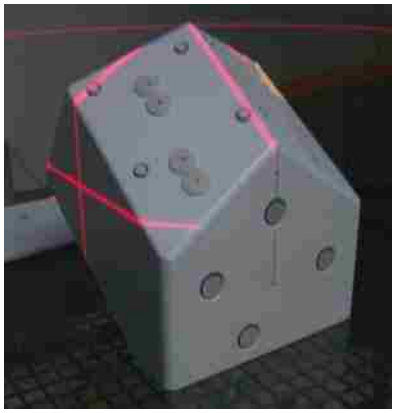

Figure 8. X-ray Calibration Phantom setup to laser isocenter. IR markers on the outside direct phantom setup. Internal markers are used for X-ray calibration.

Application of SRT can be significantly improved with increased certainty of PTV location through image guidance. Reduction of the PTV in image guided SRT will increase the amount of normal tissue that does not need to be irradiated to remain outside the volume of full dose.

The effectiveness of the Novalis ExacTrac alignment system has been evaluated in terms of its ability to reposition to isocenter. Yan *et al* (2003) reported positioning accuracy within 1 mm using a Rando phantom with embedded fiducial markers. Shifts and rotations in phantom position were simulated by moving the IR markers in relation to the phantom. The phantom was initially aligned to planned isocenter and then repositioned by the infrared camera system based on the shifted IR marker locations, thus creating a setup misalignment. Internal target

misalignment (i.e. shifting of a tumor position) was simulated using a water phantom with a submerged chamber holder, attached to a 3D scanning device, which allows for translations with sub-millimeter precision. A plastic object to which fiducial markers were attached was connected to the chamber holder as a simulated target. While this study showed the realignment capability of the ExacTrac system, it did not address the accuracy of dose delivery including the additional sources of error that occur while treating patients, such as an alignment method based on patient anatomy.

Isocentric alignment to within 1 mm was confirmed in two AAPM summer school abstracts using phantoms similar to the CIRS head phantom which was used in this study. Jin *et al* 2005 showed 1mm isocenter repositioning accuracy by placing a 2 mm diameter metal ball at isocenter inside a Rando phantom and tracking the location of the ball after application of image fusion. Li *et al* (2005) demonstrated localization to within 1 mm using an anthropomorphic head phantom which was purposely moved away from target position, then repositioned with ExacTrac image guidance. The change in treatment couch position was used to measure the system accuracy. These studies improved upon the Yan *et al* (2003) study as their image guidance was based on the patient-like anatomy of the phantom. They also, however, excluded additional error sources that might contribute to error.

Additional causes of error are encountered when delivering the prescribed treatment to the patient. Major contributing factors on the treatment side include:

(1) Discrepancies between the radiation isocenter and the image guidance isocenter. The image guidance isocenter is set to the room lasers which are subject to drift over time. A perfect image guidance system can only localize a planned target to the isocenter of the image guidance system. Offset of the radiation isocenter from this location results in dose delivery error.

(2) ExacTrac calibration is performed by manually aligning a calibration phantom to wall lasers. There is some uncertainty in the positioning of this calibration phantom that could result in a slight offset in the position of imaging isocenter.

(3) Mechanical effects on the treatment machine will affect the dose delivery and treatment. The weight of the gantry head, combined with rotational walkout of the center of each rotation axis of the treatment machine creates a wobble effect on the focal point of radiation beams from varying couch and gantry settings. Error in collimator jaw and mMLC leaf positions will also add to error in the delivered treatment. This effect can potentially result in delivered dose inaccuracy.

The radiation oncologist views the dose distribution superimposed on the anatomy as the "truth" and inaccuracies here can also create differences between the "truth" and the actual delivered dose. Major contributing factors to the accuracy of the treatment plan dose calculation include:

(1) Inaccuracies in the commissioning data

(2) Inaccuracies of the beam model and dose model

(2) CT Scanning errors such as scaling factors etc.

(3) Scaling errors between dose grid and CT grid

Therefore a method to determine the net positional accuracy of dose delivery in comparison with dose distributions from the treatment planning system would have considerable clinical relevance. For example, the patient's dose distribution from the treatment planning system is viewed by the radiation oncologist on hardcopy and CRT monitors. The radiation oncologist needs assurance that the resulting dose distribution at the time of treatment will match that of the TPS within a small, known range. Knowing quantitatively this range (i.e. the

accuracy to which the treatment plan can be reliably delivered) will apprise the radiation oncologist of the limitations of site specific treatments and allow for the generation of the optimal treatment for the patient. Presently, MBPCC radiation oncologists generally prescribe an approximately 5 mm margin outside the clinical target volume (CTV) to account for setup error in cranial treatments.

This study is designed to evaluate the accuracy of Novalis BrainLAB's delivery of the dose distribution calculated by the BrainScan treatment planning system using ExacTrac image guidance to align the phantom. Additional errors outside the scope of this study include those resulting from incorrect contouring of a tumor or PTV designation. The CT resolution (0.7 mm by 0.7 mm and slice thickness of 1.25 mm was used here) imposes a limit of tumor localization because of detail that one can be seen in the CT scan due to the finite pixel size. Cranial SRT usually involves multiple imaging modalities, most commonly MRI, where the additional image set used to determine the PTV, is fused to the CT image set. MRI-CT registration error is not included, but is low (≈ 0.3 mm) on average, but can be as much as 1.5 mm as measured at this institution.

Currently there is an established credentialing process for IMRT protocols under the Radiological Physics Center (RPC). Accuracy of IMRT deliveries are tested using an anthropomorphic head phantom with two internal PTVs and one OAR, containing both TLD and GAFchromic™ film inserts (American Association of Physicists in Medicine, RPC, M.D. Anderson Cancer Center). The phantom is anthropomorphic in that it is shaped like a human head and is filled with water, thus simulating tissue; however, it does not simulate a human head's internal anatomy (i.e. cranial bone structures) and is not meant for testing of IGRT treatment accuracy. In this RPC test measured film profiles are compared to profiles generated

in the treatment planning system, much like the analysis done in this study. The upper limit for agreement between film measured profiles and profiles generated from the dose calculation is 4 mm. An anatomical anthropomorphic phantom put to use in the same fashion as this RPC test would effectively measure the accuracy of image guided stereotactic radiosurgery/radiotherapy.

The results of this study will be highly dependent on the QA standards maintained on the CT Scanner and Novalis treatment machine, as well as the quality of commissioning data, thus, results will be institution specific. MBPCC's CT QA includes slice thickness accuracy of ± 1mm and in-plane spatial integrity of ± 1 % per millimeter. Any distortion or scaling in the CT image in any dimension can have an affect on the image fusion results, as the spatial dimensions of the DRRs used for fusion can be traced back to the nominal CT dimensions.

The treatment machine QA includes collimator jaw and mMLC positioning to ±1mm, gantry and collimator angle accuracy to ± 0.5 degrees, and 2% output constancy. The laser setup is the basis for the ExacTrac calibration, and essentially determines the accuracy of the image guidance system. At MBPCC the lasers are tuned to the center of a virtual sphere of no more than 0.75 mm radius created by the center of the radiation beams from varying gantry and table angles.

1.5 Hypothesis and Specific Aims

Cranial coplanar beam radiation therapy using the MBPCC BrainLAB ExacTrac image guidance system can achieve positional accuracy of dose delivery (i.e. displacement of delivered dose distribution from that shown by the TPS) within 1 mm for a cranial PTV in an anthropomorphic head phantom.

Three aims have been completed to test this hypothesis;

Aim 1. Film-Phantom Measurement System. Establish a method for measuring planar dose distributions in three orthogonal planes in the cranium of an anthropomorphic head phantom using film. Develop techniques for film preparation, processing, digitization, registration, and analysis, which can be used to assess accuracy of IGRT.

Aim 2. Film-Phantom Measurement System Accuracy and Precision. Assess the dosimetric accuracy for parallel irradiation geometry by comparing depth dose from film measurements with ion chamber measurements. Asses the spatial accuracy for perpendicular irradiation geometry by comparing off-axis dose profiles from film measurement with diode measurements. Estimate measurement system precision by tracking radiation isocenter variation (mid-profile location) over 5 trials for each measurement plane with constant setup.

Aim 3. Spatial Accuracy of Dose Delivery for ExacTrac IGRT. Intentionally misalign the phantom by known offsets from isocenter prior to treatment, then use the ExacTrac automatic image fusion procedure to align the phantom prior to delivering the planned treatment. Compare measured dose distributions with calculated dose distributions from the TPS to quantify spatial accuracy of dose delivery using ExacTrac IGRT.

Chapter 2 Methods and Materials

2.1 Aim 1: Film-Phantom Measurement System

Establish a method for measuring planar dose distributions in three orthogonal planes in the cranium of an anthropomorphic head phantom using film. Develop techniques for film preparation, processing, digitization, registration, and analysis, which can be used to assess accuracy of IGRT.

• • •

A major goal of this work was to simulate as closely as possible cranial SRT treatment deliveries from the BrainLAB ExacTrac system. This was accomplished by utilizing a measurement system that was able to (1) go through all phases of treatment, i.e. CT imaging, treatment planning, X-ray image guided alignment, and treatment delivery, for a true end to end test and (2) to effectively simulate patient cranial X-ray images used in IGRT. This measurement system consisted of the anthropomorphic phantom, Radiosurgery Head Phantom model 605, manufactured by CIRS (Norwalk, VA), whose materials and whose kV X-ray images are similar to those of a human head, and which was also able to house a high spatial resolution (radiographic film) detector phantom in the brain section.

This phantom holds 6.35 cm x 6.35 cm pieces of film in its internal cubicle cassette. Special templates and tools described below were required to facilitate cutting, processing, and digitizing films, and methods were designed for calibration, registration, and comparison.

2.1.1 Anthropomorphic Head Phantom

A CIRS Model 605 anthropomorphic head phantom was used to measure dose distributions resulting from stereotactic radiotherapy treatments delivered to the phantom. This phantom was selected because (1) it appears similar to patient anatomy on kV X-ray systems and

(2) the material properties of this phantom are quoted to reproduce the attenuation characteristics of a human head with 1% accuracy for the energy range of 50 keV to 25 MeV (CIRS Radiosurgery Head Phantom Model 605 Specification Sheet). Figure 9a shows how the phantom is constructed and its internal film phantom. For this study the phantom was immobilized using the with the BrainLAB mask system (c.f. Figure 9b). Figures 10 and 11 display CT and X-ray images of the phantom respectively, comparing those of an actual patient and those of the phantom (X-ray setting = 100 kVp). A comparison between the linear attenuation coefficients of the phantom and those of a human head in the energy range 0.4 MeV to 30 MeV, provided by CIRS is shown in Table 1 for the five phantom materials.

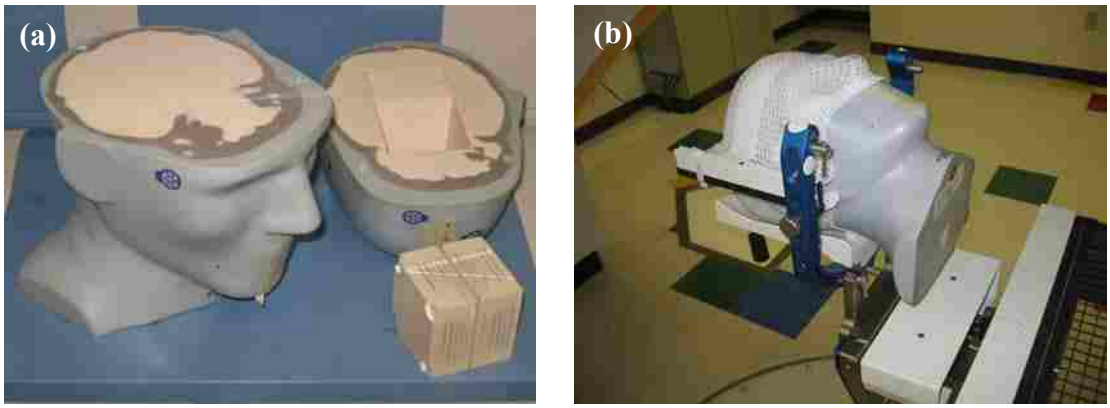

Figure 9 (a) Film phantom measurement system components (b) Phantom enclosed in immobilization mask in treatment position

2.1.1.1 Custom Film Phantom

A 6.35-cm sided cubic film block, shown in Figure 12, was custom-made by CIRS for this project. It was different from their standard film block in that the custom one sandwiches the film at 2 locations 25% and 50% across the block, as compared to the standard block that contains 13 locations for film placement (i.e. measurement planes every 0.4 cm available for measurement). The custom block can be oriented to measure dose distributions in sagittal, coronal, and axial planes for the supine patient setup used in this study. Film is held firmly in

place by four 4.1 mm diameter rods that compress the block. These rods also act as fiducials providing physical reference locations to delineate film position relative to the phantom.

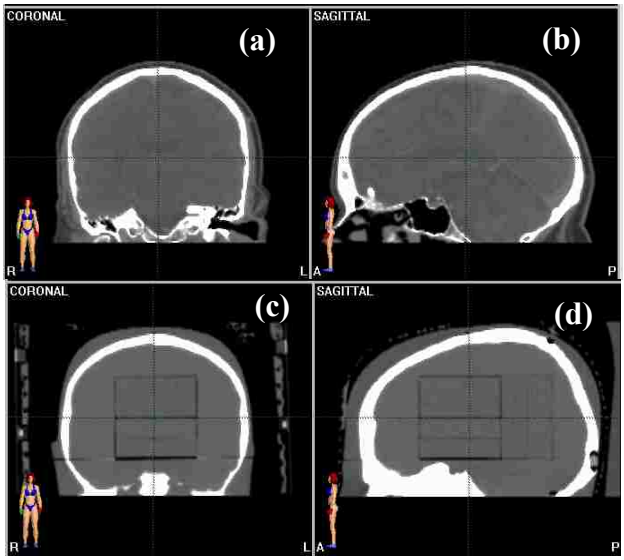

Figure 10. Coronal (a) and Sagittal (b) CT reconstructions of human head are compared with Coronal (c) and Sagittal (d) CT reconstructions of the CIRS radiosurgery head phantom. Note the film cassette edges in the CIRS head phantom.

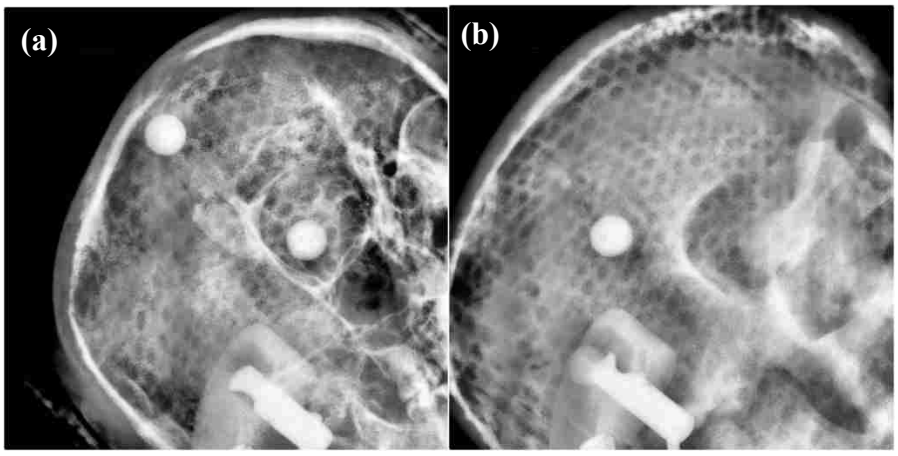

Figure 11 (a) ExacTrac X-ray of human head. (b) ExacTrac X-ray of CIRS radiosurgery head phantom. White circles seen in both images are infrared markers positioned on the patient and phantom.

Table 1. Linear attenuation coefficients, μ (cm^{-1}), physical densities, and electron densities of phantom materials versus "average human" (provided by CIRS)

		Average Soft Tissue		Average Bone Tissue		Average Brain Tissue		Spinal Cord		Spinal Discs	
		Average Human (ICRP 23, 1975)	Head Phantom	Average Human (ICRP 23, 1975)	Head Phantom	Average Human (Howard *et al* 1986)	Head Phantom	Average Human (ICRP 23, 1975)	Head Phantom	Average Human (Howard *et al* 1986)	Head Phantom
	ρ, g/cm^3	**1.030**	**1.055**	**1.577**	**1.600**	**1.040**	**1.069**	**1.037**	**1.070**	**1.100**	**1.131**
	ρ_e, $*10^{23}/cm^3$	**3.421**	**3.434**	**5.035**	**5.028**	**3.458**	**3.470**	**3.449**	**3.448**	**3.621**	**3.624**
Photon Energy, MeV	**0.04**	0.2679	0.2678	0.7884	0.7887	0.2791	0.2791	0.2769	0.2768	0.3096	0.3097
	0.1	0.1742	0.1748	0.2822	0.2819	0.1767	0.1772	0.1762	0.1761	0.1862	0.1863
	0.4	0.1086	0.1090	0.1605	0.1602	0.1098	0.1102	0.1095	0.1095	0.1150	0.1151
	1	0.0724	0.0726	0.1066	0.1064	0.0731	0.0734	0.0730	0.0729	0.0766	0.0767
	4	0.0347	0.0348	0.0521	0.0520	0.0352	0.0352	0.0351	0.0350	0.0369	0.0369
	10	0.0225	0.0225	0.0355	0.0355	0.0229	0.0228	0.0227	0.0227	0.0242	0.0242
	30	0.0171	0.0170	0.0296	0.0296	0.0176	0.0174	0.0174	0.0174	0.0189	0.0188

The threaded rods provided by CIRS were replaced with solid Delrin rods (threaded only at ends), which provide a more reproducible and rigid film placement. When the block contains one film and surrounding ready-pack layers and is inserted into the phantom, it slides into the heap cap leaving virtually no gap. Given this and the tight mechanical tolerance to which the phantom is constructed this measurement system should be able to localize dose distributions on the film for stereotactic size treatment fields within a few tenths of a millimeter.

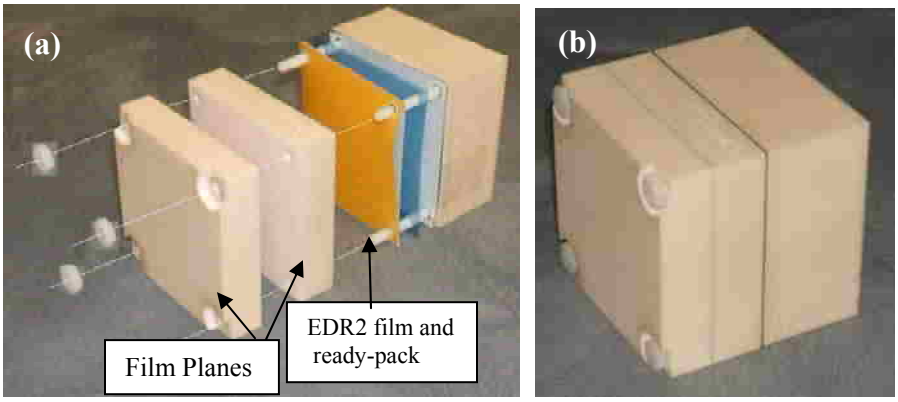

Figure 12 (a) Exploded view of film block components (b) Assembled film block

2.1.1.2 Avoidance of Phantom Artifacts in Film Dosimetry

Accurate dose measurement using film in the film block required two precautions. First, air gaps between the film and the phantom were avoided by tightening the screws on the film block to achieve maximum compression because failure to completely compress the block results in air pockets, which have been shown to result in dose measurement error as great as 10% when irradiated edge on (Suchowerska *et al* 2000). Also, the head cap of the phantom itself must be flush against the base without any gap, which was achieved by firmly compressing the phantom components together prior to treatment.

Second, the film was protected from Cerenkov light generated within the phantom (AAPM Task Group 69, AAPM Task Group 42), which overexposed the film. If not done, our measurements showed an increase in measured dose by ≈ 60% due to Cerenkov light. This was

managed by keeping the EDR2 ready-pack sleeve (white paper and black outer packaging) over the film to absorb the light generated in the film block. Although some Cerenkov light is produced in the white paper, keeping the ready-pack sleeve over the film was appropriate as it maintained the same irradiation conditions as the calibration film, ensuring proper calibration (Perrin *et al* 2007).

2.1.2 Film Dosimetry

The measurement system required a dosimeter capable of measuring 2D planar dose distributions inside of a phantom. Radiographic film was selected because of its high spatial resolution, its known dose characteristics, ease of use, ant its ability to be cut to form fit a specialized phantom. Kodak (Rochester, NY) EDR2 radiographic film was selected for its extended linear range, which allowed realistic treatment fractions (≈ 200 cGy) to be simulated. EDR2 film has been used in similar head phantom applications (Robar *et al* 2000) as well as in measurement of SRS dose distributions (Robar *et al* 1999).

Accurate film dosimetry can be problematic due to variation in film response between different batches of film, time of processing and processing conditions (Sujatha *et al* 2007, AAPM Task Group 69). Therefore in the present work, all film were from the same batch, and calibration and test film measurements were made for each measurement session and processed at the same time.

TG-69 recommends that film calibration be performed under the same conditions as the measurement. This creates a complication when measuring dose distributions from multiple fields at varying incident directions relative to film position. In this study, for example, radiation beams enter the film from many directions including parallel, perpendicular and oblique, as well as interact with the film at a variety of depths. To make sure that the effects of varying incidence

were not an issue, dose measurement with film was verified for both parallel and perpendicular incidence by comparing corresponding measurements using other dosimetry techniques (i.e. ion chambers and diodes).

2.1.3 Loading the Film Block

Each test film was prepared and loaded into the phantom in the dark room under safe-light so as to fit inside the film block in a highly reproducible way. For a single measurement set a number of films were prepared using a custom aluminum film cutting template designed and developed for this project(c.f. Figure 13) and stored in the dark room. One piece of film at a time was loaded inside the film block for irradiation. An additional un-irradiated strip (≈ 10" x 4") of film was also stored for subsequent background/fog determination.

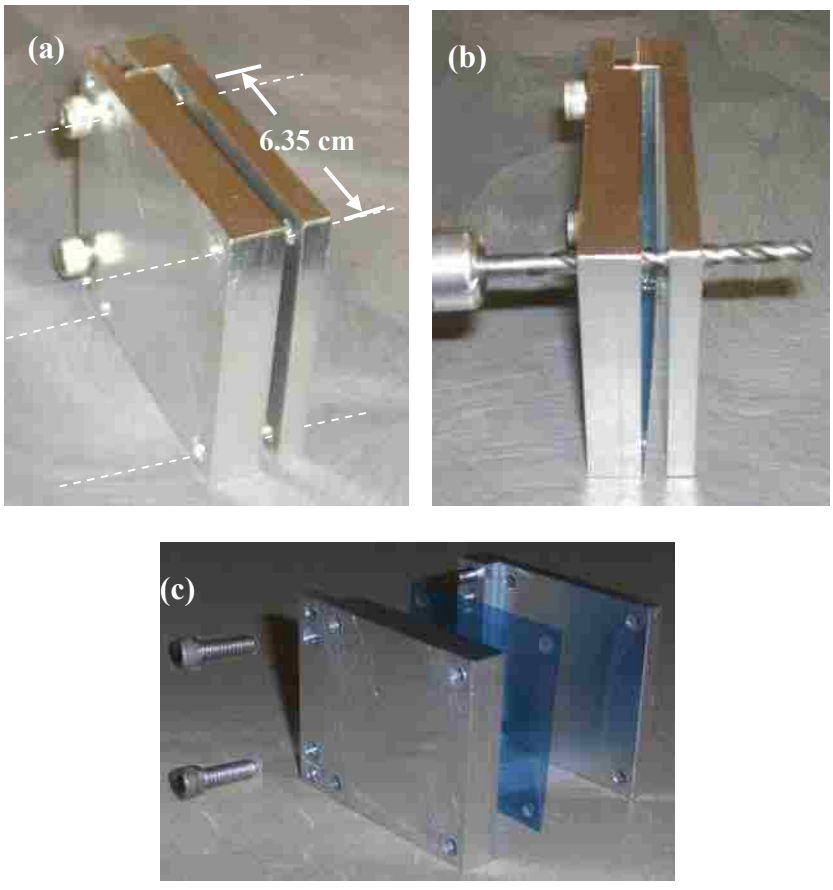

Figure 13. (a) Film cutting template. Film is placed inside the gap shown, which can be compressed by two thumb screws. (b) Film cutting template side view. The drill bit shown punctures the film and creates 4 holes. (c) Both interlocking sections of the film cutting template and thumb screws. A cut film is shown in between the two aluminum sections

The film preparation steps are listed below with images shown in Figure 14.

- A single 10" x 12" Kodak EDR2 film was cut into strips (≈ 6.3 cm x 30.5 cm) (c.f. Figure 14a).
- A single strip was inserted into the template, tightly clamped using two screws to hold the film in place (c.f. Figure 14b)
- Then, a 6.35 cm x 6.35 cm square was cut using an Exacto knife blade. This procedure was repeated until ample film squares were cut.
- For each film square holes were created using either a hand drilling tool or power drill using machined holes in the aluminum template to guide the drill (c.f. Figure 14c)
- Each film was marked to identify the film orientation (c.f. Figure 14d). The film was marked with a small pin prick at the same point on each film, which was placed in the same manner inside the film block. The film block was placed in the head phantom in a consistent manner. This allowed the appropriate orientation of the film to be analyzed.

2.1.4 Film Processing

Test films were processed using a Kodak X-OMAT 270 RA film processor, waiting at least one hour after the end of a given test session, as recommended by TG- 69. The film processor was maintained at a temperature of 94º ± 0.3º. For each processing session, prior to developing any films, at least three 11" x 14" previously developed blank films were fed through the film processor to bring the temperature and developer chemistry to stability. To prevent loss of the 6.35 cm x 6.35 cm test films in the developer, test films (up to 6 total films for one template) were inserted into the processing template, as shown in Figure 15. All test films from a given measurement set (as many as 18 total films) were processed immediately following the processing of an unexposed "fog" film and a calibration film.

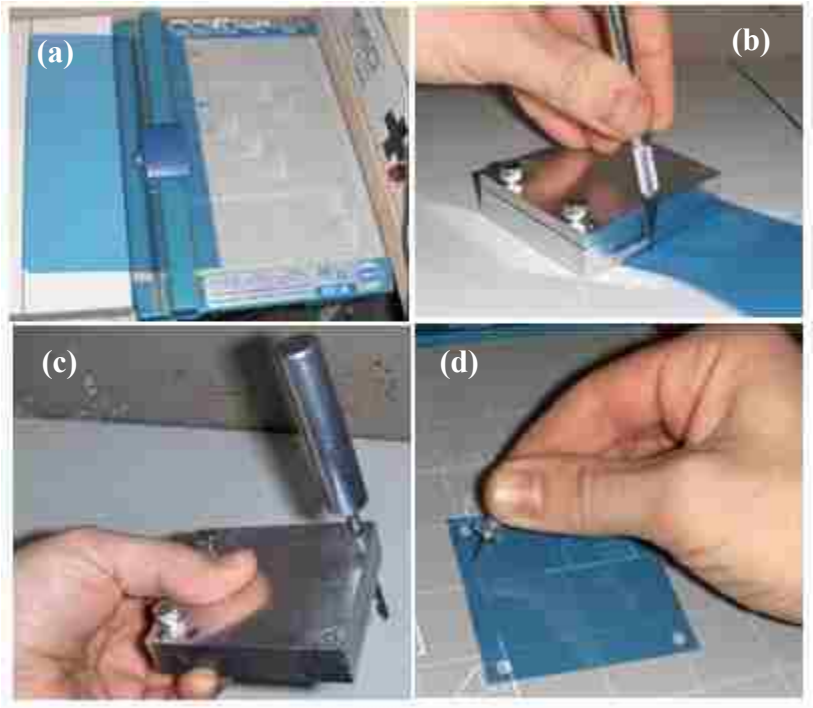

Figure 14. Film preparation sequence: (a) films were cut into slices with a paper cutter; (b) film strips were inserted into the template, compressed tightly using the screws, and cut into squares; (c) four holes were drilled at the position of each fiducial rod; (d) film was marked for orientation and either placed in the phantom or stored.

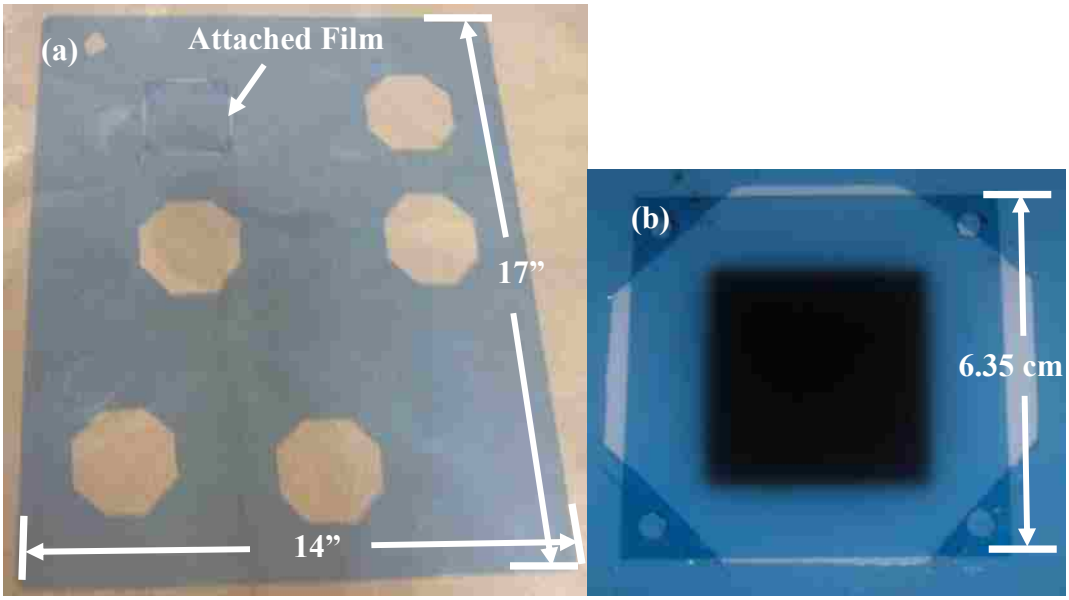

Figure 15. Film processing template: (a) test films were inserted into slots at the 4 corners of each of the six apertures; (b) Enlargement of single film section of processing template, post processing.

2.1.5 Film Digitization

A template similar to that used for film processing was used for digitizing the films. The template holds films in the same manner as that used for processing; however, the slots to insert the film were positioned closer to the center of the film such that the edge of the slot avoids the punched holes, (c.f. Figures 16). This ensured that there was no diagonal slit intersecting the punched hole that would keep the centroid algorithm from working appropriately in the registration process (Section 2.1.7.2).

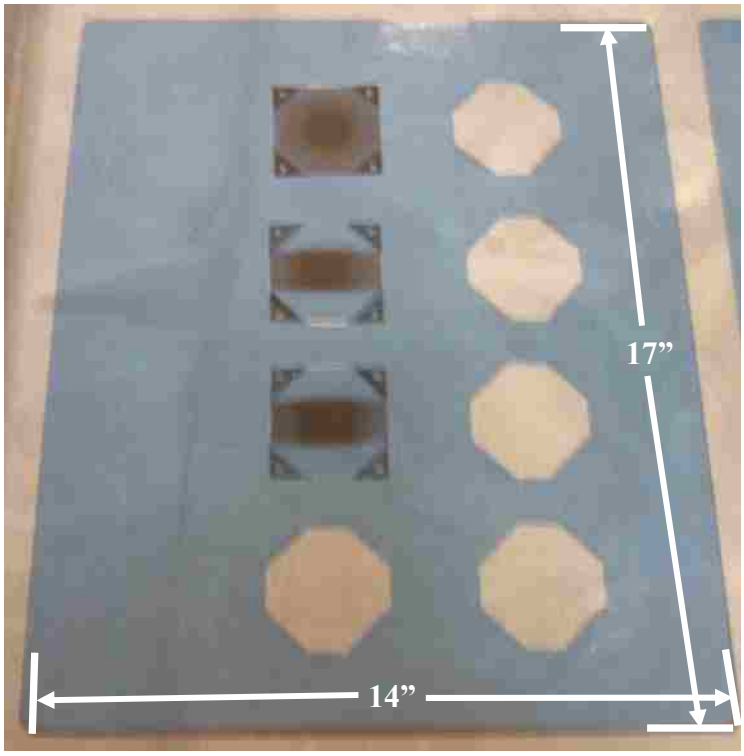

Figure 16. Film digitization template: Test films are inserted into apertures cut out of a 14” x 17” blank film.

Each test film was digitized using a Vidar Dosimetry Pro 16-bit film scanner (c.f. Figure 17). The intensity of light transmitted through the film was measured as a 16-bit A/D value from a linear array of CCD detector elements.

The scanner was calibrated at 0.089 mm resolution mode, and each test film was scanned attached to the 14" x 17" film digitization template, which was inserted into the scanner. The left third of the film digitization template did not have any test films so as to avoid a small horizontal non-uniformity, (≈ 5%) seen with our scanner at the left edge (≤10 cm from edge). Also, zero and calibration films were scanned at the center of the scanner slot, as opposed to scanning along the left edge of the slot.

Figure 17. Vidar Dosimetry Pro 16-bit film scanner; Film digitization template is shown prior to scanning.

RITv4.4 Film dosimetry software was used for all data analysis. Each test film was enclosed in a region of interest (ROI) and saved as a unique file with the test session's intensity versus dose calibration curve embedded.

2.1.6 Film Calibration

Calibration films were created for each measurement session using an 8 square 3 x 3 cm^2 field step and shoot MLC leaf sequence calibration procedure (Childress *et al* 2002) using the 6MV beam of a Varian 21 EX radiotherapy accelerator. A single 10" x 12" piece of Kodak EDR2 film was placed at 100 cm SAD between slabs of CIRS Plastic Water creating a depth of 10 cm with 5 cm of backscatter. Each square was exposed to varying doses using an MLC file previously determined by Childress *et al* 2002. Figure 18 shows a calibration film and the individual doses to the center of the 3 x 3 cm^2 squares. These dose values were independently

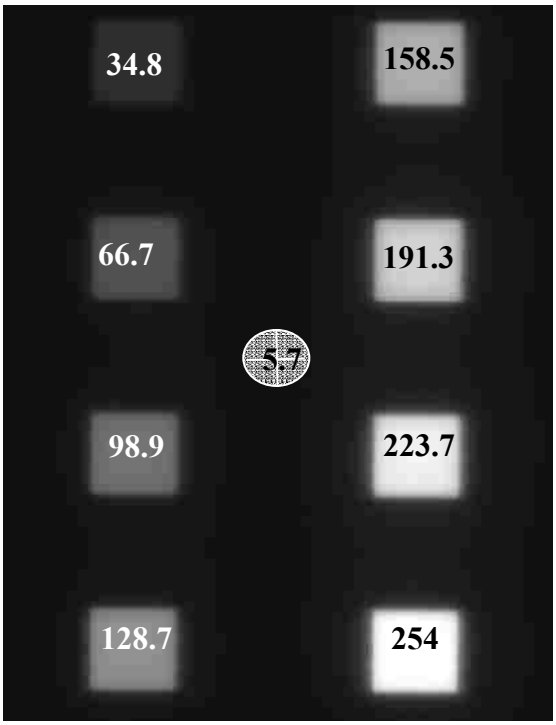

Figure 18. Example 8 square calibration film irradiated with MLC sequence. Measured doses displayed each square and center point in cGy, were used to create the film calibration curve.

verified using a calibrated Exradin A-16 ion chamber (0.007 cm^3 collecting volume). Total dose from all eight fields was measured at the center of each of the eight squares individually, and at the center of all eight squares. Total dose included scattered dose from all squares. Using the

Vidar digitizer and RIT software the calibration film is scanned as a RIT image file (file extension *.rv4). The calibration procedure calls for the user to designate a series of regions of interest to varying dose levels, creating a calibration curve, which maps the raw A/D value as measured by the Vidar scanner to dose. A 5 pixel x 5 pixel median filter is applied to each image, effectively reducing noise and artifacts. Each calibration file requires a zero dose point, which was established by scanning the unexposed strip of film.

Each dose was entered into RIT and used to generate the dose calibration curve (c.f. Figure 19). Dose points were fit to a piecewise polynomial curve. The first point on the curve (dose = 0) was determined from the unexposed film. The second point on the curve (dose =5.7 cGy), corresponded to the center of the film. The remaining 8 data points corresponded to the center of each square exposure.

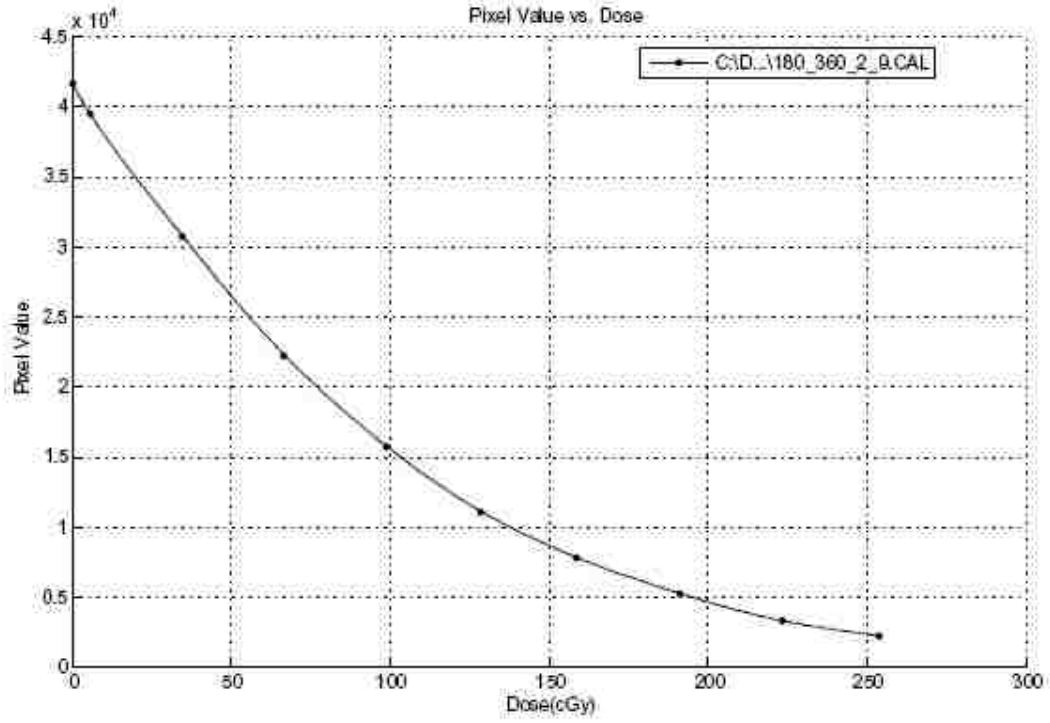

Figure 19. EDR2 Dose Calibration Curve. 10 Points were entered into RIT. Data points were fit to a piecewise polynomial curve.

2.1.7 Registration of Measured and Calculated Dose Distributions

Comparison between the measured and calculated 2D dose distributions required registration in space of at least three common points between the treatment plan and film. In the present study, the center of each of four fiducial rods that hold the film in place in the film block were used to register the measured planar dose distribution with the corresponding TPS dose distribution. For the test films, this corresponded to the centers of the holes through which the fiducial rods are inserted. RITv4.4 software has a feature that aligns two images (i.e. film and treatment plan) by rigid body point based registration and provides a number of analysis methods. Figure 20 shows a dose distribution in the TPS and the same dose distribution registered to a film measurement. The following steps are performed to register the two images.

- Coordinates of each of the four fiducial rod centers were determined in BrainScan for each measurement plane
- A dosemap from the planned treatment in each plane was exported as a data file
- The TPS dosemap was opened in RIT and pixels corresponding to each registration point were determined
- The film image was opened in RIT and the appropriate dose calibration curve was applied.
- Film registration points corresponding to hole centers were determined
- Corresponding points were registered for comparison of dose distributions

Details of the determination of location of alignment points for the calculated and measured dose distributions are detailed in the subsequent two subsections.

The calculate BrainScan dosemap was registered to the film measured dosemap. Upon

registration RIT displays an estimate of the post-registration pixel differences (ΔX, ΔY) between each registration point of the film and dosemap image. This information is an indication of the quality of the registration, (i.e. selection of registration points), and the utility of this data is described in section 2.1.7.3.

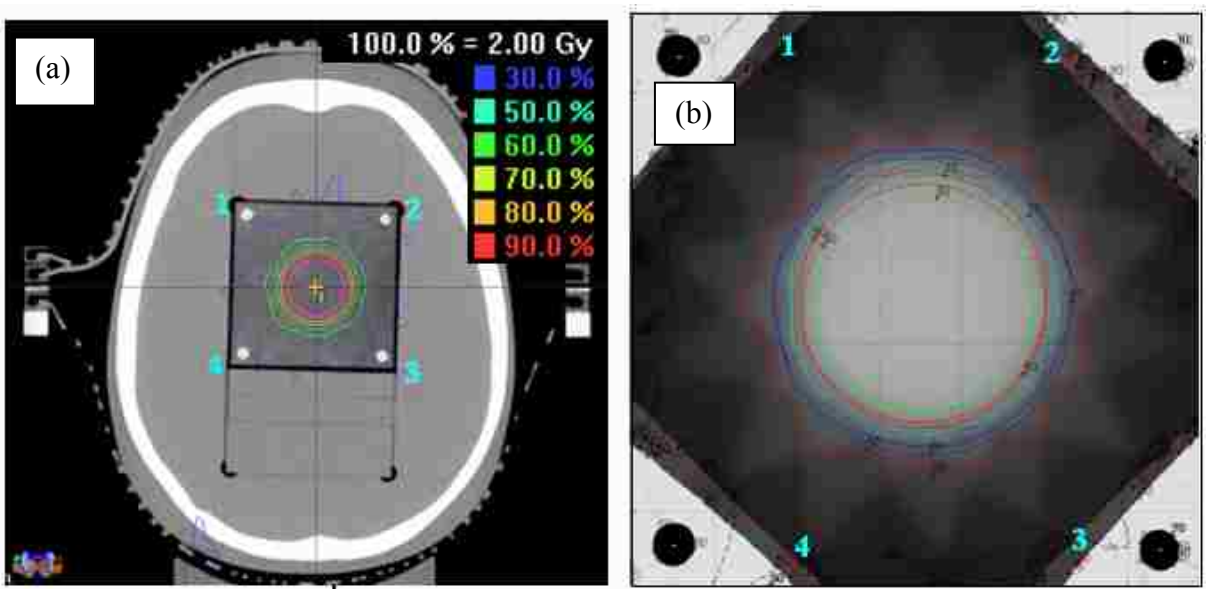

Figure 20. Film–TPS registration using RITv4.4 film dosimetry software. (a) Dose Distribution display in BrainScan treatment planning system. Registration fiducials are numbered on the screen. (b) Registered film and treatment planning dose distributions. The film image is shown, with the measured isodose lines (solid lines) and registered treatment planning isodose lines (dashed) overlaid.

2.1.7.1 Treatment Planning System Dose Distribution: Registration and Export

The coordinates of each of the 4 registration points in the treatment planning CT scan were determined by locating the center point of each fiducial rod in the treatment planning system. Determining the coordinate at the center of each fiducial rod was complicated by the pixilation effects inherent in the CT image set. The centers of the 4 rods were determined by creating a visual match between a template and the planar CT image of the film cassette rather than choosing registration points in a point by point fashion. The "in-house" template consisted of 4 circles whose diameters and locations correspond to the true physical dimensions of the film

block. The template, displayed on the computer screen was manually rotated, translated and scaled to match the circles with the fiducial rods. Figure 21 demonstrates the utilization of this software. Using windows magnification feature a close-up view of each point was displayed. How the selected template overlay holds up as the window/level setting varies was assessed. Ideally the visual center of the fiducial rod should remain centered over the range of window/level settings, otherwise adjustments were made to the template position to improve the fit. Upon finding the best match the registration coordinates were determined using the measurement tool in BrainScan.

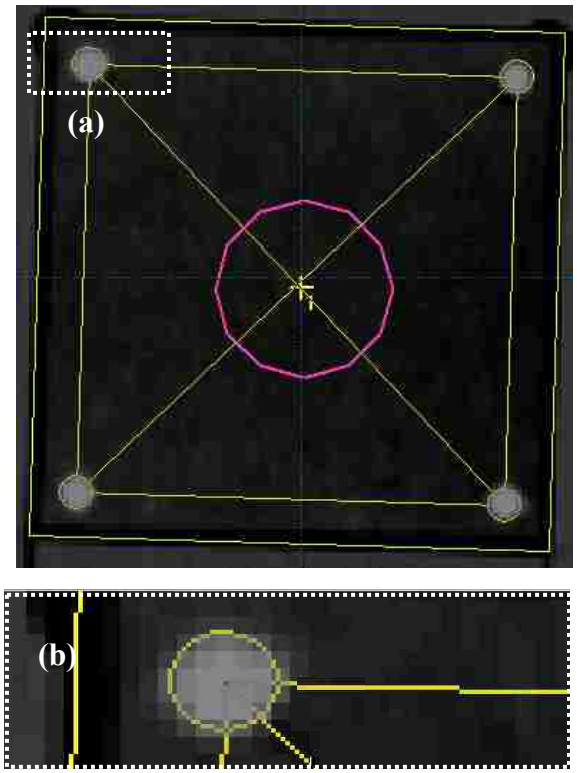

Figure 21. (a) This image illustrates final alignment of the graphics template (yellow) with the film block and fiducial rod positions in the axial plane. The pink circle is the PTV and the yellow cross is the planned isocenter. The CT image has a window/level setting on BrainScan of (Level 184, Width, 593) (b) Zoom view of point number 1 with graphics template assisting in determining the center of the fiducial rod.

The dose export tool in BrainScan was used to extract the calculated dose distribution. A matrix of dose values (i.e. planar dose grid) was outputted to a data file with user defined dimensions and increment size. For this study the size of the exported dose map was 60 mm x 60 mm with an increment of 0.1 mm. BrainLAB dose point coordinates were in mm, whereas RIT dose point coordinates were in dimensions of pixels. In order to locate registration points in RIT it was first necessary to calculate the position of each registration point in pixels in the exported dosemap from the previously determined BrainScan coordinates. Calculation of the pixel number of a particular registration point from it's TPS coordinate in the dose export was determined using equation 1, where X_{start} is the boundary (starting location) of the selected area to export, and Δ is the increment size (0.1mm was used in this study). The analogous formula (2) is used for the Row,Y coordinate.

$$Column = \left(\frac{X_{start} - X_{\mathrm{Re}\,gistrationPo\,\mathrm{int}}}{\Delta} \right) + 1 \qquad (1)$$

$$Row = \left(\frac{Y_{start} - Y_{\mathrm{Re}\,gistrationPo\,\mathrm{int}}}{\Delta} \right) + 1 \qquad (2)$$

Planar dose distributions were exported to RIT for each of the three principal planes. In order for the appropriate comparison to be made, each measured film plane coincided with the central plane of three CT data sets. To accomplish this, CT scans were taken such that the film plane was placed parallel to the CT scanner display axis physically adjusting the phantom to the correct setup, described in section 2.3.1.

2.1.7.2 Film Dose Distributions: Location of Fiducial Holes and Registration

To register the film-measured dose distributions with the BrainLAB calculated dose distributions, RIT software was used to locate the center of each of the 4 holes. For each hole a region of interest (ROI) was specified by visually selecting the region surrounding it, after which

the center of each hole was calculated by the RIT Centroid Algorithm (center of mass). In some cases the area around the hole on a result film can have a wide range of artifacts that can influence the centroid calculation. To eliminate this situation the corners of the result films were manually colored black to make the area around the hole opaque prior to film scanning (c.f. Figure 22). This results in a greater difference between optical density of the opaque outside of the hole (A/D ≈ 200) and the semitransparent hole (A/D ≈ 40,000).

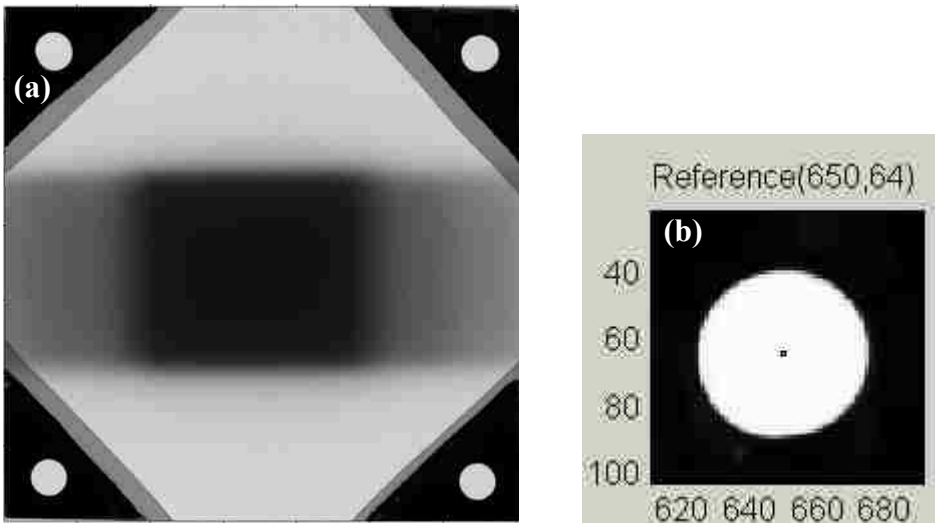

Figure 22. (a) Typical uncalibrated film image . (b) Close-up registration view of one of the 4 points used for registering film –measured and BrainLAB calculated dose distributions. The blackened corner improves the accuracy of determination of the hole center using the RIT centroid function.

Enhancement of the contrast allows the centroid calculation to reliably finds the hole center. Occasionally film artifacts such irregularly shaped holes from manually drilling the film holes result in incorrect determination of hole center. In such cases the center pixel was manually selected rather than using the RIT centroid algorithm.

Once points were defined RITv4.4 software aligned the treatment plan's calculated dose matrix to the measured dose matrix using a point based rigid body image registration technique. An image of both the TPS and film dose distributions with isodose contours is shown in Figure 23.

2.1.7.3 Quality of Registration Process

Error in the selection of the film registration points can result from (1) the inaccuracy of cutting of film holes and (2) the process of determination of hole centers in RIT. For each registration RIT displays the estimated displacement (in pixels) of each registration point on film from the corresponding point on the registered dosemap.

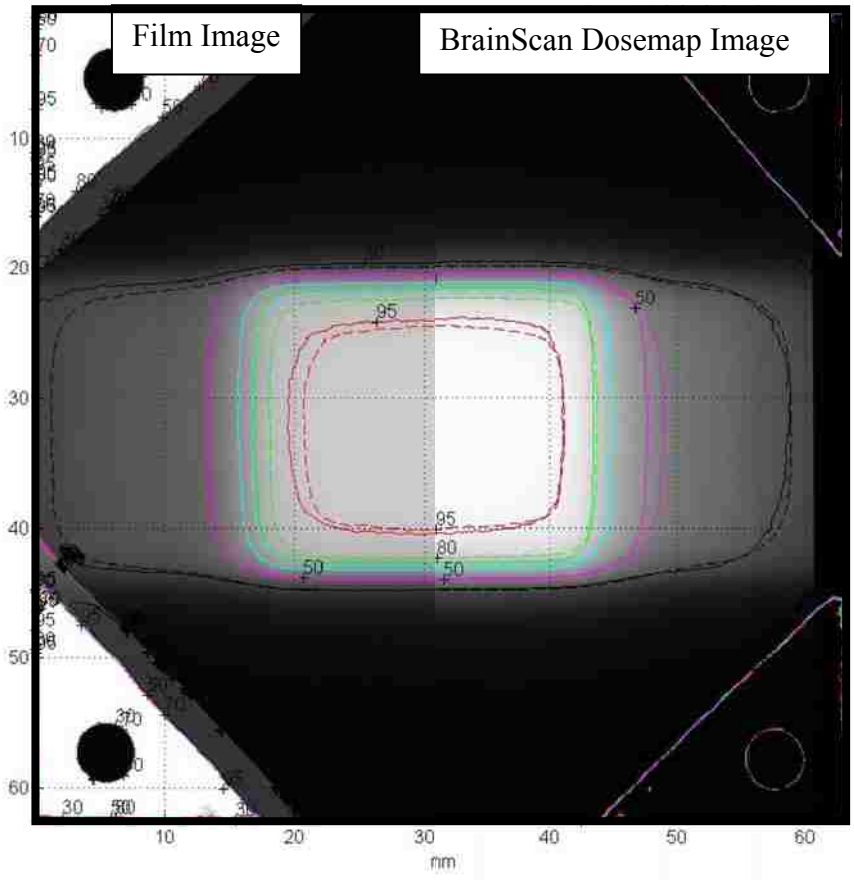

Figure 23. Registered Sagittal Film isodose overly image. The image on the left is the film image and the image on the right is the BrainScan dosemap image.

RIT also reports on-screen the standard deviation of these errors irrespective of direction, i.e. all of the displacements between points (ΔX_i and ΔY_i) are averaged and the standard deviation is computed (c.f. Figure 24). This value was taken to be a directionally independent measure of the quality of registration, the value of which henceforth defined "Q" (to indicate registration quality), as calculated by:

$$Q = \sigma_{RIT} = \sqrt{\left(\frac{1}{2N-1}\right)\sum_{j=1}^{N}\left[\left(\frac{\sum_{i=1}^{N}(\Delta x_i + \Delta y_i)}{2N} - \Delta x_j\right)^2 + \left(\frac{\sum_{i=1}^{N}(\Delta x_i + \Delta y_i)}{2N} - \Delta y_j\right)^2\right]} \quad (3)$$

where N = the number of registration points (4). This is the spread of registration error about some mean error in a given registration.

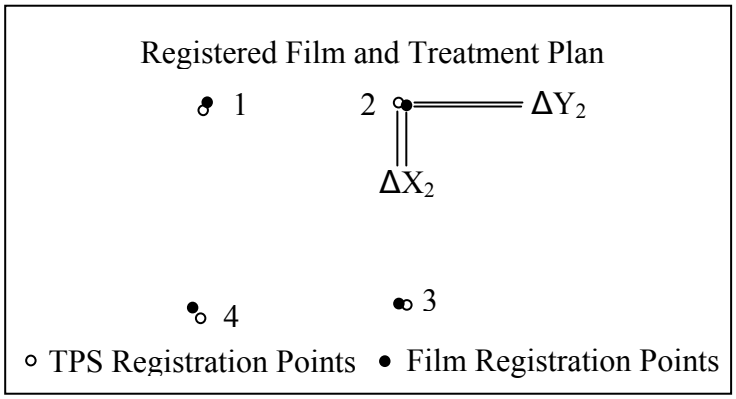

Figure 24. Diagram of RIT registration error report. After registration RIT displays the error between film registration points and corresponding TPS registration points.

In analyzing a set of registered film results there will be a number of Q's reported equal to the number of registrations in that set of results (measurement set). The distribution (σ_Q) of Q values in a particular measurement set can be thought of as a measure of consistency in registration point choice in registrations in that set of results. In measuring the precision of the

measurement system (section 2.2.3) there will be a distribution of Q values (σ_Q) associated with that measurement set. This serve as a benchmark for further results to claim the same precision as determined(i.e. other measurement sets have no more registration error. As long as each set of result films for any other set of measurements a smaller (σ_Q) than that determined from the precision test, then the reported measurement system uncertainty can be considered appropriate. This serves as a QA check for film registration point determination.

2.2 Aim 2: Film-Phantom Measurement System Accuracy and Precision

Assess the dosimetric accuracy for parallel irradiation geometry by comparing depth dose from film measurements with ion chamber measurements. Asses the spatial accuracy for perpendicular irradiation geometry by comparing off-axis dose profiles from film measurement with diode measurements. Estimate measurement system precision by tracking radiation isocenter variation (mid-profile location) over 5 trials for each measurement plane with constant setup.

• • •

The purpose of this research was to evaluate the positional accuracy of the dose delivered for Novalis IGRT cranial radiation treatments by comparing delivered (measured) dose distributions with dose distributions calculated by the BrainScan TPS. The positional accuracy was determined using relative dose distributions, i.e. dose normalized to the dose (≈ 200 cGy) delivered to isocenter (dose at isocenter for treatments in this study was taken as the average dose over a uniform region at the center of the film). Displacement of isodose lines was used as a means of determining positional error.

The type of treatment delivery being measured included seven coplanar radiation beams. Because dose was measured in three orthogonal planes, the films were irradiated from varying

orientations with respect to the film, complicating the film dosimetry. For axial plane measurements all beams were parallel to the film whereas for sagittal and coronal plane measurements beams intersected the film at a combination of perpendicular and oblique angles. Verification of the dose measurement on film in both perpendicular and parallel irradiation geometry was preformed to ensure accurate dose measurement over the entire set of irradiation conditions.

In measuring the accuracy of image guided treatment deliveries the film is inevitably exposed to kV X-rays prior to treatment. Initial testing shown a negligible effect on the measured dose due to these X-ray exposures. Nevertheless, to be consistent with the measurement conditions of film used to test image guided deliveries, film used to verify both irradiation geometries were exposed to 3 sets of ExacTrac X-rays before the test irradiation. This exposes the dosimetry verification films to the same additional background as the films used for measuring the IGRT treatments deliveries.

2.2.1 Dose Accuracy of Film-Measured Depth Dose

Measurements were taken to estimate the accuracy of dose measurement using the film phantom measurement system in parallel irradiation geometry. For treatment deliveries with the film block in the axial orientation, the film was irradiated by coplanar beams at varying angles, all of which were parallel to the film. Studies of radiographic film have shown as much as 10 % over-response for a parallel geometry due to air gaps (Suchowerska *et al* 2000) and could potentially cause inaccuracies in EDR2 film measurement in parallel irradiation geometry.

Three identical depth dose measurements taken inside the head phantom were compared to the ion chamber depth dose measurements. To approximate measurement conditions the film was loaded inside the film cassette, which was then placed inside the head cap in the sagittal

orientation. Rather than place the heap cap on top of the remaining portion of the head phantom, the head cap was turned upside down and an additional 4 cm of CIRS Plastic Water was used to increase the depth of measurement to the approximate treatment depth. Images of the measurement setup are shown in Figures 25-27.

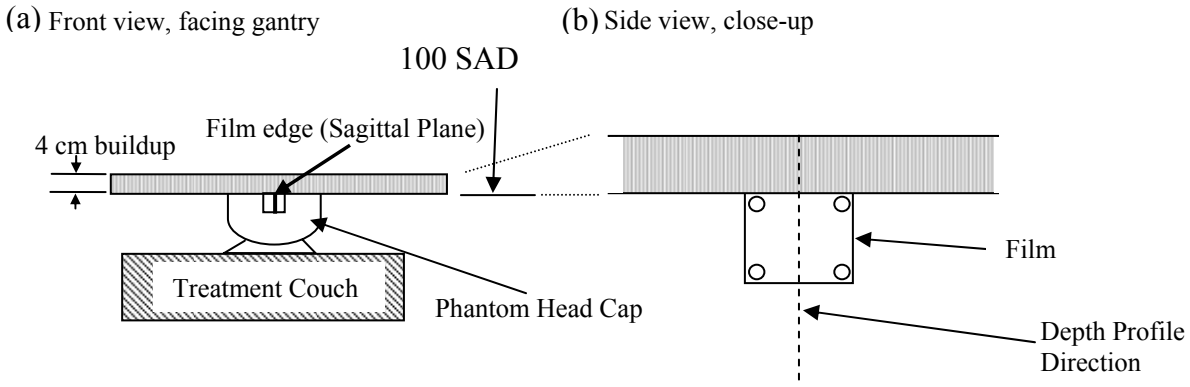

Figure 25. (a) Phantom Setup front view. The Head cap is placed upside down with the film oriented parallel to the incident radiation beam. (b) Close-up side view.

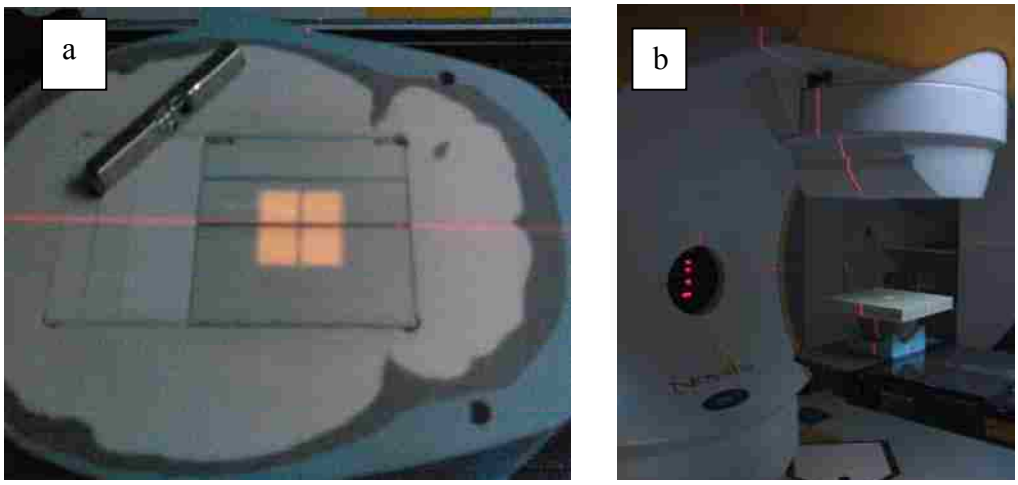

Figure 26. (a) Leveled phantom setup shown without buildup. The illuminated square is the 3 x 3 cm^2 light field projection describing the treatment beam. (b) 4 cm Plastic Water added to increase depth of measurement.

Because of the film size, only a limited portion of the depth dose was measured. 230 Monitor Units were delivered to the phantom, using a 3 x 3 cm^2 mMLC and collimator jaw setting (dose of 200 cGy at depth of 4 cm). The section of depth covered by the film (up to ≈10 cm) was compared against ion chamber depth-dose measurements in Plastic Water.

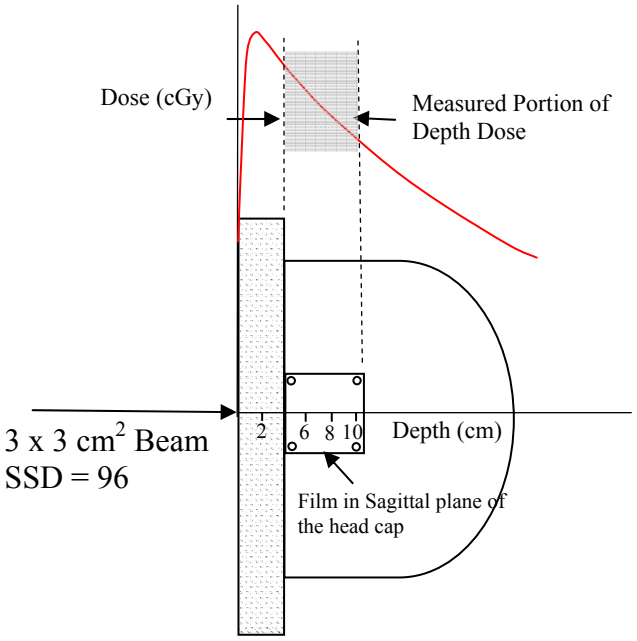

Figure 27. Schematic depicting percent depth-dose curve with respect to film position.

For comparison with film a set of point dose measurements were made along central axis using a PTW TN 30013 ion chamber. The Plastic Water was set with SSD = 96, and measurements were taken at depths of 2, 4, 5, 6, 8, 10 and 12 cm, (c.f. setup in Figure 28). Dose was determined as product of charge readings and a calibration factor, which was determined using a calibration irradiation of a 10 x 10 cm^2 field at isocenter with 10 cm depth (SSD = 90).

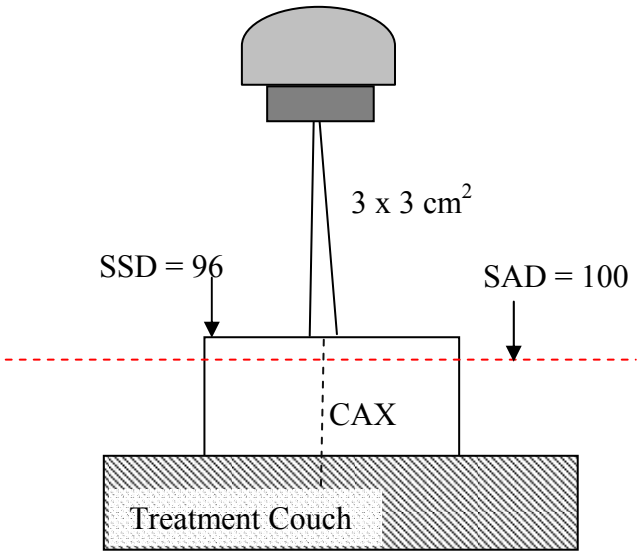

Figure 28. Ion Chamber depth-dose measurement setup. Charge readings were taken along the central axis (CAX) at depths of 2,4,5,6,8,10 and 12 cm.

2.2.2 Accuracy of Film-Measured Off-Axis Dose

The purpose of this measurement was to verify film dosimetry in phantom in the perpendicular irradiation geometry, ensuring accurate off-axis dose profiles. Verification of off-axis measurements in a perpendicular irradiation geometry was accomplished by comparing a phantom film measurement with MapCHECK (SUN Nuclear Corporation, Melbourne, FL) diode measurement. The MapCHECK system (c.f. Figure 29) is a 2D radiation measurement device with 445 silicon diodes spaced every 5 mm in the X and Y directions in the central 10 x 10 cm^2 region of the array. The thickness from the surface to the detector plane in 1.4 cm, with an effective depth (inherent buildup) of 2 cm.

For the phantom film measurement, the film was housed inside the film cassette, which was inserted into the upper phantom half only (c.f. Figure 30). As before, the head cap was placed upside down to maintain a flat surface, which was leveled on the treatment couch prior to irradiation. An off-axis dose profile comparison was made in a plane located at 100 cm SAD at a

Figure 29. MapCHECK dose measurement device. 2D dose distributions are measured on a grid of 445 diode detectors.

depth of 3.2 cm (the depth of the film plane). The MapCHECK was setup with an additional 1.2 cm buildup of Plastic Water to create an effective depth of 3.2 cm buildup above the detector plane. Results of three MapCHECK irradiations (one measurement with the diode array aligned to the beam central axis and additional measurements set up with a 2.5 mm offset in x and a 2.5 mm offset in y) were merged to create a more dense array (2.5-mm point separation).

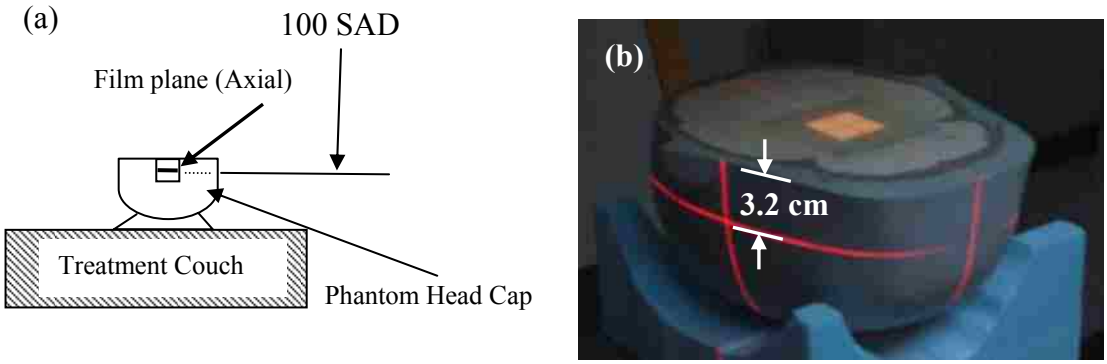

Figure 30. (a) Phantom setup schematic for perpendicular irradiation test. (b) Phantom setup image.

2.2.3 Measurement System Spatial Precision

A series of tests were performed to measure variation in the film position with respect to the phantom to estimate the positional uncertainty inherent in the film-phantom system.

Potential sources of error include (1) variability in film position on the rods and (2) block position within the head cap. By maintaining a consistent phantom setup over a series of measurements, the amount of this uncertainty can be estimated. Measurements were performed at a single gantry, couch, jaw and mMLC setting for each film block orientation (c.f. Figures 31 and 32), so that it could be assumed that the radiation beam did not vary over the course of measurements. The measurements occurred over a period of 4 hours, during which the laser

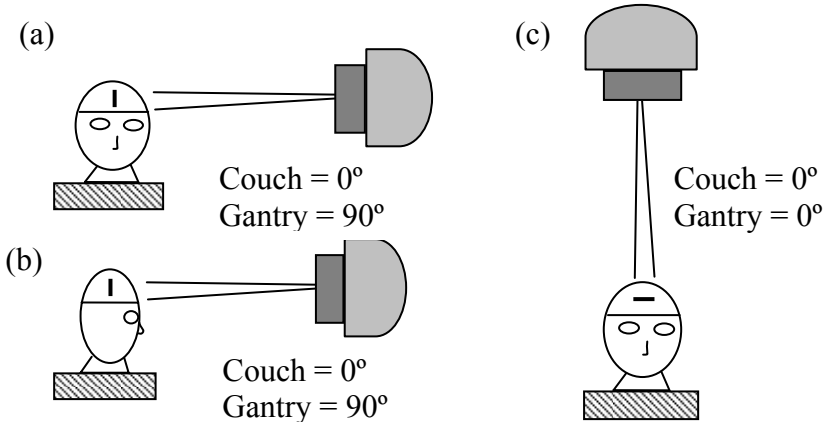

Figure 31. Precision Test Setup. Jaws and MLC set to 3 x 3 cm^2 for (a) sagittal, (b) coronal, and (c) axial irradiations.

position was assumed constant. The lasers were used for positioning by aligning crosshair marks on the phantom surface. This method is appropriate because the phantom is a rigid object and rigidly registered to the internal anatomy. Also the phantom surface can be marked using long lines along each visible laser line so that the same location can be found repeatedly with good precision (estimated to be 0.2 mm).

The mid-profile location based on common relative dose points (i.e. 50%) along radiation profiles provided a common positional measurement, and the variation in this location represented the distribution of error due to film positioning (mechanical) variability and film

registration. As manual laser positioning error ($\sigma_{laser\text{-}alignment}$) was included in the precision measurements ($\sigma_{measured}$), results provided a conservative estimate of the precision of this film phantom measurement system ($\sigma_{filmsystem}$), i.e.:

$$\sigma^2_{filmsystem} = \sigma^2_{measured} - \sigma^2_{laseralignment} \Rightarrow \sigma^2_{filmsystem} < \sigma^2_{measured} . \quad (4)$$

Five irradiations were performed for each film orientation (axial, sagittal, and coronal). Square radiation beams were delivered to the phantom perpendicular to the film plane with the Novalis Linac. The table was set to 180º and the gantry to 0 º or 90 º depending on the film orientation as illustrated in figure 30. Collimator jaws and the mMLC were both set to define 3 x 3 cm^2 field at isocenter. Exposures of 200 monitor units were delivered to each film, which were subsequently processed and digitized.

To analyze the results one film was set at the reference and all other films were registered to that film using the registration technique, previously discussed (section 2.1.7). This placed all film dose measurements in a common coordinate system. Dose for each film was normalized such that the dose on the central axis was 100%. Relative dose profiles were produced along the two lines perpendicular to and intersecting the central axis and perpendicular to the film edges.

Figure 32. View of gantry and phantom for precision test for sagittal film.

Position of the 50% isodose lines was found for each of the five profiles, and the standard deviation was determined for the midpoint of the profiles in both directions in each film plane. The process of registration and precision is illustrated in Figure 33. Hence, each film plane provided a precision measurement along the 2 principal axes.

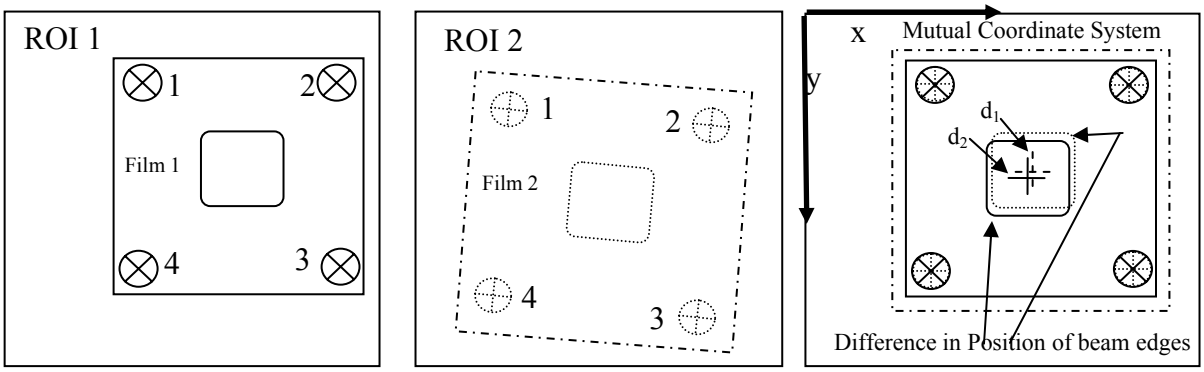

Figure 33. Film Registration for Precision test. Each film image was displayed within its own region of interest (ROI). Registration manipulates the second film image to align registration points 1-4. The distribution of error is established by measuring the standard deviation of the displacements of midpoints "d_1 and d_2" based on locations of 50% isodose lines on the mutual coordinate system.

2.3 Aim 3: Spatial Accuracy of Dose Delivery for ExacTrac IGRT

Intentionally misalign the phantom by known offsets from isocenter prior to treatment, then use the ExacTrac automatic image fusion procedure to align the phantom prior to delivering the planned treatment. Compare measured dose distributions with calculated dose distributions from the TPS to quantify spatial accuracy of dose delivery using ExacTrac IGRT.

• • •

In order to test the hypothesis, that the Novalis ExacTrac IGRT system can achieve positional accuracy of dose delivery to within 1 mm for initially misaligned patients, the film-phantom measurement system was used in a series of mock SRT treatments simulating misaligned patients. Each treatment began initialized with the phantom approximately aligned to isocenter by aligning marks on the phantom mask to the treatment room lasers, whereupon Infra-

Red tracking was used to translate the phantom to pre-determined misalignments (± 8 mm offsets along the X, Y and/or Z axes). The ExacTrac X-ray imaging system was then used to bring the patient back into alignment using the same process as used for patients, automatic 6D image fusion, prior to treatment delivery. This section details the methodology for patient, hence phantom treatments, i.e. CT scanning the phantom, planning the phantom dose distribution, aligning the phantom, and irradiating the phantom. Lastly, methods used for comparing measured with calculated (planned) dose distributions are discussed.

2.3.1 Phantom CT Scans

Three 3D CT scans, one for each film block orientation, were acquired using the large bore GE Discovery CT Scanner. Prior to each scan the phantom orientation was adjusted slightly such that the film planes were parallel with the CT image planes. This was accomplished using a tri-level platform to make fine adjustments to achieve the proper alignment, of the phantom in the CT bore. The block edges were visible in the scout image, which were compared to the onscreen axis delineating the CT image plane. Achieving adequate alignment sometimes required scanning the phantom multiple times until film plane remained flush with the imaging plane (i.e. throughout all slices). An image of the phantom prior to scanning and a close-up view of the tri-level platform used for alignment adjustments is shown in figure 34. The phantom scan parameters, in accordance with clinical SRT protocol, are shown in Table 2. Examples of the film plane alignment in each of the 3 scan orientations are shown in Figure 35. Following scanning each CT image series was exported to the BrainScan computer for treatment planning.

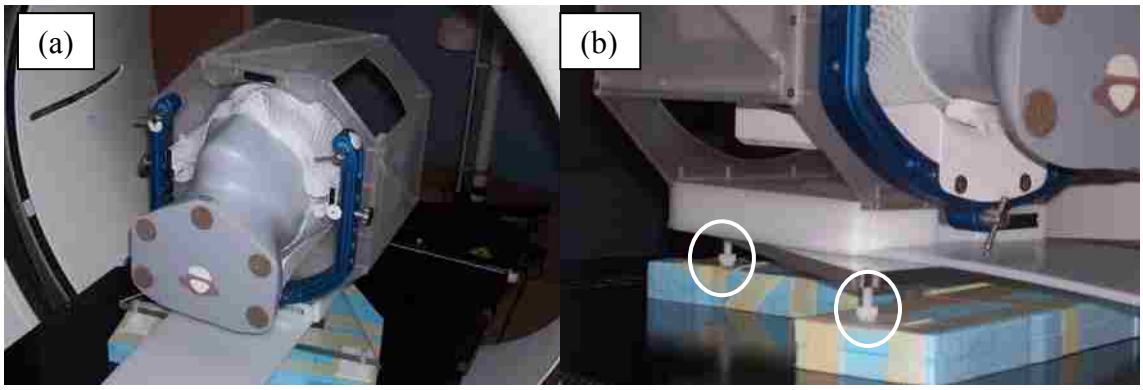

Figure 34. (a) Phantom positioned in CT bore. (b) tri-level platform: Screws (encircled) were adjusted to align film and CT planes.

Table 2. SRT Cranial Protocol, GE Discovery CT Scanner

Scan Type:	Axial
# Detector Rows	4
Slice Thickness	1.25mm
Bore diameter	80 cm
Field of view diameter	36 cm
Energy	140 kVp
Current	380 mA

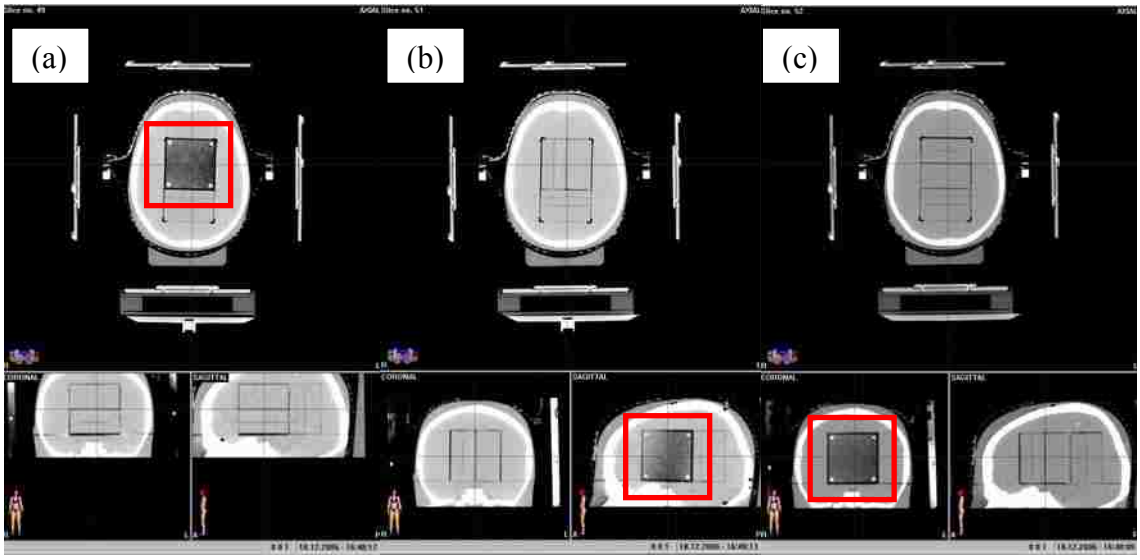

Figure 35. Phantom CT scans in BrainScan TPS for each film block orientation: (a) axial, (b) sagittal, and (c) coronal. The two film planes in the film block are visible of the small gap in phantom material. Note the film plane (red square) in each CT image series show relatively uniform grayscale, indicating their being properly aligned.

2.3.2 SRT Treatment Planning

A treatment plan was created in the Brainscan treatment planning system for each of the three block orientations. Identical 2 cm diameter by 2 cm height cylindrical PTVs were created at the center of the film block for each CT data set to simulate an approximately centrally located cranial lesion. Images of the drawn PTV are shown below in figure 36.

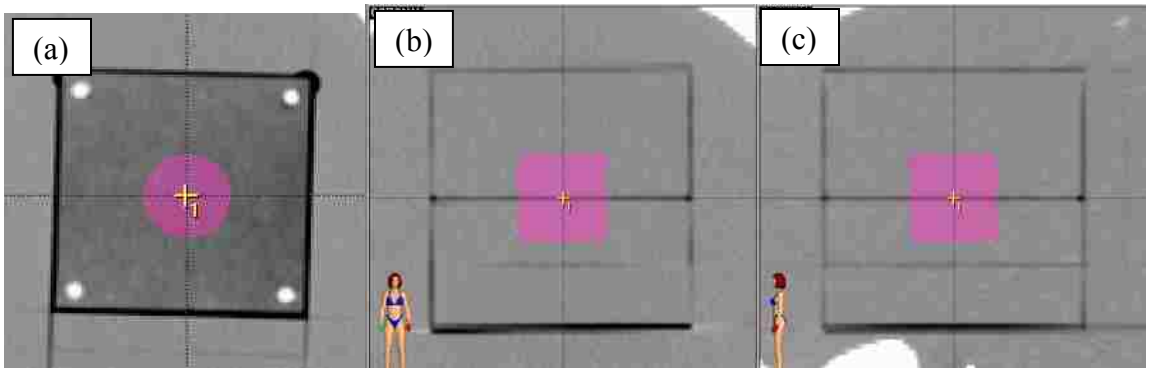

Figure 36. Cylindrical PTV views (2 cm diameter x 2 cm height) for axial CT data set. (a) Axial plane (contains film) (b) Coronal plane (c) Sagittal plane

Identical conformal beam arrangements were created in the BrainScan treatment planning computer to treat each PTV to 203 cGy at isocenter. Each plan consisted of 7 equally spaced, coplanar, axial beams, with gantry angles and monitor units delivered shown in Table 3. Monitor units vary because of the varying isocenter depth in the phantom with each beam. There was one AP beam and six oblique beams space 51.4º, spaced so as to minimize effects from cross-firing beams. Each beam had a collimator angle of 90° and independent jaws set to 2.8 x 2.8 cm^2 (size at isocenter). A single mMLC leaf arrangement was used for all beams describing a 2.4 by 2.4 cm^2 at isocenter. An isometric visualization of the treatment beams is shown in figure 37.

BrainScan dose calculation used an adaptive gird size for dose calculation, i.e. the dose grid is dependent on the dose gradient of regions surrounding a particular dose point. Whether to compute a new dose point or to interpolate between nearby points is determined by the adaptive

grid algorithm and is dependent upon the ability to approximately describe nearby dose points using linear functions (BrainScan Software Guide, Version 5.2x). Therefore, no specific parameters for dose grid size were selected.

The plan was then exported to ExacTrac. This step gives the ExacTrac console computer, which is networked with the BrainScan treatment planning computer, access to the treatment plan of the patient selected, including all data required for DRR based image guidance.

Table 3. Treatment Plan Beam Arrangement. All beams have a couch angle of 0º and field size of 2.4 cm x 2.4 cm created by the mMLC

Beam Number	Gantry Angle °	Monitor Units
1	204	51
2	255	42
3	306	42
4	0	45
5	51	41
6	102	41
7	153	47

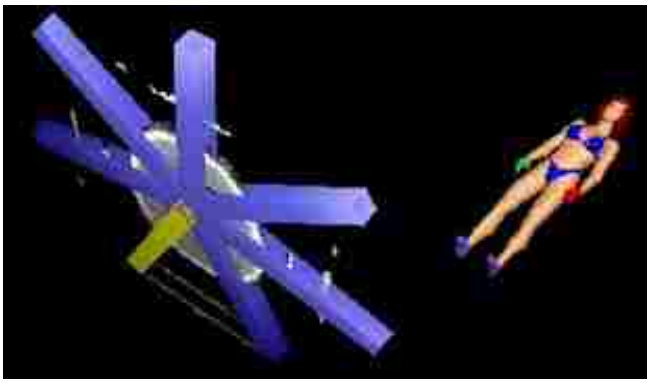

Figure 37. Rotational Conformal Beam Arrangement. Beams are shown intersecting an axial slice from an oblique perspective.

2.3.3 Initial Phantom Setup

In the darkroom, prior to each film measurement, a cut unexposed EDR2 film was placed inside the film block, which was inserted inside the phantom head cap. The phantom was first positioned on the Novalis BrainLAB treatment couch and enclosed within its thermoplastic

immobilization mask. Initial setup of the phantom was accomplished by visually aligning external laser beams to known locations on the phantom surface, roughly aligning the planned isocenter to machine isocenter. Four Infra-Red reflective markers were placed on the phantom immobilization mask surface and stereotactic U-frame, taking care to avoid ambiguities in marker placement.

The appropriate ExacTrac alignment plan (i.e. axial, sagittal or coronal, depending on block orientation) was then loaded at the ExacTrac console. On the ExacTrac console X-ray correction was selected in order to establish an initial set of IR marker positions to track the phantom movements. Following the on-screen instructions 2 orthogonal X-rays images were taken. Then Image Fusion ROIs were defined, and Automatic 6D Image Fusion was performed. The ROI was selected in the X-Ray image based on the image data to be used for image fusion. By contouring the ROI in the X-ray image the user can emphasize a particular part of the bony anatomy in the fusion or remove an area from the fusion calculation that might negatively affect the results. In this study the rind of the skull was excluded due to its rotational symmetry, leaving strong edges in the bony orbital area of the skull as the primary region of the image used for fusion (c.f. Figure 38).

This results in numerical values of the initial setup error in 6 dimensions (x, y, z, translational axes and tilt, roll and couch rotational axes) (c.f. Figure 39). Running Image Fusion on this initial setup allows the IR tracking system to be used as a feedback to ensure that the both the offsets and realignments were made with high accuracy.

2.3.4 Intentional Misalignments

The onscreen readout shows the amount of current misalignment in 6 dimensions. To move the phantom to an intentional misaligned position, the phantom was shifted by manually

moving the couch position. Misalignment distance was viewed by noting the IR positioning readout on the ExacTrac display, which changes in real time with changes in IR marker locations. In the normal treatment case the patient is moved according to the suggested shifts for correct setup; however, for testing purposes shifts were imposed by manually moving the treatment couch to intentional misalignments, as specified by a given sample space point for each treatment (section 2.3.5). Screenshots of the ExacTrac computer using Infra-Red positioning are shown in figures 40 and 41.

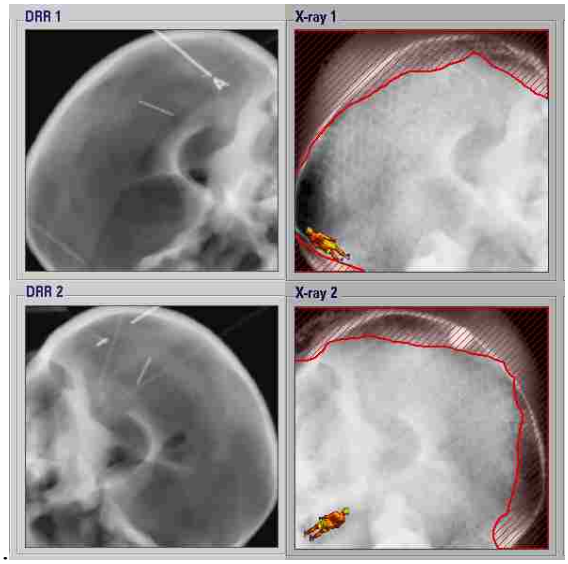

Figure 38. ExacTrac X-Ray Correction Setup. ROIs (shown in red) are contoured leaving the bony orbit area to the used for fusion.

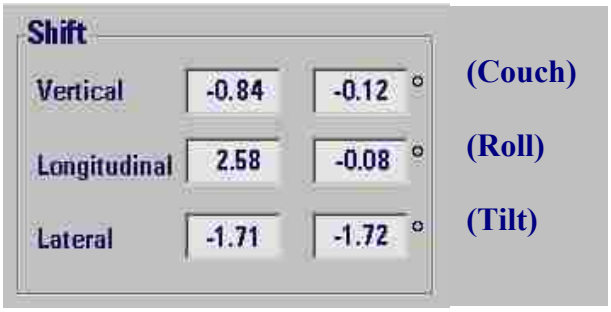

Figure 39. ExacTrac Shift Report. Each of 6 dimensions can be corrected by the shifts shown.

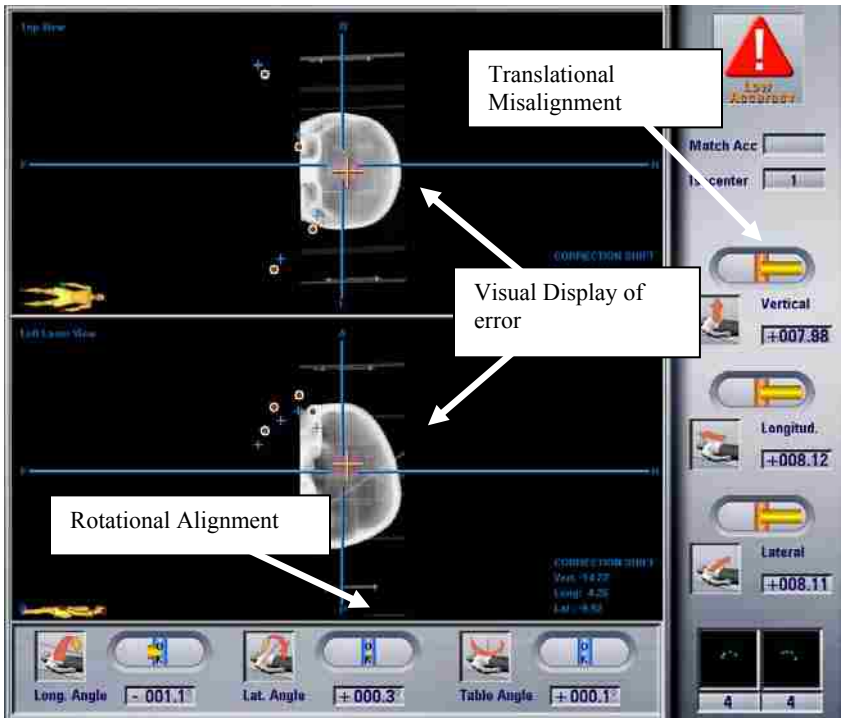

Figure 40. ExacTrac screenshot for misaligned phantom. The imposed shift is (8 mm, 8mm, 8mm) in vertical, longitudinal and lateral directions.

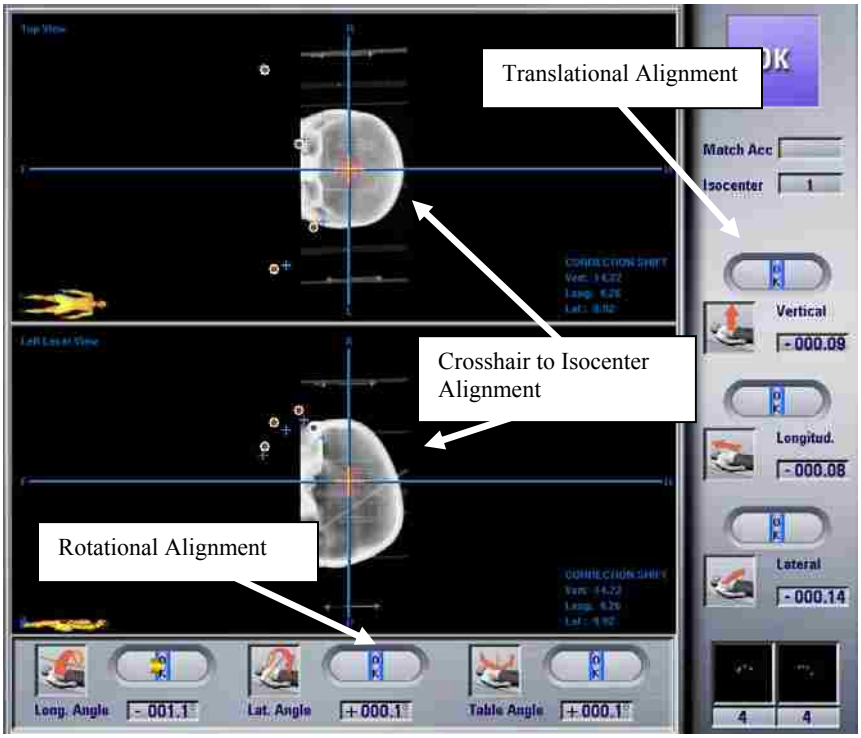

Figure 41. ExacTrac screenshot for aligned phantom, after ExacTrac X-ray is applied.

2.3.5 Sample Space

The extent of intentional misalignments was 8 mm translations in the longitudinal, vertical and lateral directions, which encases the great majority of initial misalignments seen at MBPCC for cranial cases. There were no intentional rotational misalignments, although small rotational misalignments occurred at random. Treatments were delivered, and dose was measured for initial misalignments corresponding to the center of cube (i.e no shift) and the corners of the cube (c.f. Table 4 and Figure 42). An example of a corner point had a misalignment of (8 mm, 8 mm, 8mm) in vertical, lateral, and longitudinal axes, respectively. The reason for varying the offset position was to determine if there were any locational dependence on image guided treatment outcome.

Table 4. Sample Space Points (distance from center in mm)

Point	Vertical (Anterior-Posterior)	Longitudinal (Inferior-Superior)	Lateral (Right-Left)
0	0	0	0
1	-8	8	8
2	8	-8	8
3	-8	-8	8
4	8	8	8
5	8	8	-8
6	-8	-8	-8
7	8	-8	-8
8	-8	8	-8

Four sets of measurements were taken on four separate dates (12/3/06, 1/9/07, 1/24/07 and 2/9/07). For each set, measurements were taken with the phantom's initial misalignment set to various offset positions according to predetermined sample space point coordinates. The offset points used in each measurement set were chosen on the following basis: Initially, the

goal was to test each sample point at least once with the film block in each of the 3 film plane orientations. During the first set of measurements, each point (0-8) was tested; however, 3 offset points (3,4, and 5) were not analyzed due to a treatment delivery error and had to be removed from the data set. The second set of measurements repeated those measurements. These first 2 measurement sets (measurement sets 1 and 2) were based on a fusion acceptance criteria

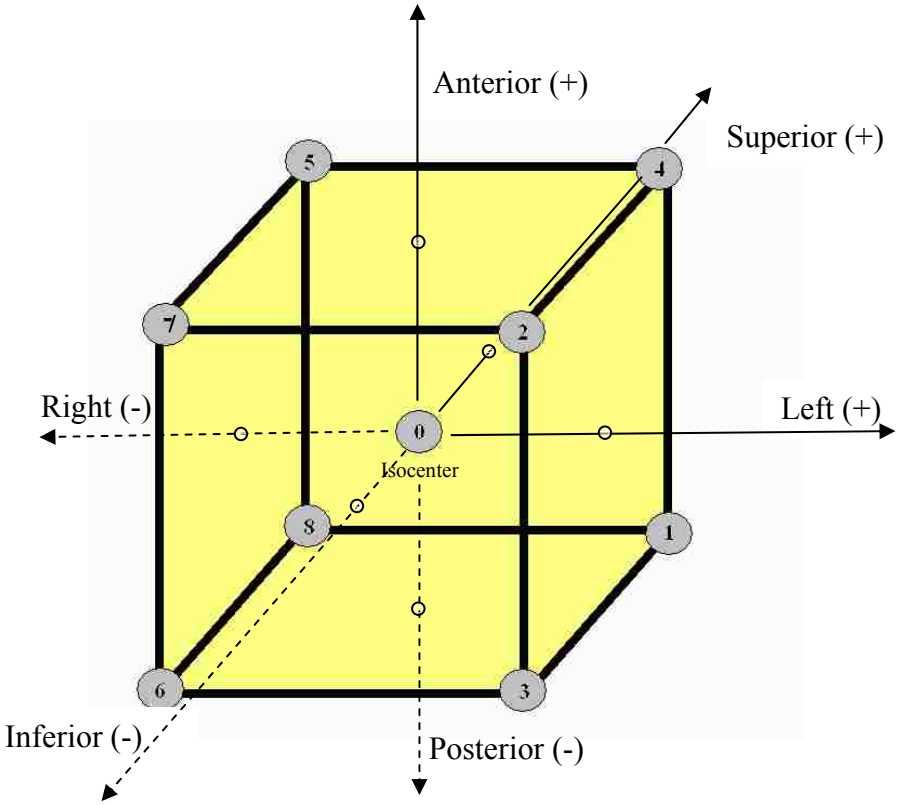

Figure 42. Representation of Sample Space points. Isocenter is represented by point number 0.

(ExacTrac accuracy required to treat the phantom, as reported using automatic image fusion) of 1mm and 1º for all 6 degrees of freedom. For the next two sets (measurement sets 3 and 4) an arbitrary subset of offset points were chosen, and treatments were made using an acceptance criteria of 0.4 mm and 0.4º. The reason for varying the acceptance criteria was to see whether

the resulting measurements of accuracy of the delivered dose distribution correlated with the acceptance criteria (i.e does a more stringent alignment requirement result in a better treatment). Table 5 summarizes the measurement points and acceptance criteria for the 4 measurement sets.

Table 5. Measurement set acceptance criteria, offsets and number of treatments (N) performed at each sample space point. (N = 3 generally implies 1 axial, 1 sagittal, and 1 coronal film treatment.)

Measurement Set 1 12/3/06			**Measurement Set 2 1/9.07**			**Measurement Set 3 1/24/07**			**Measurement Set 4 2/9/07**		
Sample Space Point	**Offset Coordinates (mm)**	**N**	**Sample Space Point**	**Offset Coordinates (mm)**	**N**	**Sample Space Point**	**Offset Coordinates (mm)**	**N**	**Sample Space Point**	**Offset Coordinates (mm)**	**N**
0	(0,0,0)	3	3	(-8,-8,8)	3	0	(0,0,0)	2	0	(0,0,0)	3
1	(-8,8,8)	3	4	(8,8,8)	3	2	(8,-8,8)	2	3	(-8,-8,8)	3
2	(8,-8,8)	3	5	(8,8,-8)	3	3	(-8,-8,8)	3	5	(8,8,-8)	3
6	(-8,-8,-8)	3				4	(8,8,8)	3			
7	(8,-8,-8)	3				5	(8,8,-8)	3			
8	(-8,8,-8)	3									
Acceptance Criteria 1 mm / 1°						Acceptance Criteria 0.4 mm / 0.4°					

2.3.6 ExacTrac X-ray Image Fusion Correction

Following intentional misalignments the patient plan was closed and reopened, as if the patient had just been setup. X-ray correction was again selected, establishing the new initial IR coordinates, and 2 orthogonal X-rays are taken. Then ROIs were defined, and Automatic 6D Image fusion was performed. Next, the suggested shifts were documented, and all suggested shifts and rotations were made bringing the phantom as close to perfect setup as possible by moving all ExacTrac IR readouts to as close as practical to 0.00 in all dimension. For optimal results the following correction shift order was used. First, major translations were corrected to bring the setup to approximately within 1 mm by manually moving the treatment couch, then the rotation angles were adjusted by adjusting the couch mount rotation knobs (about the longitudinal and lateral axes) and table angle, using the IR readout for positional feedback.

Finally the translations were fine tuned, necessary because of the interplay between angular adjustment and translational misalignment.

X-ray verification was selected as is done clinically, and another pair of orthogonal X-rays were taken to confirm alignment. Treatment commenced as long as the reported translational and rotational misalignments were within the specified acceptance criteria, either (1 mm, 1 º) or (0.4 mm, 0.4º) depending on the measurement set. One reason for testing on various dates was to determine the extent of drift in the ExacTrac calibration over time. The 7-beam treatment was delivered taking care not to bump the treatment couch or disturb the phantom setup. Following treatment the phantom was removed from the immobilization mask and taken into the dark room. There the film was removed and stored in the dark room for subsequent processing. This image guidance–misalignment-treatment procedure was repeated for each measurement point for each of the 3 film plane orientations.

2.3.7 Analysis Techniques

Films were digitized and calibrated to dose using a Vidar Dosimetry Pro 16 bit scanner at 0.089 mm resolution and RIT v4.4 film dosimetry software as explained previously. For comparison with the measured dose distributions delivered to the phantom, the corresponding dose export images from BrainScan were opened in the RIT system as the target image dose map. These films were registered as outlined in section 2.1.7, and isodose plots were generated for comparison (c.f. Figure 43a). To obtain a more quantitative measure of shifts between the planned and delivered dose distributions, film profiles along the vertical and horizontal axes were generated (c.f. Figure 43b). Errors were specified as follows: Positional alignment error (Δc) was determined as the displacement between the midpoint (center) locations of the 70%

dose contours (on each side of the profile) on the delivered (film) and planned dose distributions, i.e.

$$\Delta c = {}^{1}/_{2}\,(70\%_{film2} - 70\%_{film\ 1}) - {}^{1}/_{2}\,(70\%_{TPS2} - 70\%_{TPS1}), \quad (5)$$

where 70% refers to the position of the 70% dose contour and subscripts 1 and 2 refer to the posterior, right, and anterior) dose falloff regions and the (anterior, left, and superior) dose falloff regions respectively. The 70% dose level was selected because it is close to the location of steepest dose gradient. This value is a measure of the alignment error in a particular measurement.

However, comparison of shifts in 80% dose contours has greater clinical relevance to the radiation oncologist on the basis of clinical decisions. 80% isodose shifts were defined as follows:

$$\Delta 80_1 = 80_{TPS,\,1} - 80_{film,1} \quad (6a)$$

$$\Delta 80_2 = 80_{film,\,2} - 80_{TPS,\,2} \quad (6b)$$

where subscripts 1 and 2 indicate the negative and positive axis being measured (e.g. $\Delta 80_1$ corresponds to the 80% error on the posterior (negative) axis along a Posterior –Anterior profile), therefore:

$$\{\Delta 80_P, \Delta 80_R, \Delta 80_I\} \in \Delta 80_1 \quad (7a)$$

$$\{\Delta 80_A, \Delta 80_L, \Delta 80_S\} \in \Delta\, 80_2\,, \quad (7b)$$

where subscripts P, A, R, L, I and S denote posterior, anterior, right, left, inferior and superior respectively. This definition designates positive values as 80% isodose line coverage of the planned 80% isodose contour. Conversely a negative value indicates a measured under-dose at planned 80 %, which can be clinically important.

The displacement between the delivered (measured) 80% and the planned (calculated) 80% isodose lines (Δ80) was documented for each film result. Also the displacement between the midpoints of the 70 % isodose levels (Δ 70c) was also determined as a measure of alignment error.

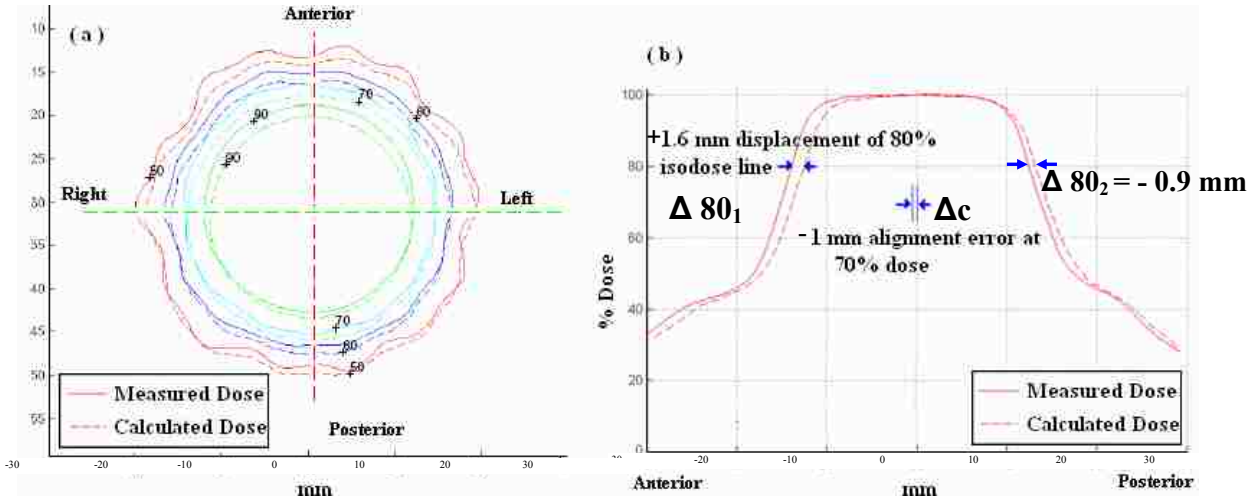

Figure 43. (a) Isodose comparison between TPS and film. (b) AP Profile showing error definition.

2.3.8 Discussion of Errors

Differences between the measured and calculated dose distributions, could be due to of a number of factors.

- Automatic Image Fusion Result: There is a limit to the image fusion ability to perfectly align the DRRs and X-ray images. One limiting factor is the CT voxel dimensions, in this case (0.703 x 0.703 x 1.25 mm^3). The choice of the ROI selected for image fusion can also affect the fusion result.
- Laser – Radiation isocenter coincidence: A perfect ExacTrac calibration will ideally place the patient at laser isocenter upon X-ray correction. Laser isocenter is set as the best approximation of the center point of the virtual sphere created by the central ray of the radiation

beam delivered under varying table and gantry angles. This sphere is created as the result of mechanical variability of the linac, e.g. gantry sag, gantry wobble, and table or collimator rotational wobble (sometimes referred to as "walkout"). Additionally, wall-mounted lasers are subject to drift over time. In such a case the lasers do not intersect at the true center of this sphere, and the ExacTrac system will be calibrated to the incorrect isocenter position; therefore, the patient (or phantom) will be set up with a small amount of positional error with respect to the delivered radiation. Furthermore the treatment parameters for a particular treatment can create a situation for additional error if the displacement between laser and radiation isocenter is in the same direction for each of the gantry and table angles chosen for a particular treatment. Typically a treatment will be comprised of multiple couch, gantry and collimator angles, which would offset the degree of this type of error.

- ExacTrac Calibration: The previous assumes that the ExacTrac calibration isocenter phantom is perfectly aligned to room lasers upon calibration. Slight deviations are possible which would set the IR isocenter with a positional misalignment. This misalignment would then result in incorrect placement of the X-ray phantom and therefore incorrect determination of X-ray projection parameters which will affect the image fusion results. This could potentially contribute to a translational error in dose delivery.
- Error in the TPS dose calculation will obviously affect comparisons with measured dose distributions. This will be more prevalent with $\Delta 80_1$ and $\Delta 80_2$ given the symmetry of the dose distribution used in this study. Values of Δc should not be significantly influenced by the calculation of beam edges – however $\Delta 80_1$ and $\Delta 80_2$ are directly related to these calculations. The beam model for this study was different than that used clinically, i.e. during the course of this study, more accurate TPS parameters for the mMLC beams were determined.. Details of these changes are found in Appendix 2.

Chapter 3 Results and Discussion

3.1 Aim 1: Film-Phantom Measurement System

The film phantom measurement system as described in section 2.1 was developed for measuring dose distributions from image guided radiation therapy treatments in the cranium. Its film-measured dose distributions were registered to and compared with dose distributions from the BrainLAB treatment planning system. The final version of the film phantom system was composed of the following components, features and techniques:

- CIRS anthropomorphic head phantom with internal film cassette
- Custom 3-piece internal film cassette with modified rods to improve indexing
- Custom aluminum template for cutting in the darkroom, 6.35 cm x 6.35 cm EDR2 film sections having 4 indexing holes
- Utilization of ready-pack container to shield film from Cerenkov light produced in the phantom
- Film templates for mounting film during film processing and scanning (digitization)
- Film dose calibration technique using a Varian 21 EX 6 MV beam and MLC
- RIT film software analysis techniques for film and BrainScan dose import
- Point-based registration method aligning the center of fiducial rods (TPS) and film holes in RIT (film image)
- Custom software template to assist in localizing the center of fiducial rods in BrainScan TPS

These devices and procedures provided a means of measuring dose delivery, which are useful for evaluation of the spatial accuracy of IGRT delivered dose distributions.

3.2 Aim 2: Film-Phantom Measurement System Accuracy and Precision

Results of measuring the accuracy and precision of film dosimetry using the film phantom measurement system are contained in the following subsections.

3.2.1 Dose Accuracy of Film-Measured Depth Dose

Evaluation of the film dosimetry system for the parallel irradiation geometry (c.f. Figure 27) utilized measured dose values on film (N=3) that corresponded to a portion of the Novalis 6MV depth-dose curve where the incident radiation beam intersected the film section. The results shown in Figure 44 compare the measured depth-dose curves on film to ion chamber point dose measurements made along the central axis.

Film dose values agree to within 2% of ion chamber values (considered "gold standard"), giving confidence that film accuracy is within 2% for measurement of IGRT treatment deliveries. Note only three measurement points coincided within the film measured section. The remaining ion-chamber depth-dose measurements were useful in comparing both measurements to the BrainScan calculated depth dose. This has an impact on the calculated dose distribution. Details on the agreement between calculation and measurement can be found in Appendix 1. Film data at a few mm from the outer edges of the film is omitted as it was not used and was more susceptible to artifacts from the film cutting process and developing.

The significance of errors are dependent upon the dose distribution being analyzed, specifically the dose gradient at a given location on film. For testing of the hypothesis, the measured depth-dose error seen here will result in virtually no positional isodose error in the steep dose gradient regions, which are used to define the alignment errors.

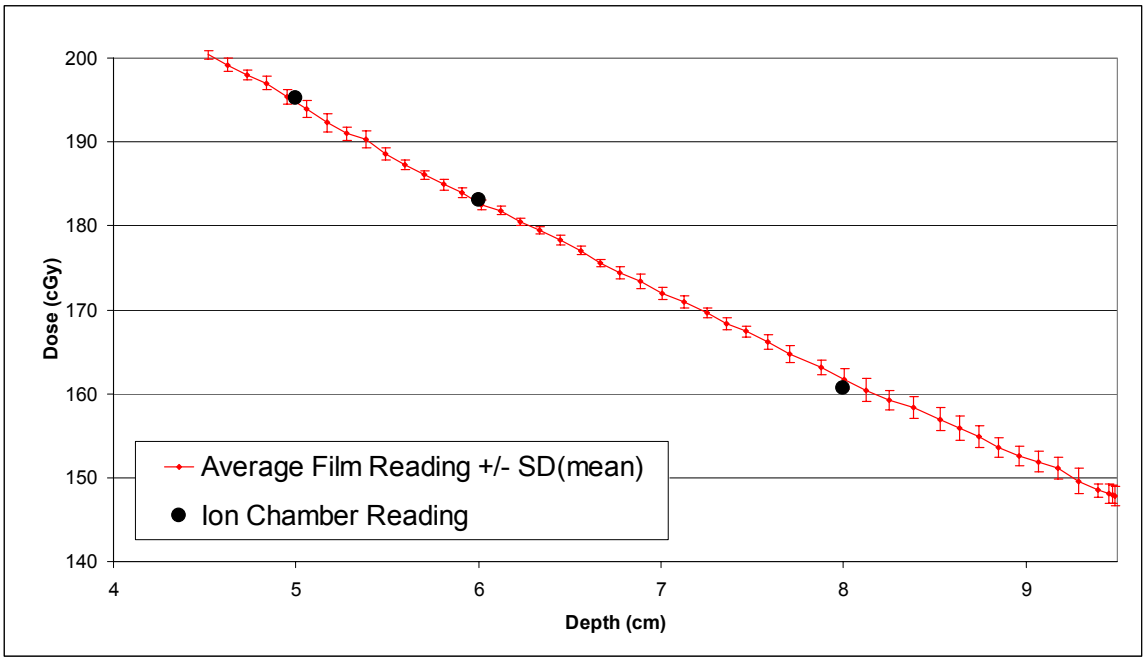

Figure 44. Film depth-dose measurements compared to corresponding ion chamber measurements. Film results have been averaged and sampled. Error bars indicate the standard deviation of the mean.

3.2.2 Accuracy of Film-Measured Off-Axis Dose

Results of evaluation of the spatial accuracy of film dosimetry measurements perpendicular to the beam direction are shown in Figures 45 and 46. Measured film profiles and MapCHECK diode measurements were taken across both major axes. Figure 45 shows the profile in the X direction, which corresponds to the direction of mMLC leaf motion. Figure 46 shows the dose profile across the tongue and groove edge of the mMLC leaf.

Points from the MapCHECK diode array agree with the film profile along the off-axis dose falloff within 0.2 mm in the high dose gradient region (10% - 90%), and within 2% in the uniform dose regions. This established that the off –axis dose was accurately measured by the film phantom system throughout the penumbra region (0.2mm) in the same measurement conditions used to test the hypothesis (i.e. film held inside the film cassette, housed in the

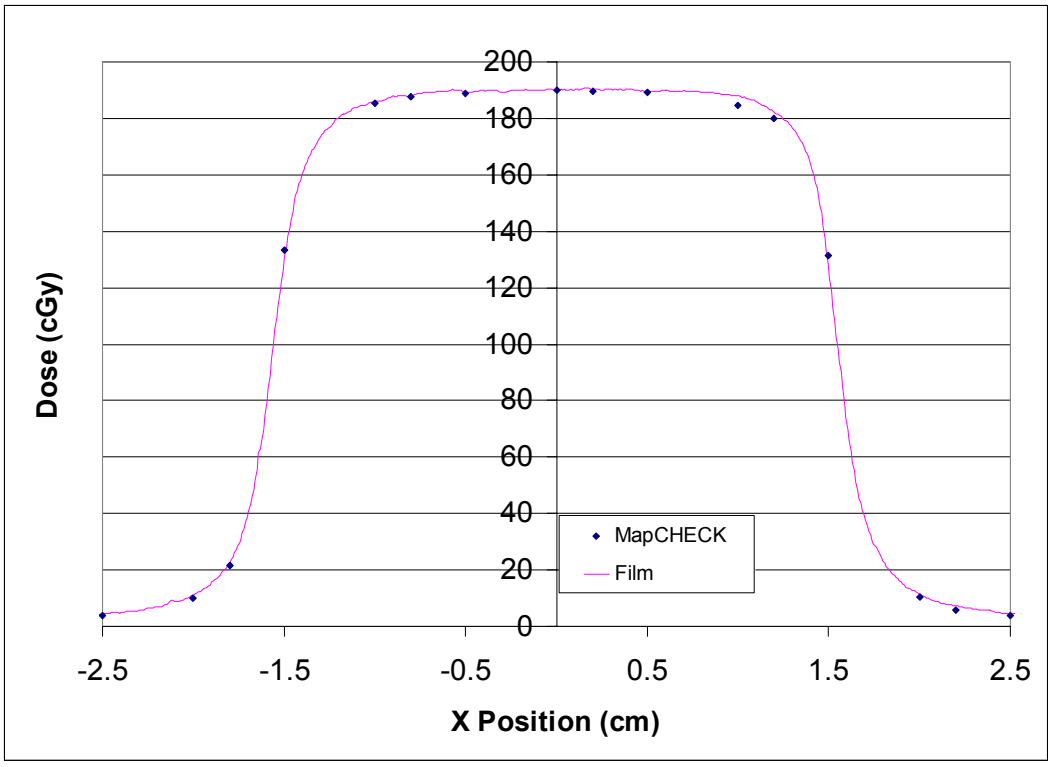

Figure 45. Perpendicular film verification of off-axis profiles in the mMLC leaf motion direction.. Film Measurements are compared with MapCHECK diode measurements. SAD = 100 cm, d/deff = 3.2 cm, 3 cm x 3 cm field size.

phantom, and calibrated to dose as described). Radiation was delivered to both phantom setups with SAD = 100 cm and d = 3.2 cm. Effectively the shape of the fall off is preserved. The 0.2 mm error along the edges is likely partly due to the result of beam divergence due to a slightly different source to measurement distance between the test films and the MapCHECK diode array. Absolute dose at the central axis for both measurement techniques agree within 0.5%.

Note the width of each profile (i.e. FWHM) is not the same in both directions with respect to the mMLC leaves despite a planned square filed of 3 x 3cm^2. This would have an impact on film measurements in comparisons to beam edges generated in the treatment planning system; however, the beam model was adjusted to reflect this measured asymmetry, as described in Appendix 2.

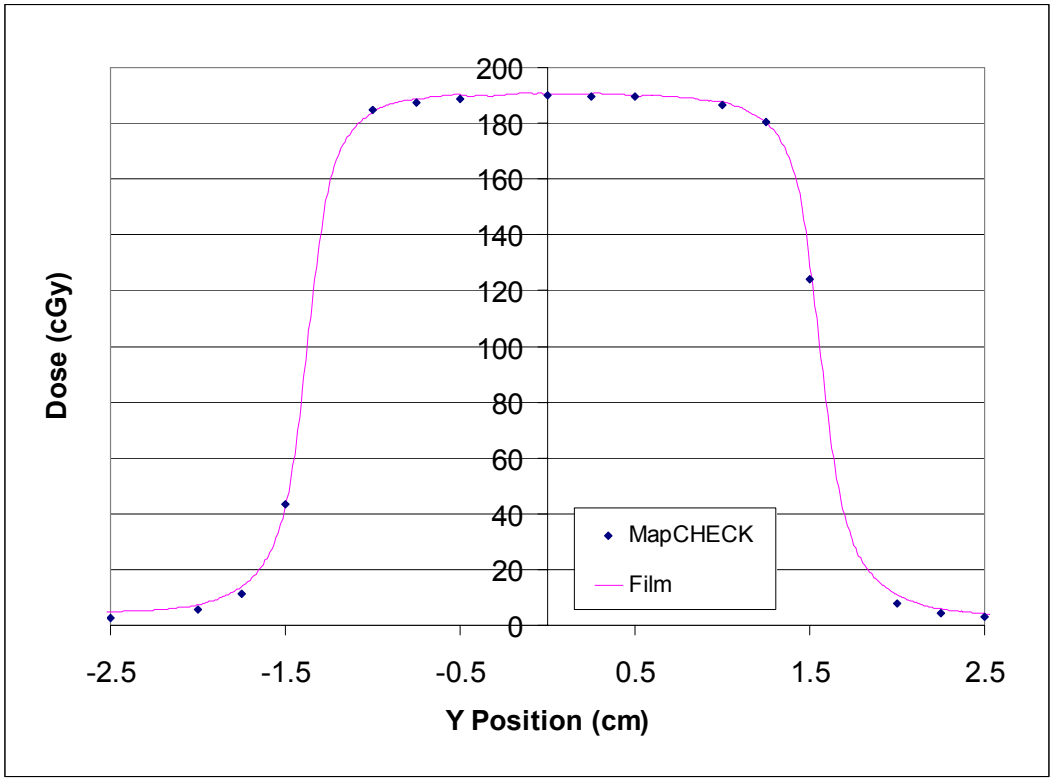

Figure 46. Perpendicular film verification of off-axis profiles in the tongue and groove edge direction. Film measurement are compared with MapCHECK diode measurements. SAD = 100 cm, d/deff = 3.2 cm, 3 cm x 3 cm field size.

3.2.3 Measurement System Spatial Precision

Measurement of the spatial precision of the film measured dose distributions followed the procedures in section 2.2.3. The precision was determined by measuring the statistical spread (i.e. standard deviation) of the mid-profile positions (based on midpoint of 50% OARs), results being shown in Table 6.

Table 6. Results of Film Precision Test: Measure of distribution (95%) of mid-profile (2σ) location for repeated measurements in each film plane in the same setup. Each film plane contained 2 measurement axes.

2σ (mm): 95% Confidence Limits			
	Posterior - Anterior	Right – Left	Inferior - Superior
Axial	0.23	0.25	
Sagittal	0.32		0.21
Coronal		0.15	0.21

This variation, expressed as 2σ estimates the 95% confidence limit of the positional uncertainty for each film measurement. All values are within 0.32 mm, and it is reasonable to suggest that the true value of uncertainty is actually lower, based on the fact that the phantom was setup manually according to the lasers for the irradiation used to determine 2σ, i.e. error associated with manual alignment of the phantom to the lasers (as opposed to using image guidance) is included in this uncertainty estimate. The uncertainty present in each measurement for testing the hypothesis included the "true" positional uncertainty ($2\sigma < 0.32$mm), of which film registration uncertainty, and dosimetric uncertainty were included; however the uncertainty of manual laser positioning was not included.

The reported Q value by RIT (defined in section 2.1.7.3) was cataloged for each measurement (registration) in the set of measurements of the precision test, and these results have a standard deviation ($2\sigma_Q$) of 0.01 mm. This serves an indication of the quality of the registration point choices in RIT and the consistency of the film preparation technique for a given set of measurements. Therefore in order to achieve the stated precision as quoted above (within 0.321 mm) the registration standard deviation of error, σ_Q, statistics for measurement films used for testing the hypothesis must be less than the that specified, i.e. 0.01 mm. This parameter was used as a quality assurance check on subsequent measurements.

Table 10 lists standard deviation ($2\sigma_Q$) for RIT registrations in each measurement set and for all treatments combined. In comparing the ($2\sigma_Q$) in all result films (0.072 mm) to ($2\sigma_Q$) measured from the precision test (0.092 mm), the result film value is less than that of the precision test indicating that the positional uncertainty in measurement is within 0.321 mm.

Table 7. Film Registration Quality ($2\sigma_Q$). The average listed is the mean Q value reported for a set of measurements. Also reported is spread (95%) of Q values in a given set of measurements about the mean.

Measurement Set/Date	Average (mm)	$2\sigma_Q$ (mm)
1 (12/3)	.096	0.066
2 (1/9)	0.116	0.092
3 (1/24)	0.093	0.072
4 (2/9)	0.107	0.067
ALL	**0.101**	**0.072**

3.3 Aim 3: Spatial Accuracy of Dose Delivery for ExacTrac IGRT

There were a total of four measurement sessions (dates). For each session the delivered dose distribution in each principal plane was measured after ExacTrac corrections were made following intentional phantom misalignments according to all 9 sample space points. Subsequently, the displacements between the film measured 80% and the calculated 80% isodose lines ($\Delta 80_1$ and $\Delta 80_2$) for both orthogonal profiles were documented for each film result (subscripts 1 and 2 referring to the ascending [posterior, right, inferior] and descending [anterior, left, superior] portions of each relative dose profile respectively). Also, the displacements between the midpoints (centers) of the 70% isodose levels for both orthogonal profiles (Δc) were also determined as a measure of alignment error. As an example, results in each measurement plane from a single measurement session (#3), for a single sample space point (#5), are shown in Figure 47. Point #5 refers to an intentional offset of +8 mm, +8 mm and -8 mm in the Posterior - Anterior, Inferior - Superior, and Right - Left directions respectively.

Corresponding profiles are shown side by side in Figure 47, and as can be easily seen, there are errors indicated a shift in delivered dose in the Anterior and Superior directions. As seen throughout the entire data set, errors in a particular direction show up in both profiles along a given direction when measured using 2 different film block orientations containing that direction. This indicates that errors are "real" in that it is not due to a systematic measurement error. The complete set of treatment results are shown in Table 8.

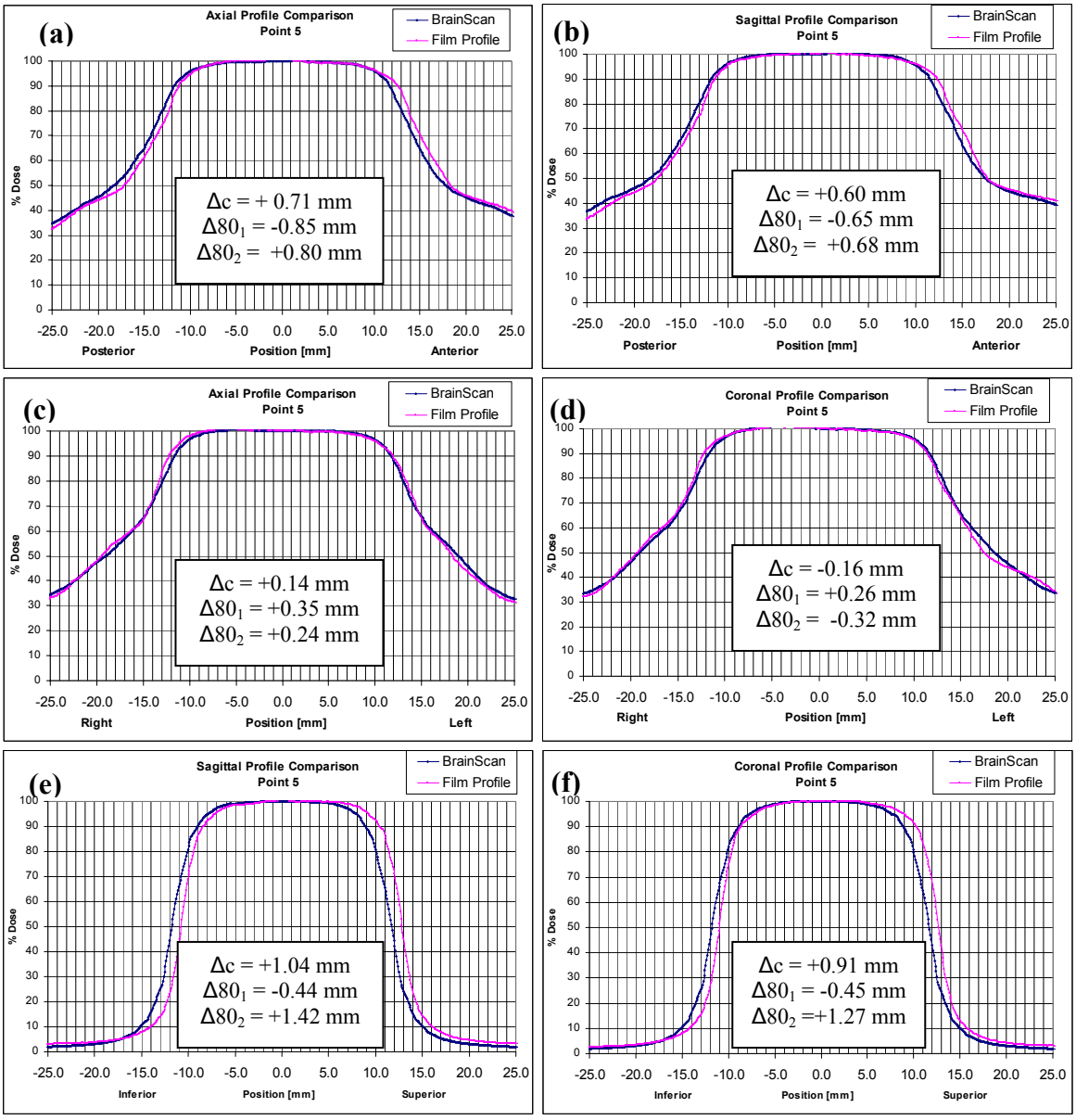

Figure 47. Relative Dose Profile Comparisons. BrainSCAN dose calculation versus measured (delivered) dose distribution. Results are shown for the initial misalignment point 5 (8,8,-8) of measurement set 2 (1/9/07). (a) Axial Plane, Posterior-Anterior Axis (b) Sagittal Plane, Posterior – Anterior Axis (c) Axial Plane, Right – Left (d) Coronal Plane , Right –Left (e) Sagittal Plane, Inferior – Superior (f) Coronal Plane, Inferior – Superior. Inserts show the measured errors (Δc, $\Delta 80_1$, $\Delta 80_2$) for each profile comparison

Table 8. Complete Data Set (Distances in mm).

Measurement Set 1		AXIAL FILM PLANE						SAGITTAL FILM PLANE						CORONAL FILM PLANE					
		Right - Left			Posterior - Anterior			Posterior - Anterior			Inferior - Superior			Inferior - Superior			Right - Left		
Sample Space Point	Offset Coordinates	$\Delta 80_1$	$\Delta 80_2$	Δc	$\Delta 80_1$	$\Delta 80_2$	Δc	$\Delta 80_1$	$\Delta 80_2$	Δc	$\Delta 80_1$	$\Delta 80_2$	Δc	$\Delta 80_1$	$\Delta 80_2$	Δc	$\Delta 80_1$	$\Delta 80_2$	Δc
0	(0,0,0)	0.91	-0.56	-0.62	-0.43	1.04	0.67	-0.35	0.95	0.69	-0.64	1.42	0.99	0.37	0.59	0.14	0.26	0.06	-0.01
1	(-8,8,8)	0.72	-0.48	-0.63	-0.58	0.82	0.64	-0.07	0.51	0.24	-0.01	0.79	0.38	0.48	0.68	0.13	-0.20	0.43	0.51
2	(8,-8,8)	0.48	-0.25	-0.33	-0.02	0.40	0.10	-0.05	0.85	0.56	-0.08	1.01	0.59	0.71	0.37	-0.14	0.45	-0.01	-0.29
6	(-8,-8,-8)	0.76	-0.54	-0.66	0.34	0.30	0.11	-0.34	0.71	0.55	0.00	0.99	0.54	0.71	0.19	-0.25	0.39	-0.15	-0.18
7	(8,-8,-8)	0.90	-0.70	-0.86	-0.07	0.06	-0.06	-0.09	0.26	0.12	0.09	0.93	0.39	0.49	0.26	-0.16	0.01	0.15	0.16
8	(-8,8,-8)	0.46	-0.41	-0.36	0.12	0.01	-0.12	0.15	-0.03	-0.02	-0.10	0.86	0.52	0.38	0.69	0.11	-0.04	0.25	0.16

Measurement Set 2		AXIAL FILM PLANE						SAGITTAL FILM PLANE						CORONAL FILM PLANE					
		Right - Left			Posterior - Anterior			Posterior - Anterior			Inferior - Superior			Inferior - Superior			Right - Left		
Sample Space Point	Offset Coordinates	$\Delta 80_1$	$\Delta 80_2$	Δc	$\Delta 80_1$	$\Delta 80_2$	Δc	$\Delta 80_1$	$\Delta 80_2$	Δc	$\Delta 80_1$	$\Delta 80_2$	Δc	$\Delta 80_1$	$\Delta 80_2$	Δc	$\Delta 80_1$	$\Delta 80_2$	Δc
3	(-8,-8,8)	0.21	0.22	0.02	-1.20	1.41	1.39	-0.61	0.77	0.82	-0.42	1.18	0.82	0.00	0.81	0.43	-0.35	0.50	0.62
4	(8,8,8)	0.29	-0.28	-0.12	-0.79	0.81	0.79	-0.94	1.02	0.93	-0.76	1.65	1.26	0.08	0.66	0.33	1.02	-0.59	-0.93
5	(8,8,-8)	0.35	0.24	0.14	-0.85	0.80	0.71	-0.65	0.68	0.60	-0.44	1.42	1.04	-0.45	1.27	0.91	0.26	-0.32	-0.16

Measurement Set 3		AXIAL FILM PLANE						SAGITTAL FILM PLANE						CORONAL FILM PLANE					
		Right - Left			Posterior - Anterior			Posterior - Anterior			Inferior - Superior			Inferior - Superior			Right - Left		
Sample Space Point	Offset Coordinates	$\Delta 80_1$	$\Delta 80_2$	Δc	$\Delta 80_1$	$\Delta 80_2$	Δc	$\Delta 80_1$	$\Delta 80_2$	Δc	$\Delta 80_1$	$\Delta 80_2$	Δc	$\Delta 80_1$	$\Delta 80_2$	Δc	$\Delta 80_1$	$\Delta 80_2$	Δc
0	(0,0,0)	0.51	0.10	-0.07	-0.16	0.84	0.46							0.51	0.59	0.03	0.23	0.37	0.17
2	(8,-8,8)	0.39	0.12	0.08	-0.17	0.98	0.58							0.89	0.37	-0.26	0.13	0.61	0.43
3	(-8,-8,8)	0.37	0.14	0.11	-0.55	1.38	0.81	-0.36	1.22	0.77	0.34	0.79	0.16	1.00	0.07	-0.49	0.40	0.33	0.05
4	(8,8,8)	0.26	0.34	0.06	-0.04	0.85	0.41	-0.32	1.15	0.80	0.34	0.75	0.24	0.84	0.35	-0.18	0.15	0.39	0.30
5	(8,8,-8)	0.35	0.24	0.14	-0.06	0.98	0.44	-0.02	1.29	0.76	0.57	0.68	0.16	0.55	0.62	0.02	0.00	0.52	0.39

Measurement Set 4		AXIAL FILM PLANE						SAGITTAL FILM PLANE						CORONAL FILM PLANE					
		Right - Left			Posterior - Anterior			Posterior - Anterior			Inferior - Superior			Inferior - Superior			Right - Left		
Sample Space Point	Offset Coordinates	$\Delta 80_1$	$\Delta 80_2$	Δc	$\Delta 80_1$	$\Delta 80_2$	Δc	$\Delta 80_1$	$\Delta 80_2$	Δc	$\Delta 80_1$	$\Delta 80_2$	Δc	$\Delta 80_1$	$\Delta 80_2$	Δc	$\Delta 80_1$	$\Delta 80_2$	Δc
0	(0,0,0)	0.49	0.21	0.10	-0.55	1.40	0.93	-0.70	1.10	0.88	0.55	0.38	0.44	1.12	-0.23	-0.66	-0.02	0.24	0.33
3	(-8,-8,8)	0.50	-0.15	-0.21	-0.52	1.31	0.83	-0.32	1.02	0.68	0.66	0.43	-0.06	1.20	-0.16	-0.64	0.54	-0.30	-0.14
5	(8,8,-8)	0.43	0.00	-0.07	-0.49	1.04	0.75	-0.62	1.17	0.91	0.69	0.23	-0.25	0.87	0.03	-0.46	0.20	0.30	0.14

3.3.1 Treatment Results

Positional alignment error, (Δc) and 80% isodose errors ($\Delta 80_1$ and $\Delta 80_2$) on each principal axis are shown in Figures 48 -50, grouped by the acceptance criteria used for treatment. All results discussed here have units of millimeters. For the first two measurement sets with an acceptance criteria of 1mm/1° the measured mean errors ($\overline{\Delta c} \pm \sigma$) between mid-profiles of the planned and measured dose distributions based on the 70% isodose contour were 0.48 ± 0.40, -0.20 ± 0.45, and 0.45 ± 0.43 mm in the Posterior-Anterior, Right-Left and Inferior-Superior directions respectively. For this data set, results ranged from -0.93 to 1.39 mm. For the second two measurement sets with an acceptance criteria of 0.4 mm/0.4° the measured mean errors ($\overline{\Delta c} \pm \sigma$) were 0.72 ± 0.18, 0.12 ± 0.18, and -0.14 ± 0.34 mm along each axis, respectively. The data ranged from was -0.66 to 0.93 mm.

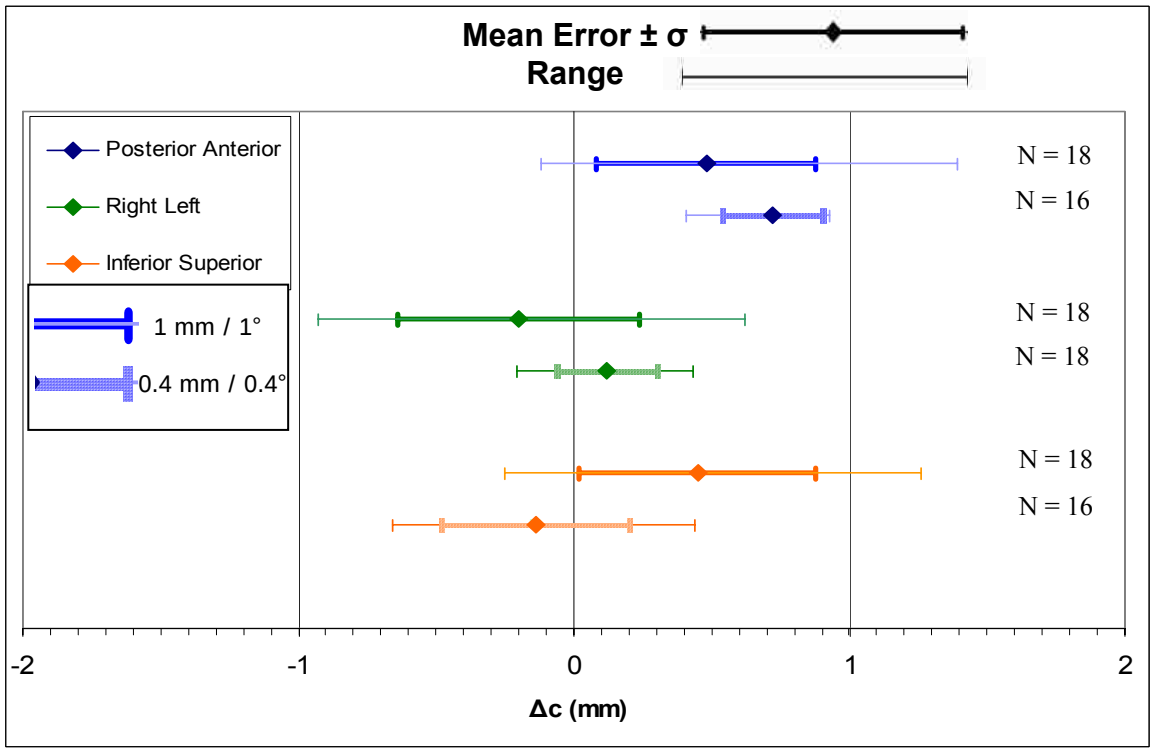

Figure 48. Treatment results for parameter Δc. Error bars indicate the standard deviation and range of each group of measurements. Dark and light error bars indicate the first and second acceptance criteria respectively.

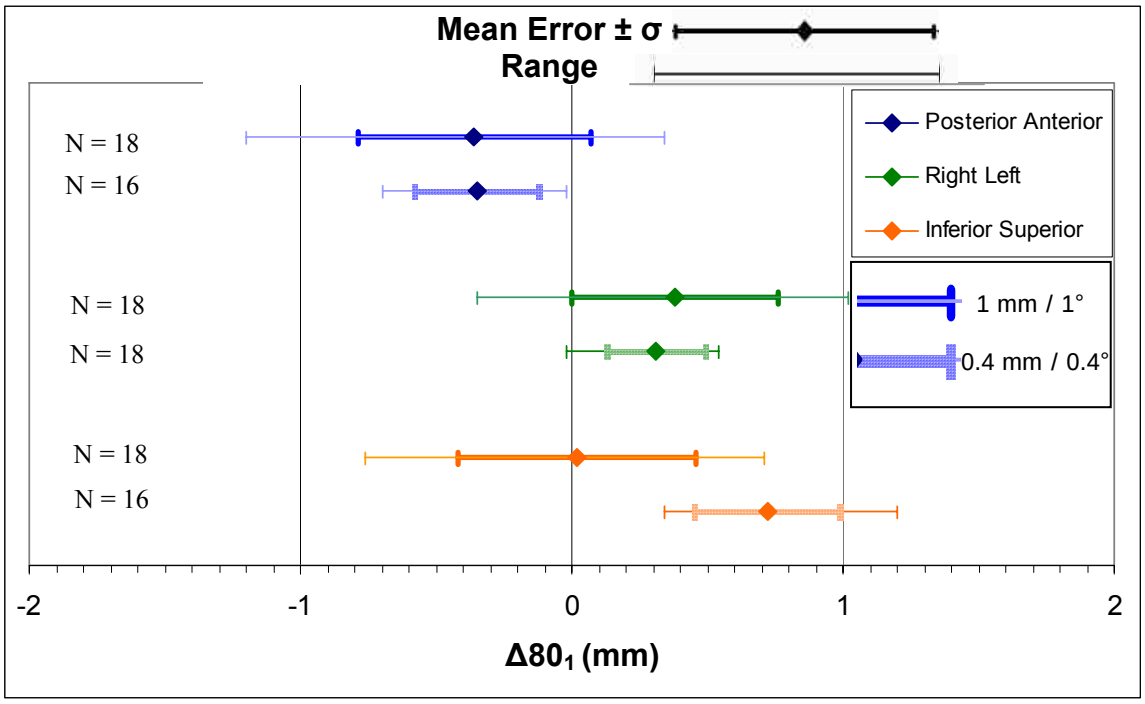

Figure 49. Treatment results for parameter $\Delta 80_1$. Error bars indicate the standard deviation and range of each group of measurements. Dark and light error bars refer to the first and second acceptance criteria respectively.

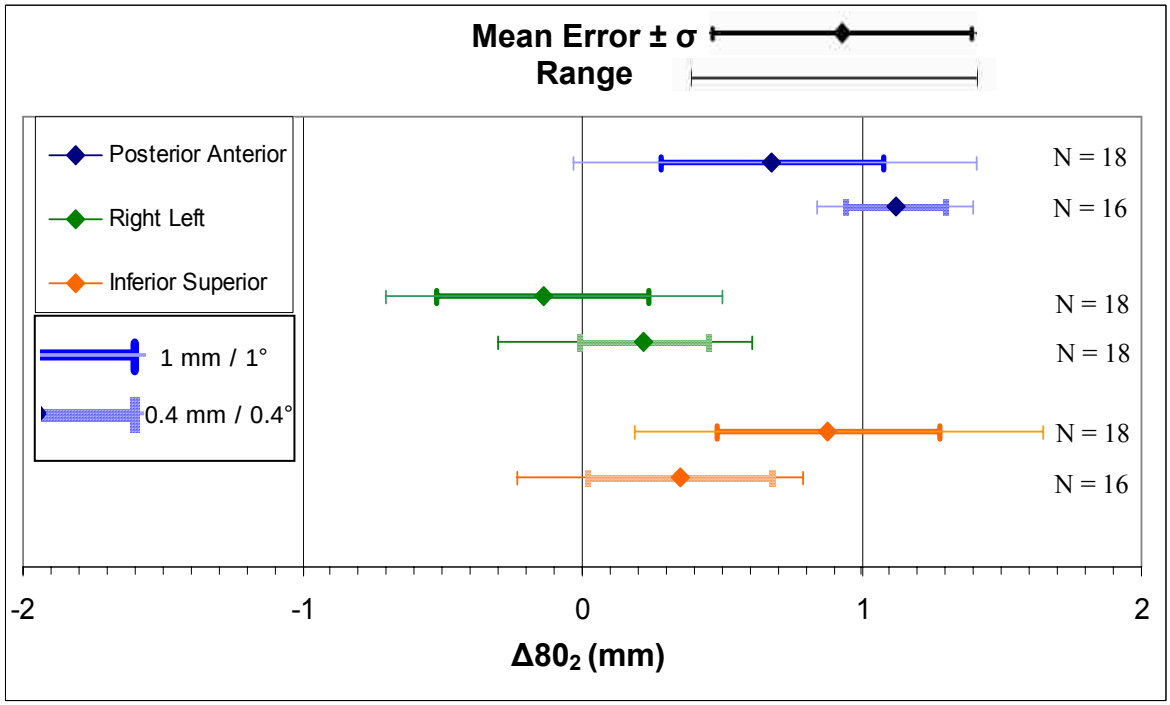

Figure 50. Treatment results for parameter $\Delta 80_2$. Error bars indicate the standard deviation and range of each group of measurements. Dark and light error bars refer to the first and second acceptance criteria, respectively.

The mean and standard deviation of the displacement of the measured 80% isodose locations compared to calculated 80% isodose locations, ($\Delta 80_1$ and $\Delta 80_2$) are shown in Figures 49 and 50. For the first two measurement sets (1mm/1°) the error along the negative axis ($\Delta 80_1$) was -0.36 ± 0.43, 0.38 ± 0.38, and 0.02 ± 0.44 mm on the Posterior, Right, and Inferior portions of measured dose profiles, respectively. The range for this set of results was -1.20 to 1.02 mm. For the second two measurement sets (0.4 mm/0.4°) $\Delta 80_1$ was -0.35 ± 0.23, 0.31 ± 0.18, and 0.72 ± 0.27 mm on each axis respectively. Values ranged from -0.7 to 1.2 mm.

For the first two measurement sets (1mm/1°) the errors on the positive axis ($\Delta 80_2$) were 0.68 ± 0.4, -0.14 ± 0.38, and 0.88 ± 0.4 mm on the Anterior, Left, and Superior axes, respectively. The range for this set of results was -0.7 and 1.7 mm. For the second two measurement sets (0.4 mm/0.4°) $\Delta 80_2$ was 1.12 ± 0.18, 0.22 ± 0.23, and 0.35 ± 0.33 mm on each axis respectively, with a range of -0.3 to 1.4 mm.

In some cases the mean error of isodose edges ($\Delta 80_2$) are higher than expected (i.e. 1.12 mm in the Posterior-Anterior direction). These high errors come about as a combination of both increased alignment error (Δc) and isodose error ($\Delta 80$) due to effects stated above (Section 2.3.8).

Negative values for $\Delta 80_1$ and $\Delta 80_2$ indicate an underdose to the prescribed 80% isodose line, certainly of clinical interest. Even with average positive values for $\Delta 80_1$ and $\Delta 80_2$, most directions had at least one treatment with large negative margins, i.e. each axis had at least one case where $\Delta 80_1$ or $\Delta 80_2 \leq -0.7$.

These results are specific to the beam model used for dose calculation which was adjusted from the model used clinically as described in Appendix 2. Also, the BrainScan dose calculation is an approximation and may not perfectly model the treatment beams

even with adjustments made to the beam profile. If the treatment plans were analyzed using calculations using the clinical beam model the Δ80 results would certainly change. For example a perfectly aligned (Δc = 0) phantom would still have positive Δ80 values in the A-P and R-L directions due to the field size asymmetry not reflected in the clinical beam model (Appendix 2).

The standard deviation (σ) of all alignment errors (Δc) is a measure of the reproducibility of alignment of ExacTrac to the IR calibrated isocenter. Values of 0.40, 0.44 and 0.43 mm were measured in the PA, RL and IS directions respectively for an acceptance criteria of 1mm/1°. This suggests that the ExacTrac reproducibility (2σ) is at least within 0.8 mm for all directions using these acceptance criteria. With such treatment precision, the ability to reduce the mean value $\overline{\Delta c}$, to very small values (<0.2mm) would result in sub-mm accuracy alignment with 95% confidence. The standard deviations for all parameters (Δc, $\Delta 80_1$ and $\Delta 80_2$) were between 0.38 and 0.44 mm for acceptance criteria of 1mm/1° while for 0.4mm 0.4 degrees they ranged from 0.18 to 0.34 mm which is indicative of increased precision of the ExacTrac alignment using the smaller criteria. In each case the highest value is in the Inferior-Superior direction might be a consequence of the voxel dimensions. CT scans used had a 1.25 mm slice separation versus 0.7 mm pixel size in the transverse plane; therefore, the DRR based fusion might have the most uncertainty in the Superior –Inferior direction.

3.3.2 Correlation of Spatial Error with Lutz Tests.

The data was grouped by each individual measurement set to asses the variation of Δc over time, in comparison to the variation in machine QA results. The Δc data is displayed graphically in Figure 51 and tabulated in Table 9.

It is apparent from the changes in the amount alignment error (Δc) along each axis that the systematic error due to affects described in section 3.3 is variable over time. The best treatments, in terms of alignment occurred during measurement set 1 with a maximum mean misalignment of 0.29 mm. The large average misalignment (Δc) in the Anterior direction, averaging up to approximately 0.9 mm, was seen for the last three measurement dates.

Clinical Winston-Lutz tests (c.f. Figure 52) recorded throughout the measurement period were reviewed by measuring the distance between the center of the circle created by the Lutz pointed and the center of the circle defined by a 1 cm diameter radiation beam delivered by the Novalis. Each Lutz film was marked prior to irradiation so that each principal direction (e.g. Posterior-Anterior) could be determined for each field as a function of the gantry and couch positions. The displacement vector between the laser isocenter (location of spherical radio-opaque marker) and radiation center (center of collimated beam) was determined from the film image for each gantry and couch angle combination.

These test results demonstrated a consistent, (within specification) misalignment between the laser and radiation isocenter position in the AP direction over the dates for measurement sets 2 – 4. This misalignment was not seen in Winston-Lutz results taken on the dates surrounding measurement set 1, which suggests that a systematic error independent of the ExacTrac calibration is this cause. Laser-radiation offset due to laser drift results in an offset IR/imaging isocenter and thus fusion result.

The treatment threshold used to decide when the fusion result was "good enough" did have effect on the results, as evidenced by differences in the standard deviations between sets 1 and 2 versus sets 3 and 4. The average standard deviation was 0.4 mm for sets 1 and 2 (1mm/1º) combined versus 0.2 mm for measurement sets 3 and 4 (0.4 mm/0.4º). Therefore maintaining a more stringent acceptance criteria leads to higher precision.

Table 10 lists the average and standard deviations of final verification shifts suggested by ExacTrac. These shifts were never made to the phantom. The grouping is based on the treatment thresholds of 1mm/1º used in measurement sets 1 and 2 and 0.4 mm/0.4º used in measurement sets 3 and 4. Again, measurement sets 1 and 2 have a standard deviation that is twice that of sets 3 and 4, indicating more spread in the data which is certainly reflected in the previously discussed. This is to be expected as these are a direct result of the acceptance criteria used from a given treatment set.

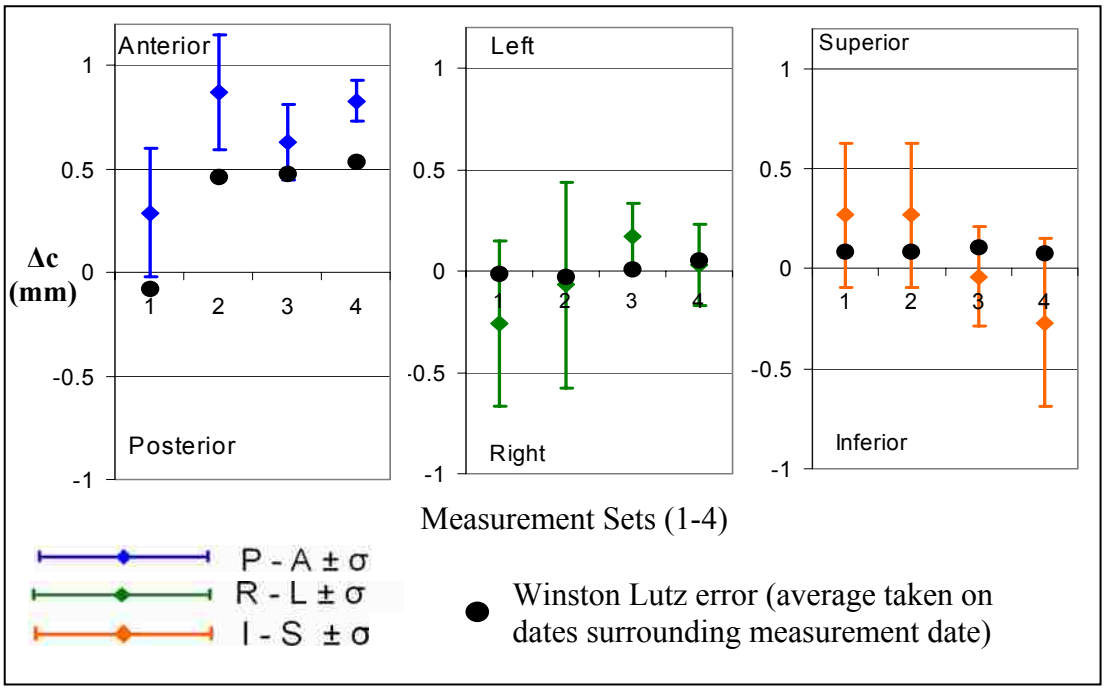

Figure 51. Measurement Set Dependence. Winston Lutz results involved averaging the displacements between the center of the Lutz ball and the center of the radiation field, using the couch/gantry angles corresponding to the principal axis being investigated.

Table 9. Alignment error (Δc) and 80% isodose line deviations ($\Delta 80_1$ and $\Delta 80_2$) grouped by the date of measurement (measurement set) Δc is the displacement of the center of the measured film profile from the calculated film profile based on 70% isodose locations. $\Delta 80_1$ is the displacement of the measured 80% line form the calculated 80% line on the negative aspect (posterior, right, inferior) of a given axis. $\Delta 80_2$ corresponds to the positive aspect (anterior, left, superior) of a given axis. For Δ80, + and – denote positive and negative margins about the planned 80 % isodose contour respectively. All values are in (mm).

	Posterior – Anterior (N = 12)			Right – Left (N = 12)			Inferior – Superior (N = 12)		
Set 1 12/3	**Δc**	**Δ 80_1**	**Δ 80_2**	**Δc**	**Δ 80_1**	**Δ 80_2**	**Δc**	**Δ 80_1**	**Δ 80_2**
	+0.29 ± 0.31	-0.12 ± 0.26	+0.49 ± 0.38	-0.26 ± 0.41	+0.43 ± 0.37	-0.18 ± 0.36	+0.27 ± 0.36	+0.20 ± 0.40	+0.73 ± 0.35
	[-0.12, +0.69]	[-0.58, +0.34]	[-0.03, +1.04]	[-0.86, +0.51]	[-0.20, +0.91]	[-0.70, +0.43]	[-0.25, +0.99]	[-0.64, +0.71]	[+0.19, +1.42]
	Posterior – Anterior (N = 6)			**Right – Left (N = 6)**			**Inferior – Superior (N = 6)**		
Set 2 1/9	**Δc**	**Δ 80_1**	**Δ 80_2**	**Δc**	**Δ 80_1**	**Δ 80_2**	**Δc**	**Δ 80_1**	**Δ 80_2**
	+0.87 ± 0.28	-0.84 ± 0.22	+0.91 ± 0.27	-0.07 ± 0.51	+0.30 ± 0.44	-0.04 ± 0.42	+0.27 ± 0.36	-0.19 ± 0.44	+1.16 ± 0.37
	[+0.60, +1.39]	[-1.20, -0.61]	[+0.68, +1.41]	[-0.93, +0.62]	[-0.35, +1.02]	[-0.59, +0.50]	[+0.33, +1.26]	[-0.76, +0.44]	[+0.66, +1.65]
	Posterior – Anterior (N = 8)			**Right – Left (N = 10)**			**Inferior – Superior (N = 8)**		
Set 3 1/24	**Δc**	**Δ 80_1**	**Δ 80_2**	**Δc**	**Δ 80_1**	**Δ 80_2**	**Δc**	**Δ 80_1**	**Δ 80_2**
	+0.63 ± 0.18	-0.21 ± 0.19	+1.09 ± 0.20	+0.17 ± 0.16	+0.28 ± 0.15	+0.32 ± 0.17	-0.04 ± 0.25	+0.63 ± 0.25	+0.53 ± 0.24
	[+0.41, +0.81]	[-0.55, -0.02]	[+0.84, +1.38]	[-0.07, +0.43]	[0.00, +0.51]	[+0.10, +0.61]	[-0.49, +0.24]	[+0.34, +1.00]	[+0.07, +0.79]
	Posterior – Anterior (N = 6)			**Right – Left (N = 6)**			**Inferior – Superior (N = 6)**		
Set 4 2/9	**Δc**	**Δ 80_1**	**Δ 80_2**	**Δc**	**Δ 80_1**	**Δ 80_2**	**Δc**	**Δ 80_1**	**Δ 80_2**
	+0.83 ± 0.10	-0.53 ± 0.13	+1.17 ± 0.15	+0.03 ± 0.20	+0.36 ± 0.22	+0.05 ± 0.24	-0.27 ± 0.42	+0.85 ± 0.26	+0.11 ± 0.28
	[+0.68, +0.93]	[-0.70, -0.32]	[+1.02, +1.40]	[-0.21, +0.33]	[-0.02, +0.54]	[-0.30, +0.30]	[-0.66, +0.44]	[+0.55, +1.20]	[-0.23, +0.43]

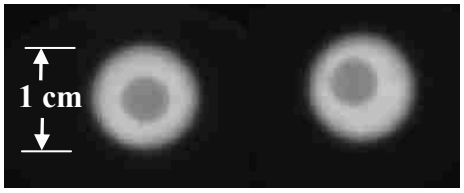

Figure 52. Example of Winston Lutz test results. The radiation field on the left shows greater radiation/isocenter coincidence than the field on the right.

Table 10. Final ExacTrac Suggested Shifts. Reported shifts were not made to phantom as they were within the acceptance criteria, and served as a verification of phantom alignment.

Translation		**Posterior - Anterior**	**Inferior - Superior**	**Right - Left**
Average ± σ (mm)	**Sets 1 and 2**	-0.07 ± 0.22	0.00 ± 0.21	0.13 ± 0.21
	Sets 3 and 4	-0.06 ± 0.13	-0.02 ± 0.14	0.03 ± 0.13
Rotation		**Couch Angle**	**Roll Angle**	**Tilt Angle**
Average ± σ (°)	**Sets 1 and 2**	0.16 ± 0.35	-0.07 ± 0.24	0.06 ± 0.25
	Sets 3 and 4	0.04 ± 0.17	-0.03 ± 0.16	-0.02 ± 0.20

Chapter 4 Conclusions

4.1 Summary of Results

Coplanar beam therapy using ExacTrac image guidance with Novalis at this treatment center(MBPCC) can achieve patient alignment within 1.4 mm for patients whose initial misalignment is within ± 8 mm from isocenter for an ExacTrac acceptance criteria of 1 mm, 1°. Using this acceptance criteria the maximum error in the location of the measured 80% isodose compared to the calculated 80% isodose line was 1.7 mm. When the acceptance criteria was reduced to 0.4 mm, 0.4° the maximum alignment error reduced to 0.7 mm, and the maximum error in 80% isodose location reduced to 1.4 mm. Alignment error in the A-P direction showed a correlation with the deviation of laser and mechanical isocenter as determined from Winston-Lutz testing.

These results are dependent on a combination of (1) MBPCC calibration protocol and QA specifications and (2) adjustments to the standard clinical procedures made specifically for this study (i.e. methods in the treatment process not used clinically at the time of this study). Results are also affected by the day-to-day accuracy of ExacTrac calibration used in the clinic. However, the accuracy required for treatment (acceptance criteria) used in the study was lower than the current clinical requirements at MBPCC (2.5 mm, 2.5°). By implementing a tighter accuracy acceptance criteria for treatment leads to (1) more precise treatments and (2) independence of large initial misalignments.

The quality of the dose calculation to which the measured treatments were compared has a large effect on determined error results, primarily in the $\Delta 80$ values. The three main components of the dose calculation are (1) Treatment Machine Commissioning Data, (2) Beam model settings and (3) Dose calculation algorithm

(PBA). For this study the beam model was adjusted to account for a small asymmetry in the delivered radiation field as descried in Appendix 2.

4.2 Evaluation of Hypothesis

My hypothesis *"Cranial coplanar beam radiation therapy using the MBPCC BrainLAB ExacTrac image guidance system can achieve positional accuracy of dose delivery (i.e. displacement of delivered dose distribution from that shown by the TPS) within 1 mm for a cranial PTV in an anthropomorphic head phantom."* was not proven, as measured errors were > 1 mm. However, it is believed that this could be easily met, possibly significantly exceeded (e.g. <0.5 mm) by following the clinical and vendor recommendations listed below.

4.3 MBPCC Clinical Recommendations

Recommendations for MBPCC are (1) to put into place tighter action levels such that consistent deviations between the lasers and radiation are quickly recognized so that the lasers can be adjusted. There is random variability in this parameter, so differentiating a random offset on a given Winston-Lutz test results from a systematic discrepancy must be realized. It is also recommended that (2) the appropriate adjustments be made to the beam model to account the treatment field asymmetry. This would make this study clinically valid and could lead to treatment recommendations based on this study. The recommended PTV margin would be approximately 2 mm based on 80% deviation to 1.7 mm and acceptance criteria of 1mm, 1°.

4.4 Vendor Recommendations

It is also recommended that the vendor (1) provide tools to ensure that the highest possible accuracy of the system is achieved, with the normal variations seen in this study.

For example, with addition of the 6D treatment couch, it should be feasible to add an inherent, automatic correction for any offsets between laser and radiation isocenter due to table or gantry wobble. This would make the isocenter wobble essentially disappear on the Lutz test. It is also suggested that (2) the vendor should provide tools to measure the system accuracy as it is used clinically. By providing tools to measure the accuracy in an "end to end" test (i.e. similar to this study) the accuracy of clinical treatments could be evaluated readily.

4.5 Future Work

Future work could include measuring the accuracy of treatments at various treatment sites, both cranial and an extra-cranial, using similar methodology. This could be done using the existing phantom by moving the target to other areas on the film block. Anthropomorphic phantoms with internal film inserts in other areas of the head would allow for measurements of treatment sites such as trigeminal neuralgia, or acoustic neuroma. Testing of non-coplanar beams would be useful as most treatments are planned using a non-coplanar beam arrangement. Regulation of such test procedures could be used to provide a means of inter-comparison between treatment centers, by using similar phantom studies to measure IGRT treatment deliveries. Evaluation of other image guided treatment modalities e.g. TomoTherapy, would also be worthwhile.

References

Alheit H, Dornfeld S, Dawel M, Alheit M, Henzel B, Steckler K, Blank H and Geyer P 2001 Patient position reproducibility in fractionated stereotactically guided conformal radiotherapy using BrainLAB Mask System *Strahlentherapie und Onkologie* **5** 264-268

Childress N L, Dong L and Rosen I I 2002 Rapid radiographic film calibration for IMRT verification using automated MLC fields *Med.Phys.* **29** 2384-2390

Cosgrove V P, Jahn U, Pfaender M, Bauer S, Budach V and Wurm R E 1999 Commissioning of a micro multi-leaf collimator and planning system for stereotactic radiosurgery *Radiotherapy and Oncology* **50** 325-336

Jin J, Ryu S, Faber K, Movsas B 2005 An Image Guided Target localization system for brain radiosurgery and fractionated stereotactic radiotherapy using a non-invasive fixation *Med Phys.* **32** 2041-2042 SU-FF-T-394

Li S, Ayyangar K, Pillai S, Nehru R, Fung A, Djajaputra D, Thompson R, Raman N, Zhen W, Enke C 2005 Target localization of intensity modulated Radio-surgery patients using ExacTrac system *Med. Phys.* **32** 2045 SU-FF-T-410

Lutz W, Winston K R and Maleki N 1988 A system for stereotactic radiosurgery with a linear accelerator *Int. J. Radiat. Oncol. Biol. Phys.* **14** 373

Robar J L and Clark B G 1999 The use of radiographic film for linear accelerator stereotactic radiosurgical dosimetry *Med.Phys.* **26** 2144-2150

Robar J L and Clark B G 2000 A practical technique for verification of three-dimensional conformal dose distributions in stereotactic radiosurgery *Med. Phys.* **27** 978-987

Robar J L, Clark B G, Schella J W and Kim C S 2005 Analysis of patient repositioning accuracy in precision radiation therapy using automated image fusion *Journal of Applied Clinical Medical Physics* **6** 71-83

Schell M C, Bova F J, Larson D A, Leavitt D D, Lutz W R, Podgorsak E B, Wu A 1995 Stereotactic Radiosurgery; AAPM Report 54, Task Group 42 *American Institute of Physics*

Solberg T, Selch M, Smathers J, DeSalles J A 1998 Fractionated Stereotactic Radiotherapy: Rationale and Methods *Med. Dosimetry* **23** 209–219

Suchowerska N, Hoban P, Butson M, Davison A, Metcalfe P 2001 Directional dependence in film dosimetry: radiographic and radiochromic film *Phys. Med. Biol.* **46** 1391-1397

Sujatha P, Das I J, Dempsey J F, Lam K L, LoSasso T J, Olch A J, Palta J R, Reinsein L E, Wilcox E E 2007 TG-69: Radiographic film for megavoltage beam dosimetry *Med. Phys.* **34** 2228-2257

Woodard H Q and White D R 1986 The Composition of Body Tissues *The British Journal of Radiology* **59** 1209-1219.

Yan H, Kim F and Kim J H 2005 A phantom study on the positioning accuracy of the Novalis Body system *Med. Phys.* **30** 3052-3059

Perrin D, Hogstrom K, and Cheek D 2007 Cerenkov light from phantom cassettes in absolute dose measurements using radiographic film *Med. Phys.***30** 2629 TH-C-M100E-04

ICRP 23 1975 Report of the Task Group on Reference Man

Clinical Users Guide Revision 1.0, Novalis Body/ExacTrac Version 5.0 2005 BrainLAB AG, Heimstettan Germany

Software Guide Revision 1.0, BrainSCAN Version 5.2x 2002 BrainLAB AG, Heimstettan Germany

Appendix 1 BrainScan Calculated Depth-Dose Generation

A depth-dose calculation was extracted from a treatment plan in BrainScan of a single beam incident on a flat solid-water phantom set to match the measurement conditions of depth dose measurements on film and ion chamber measurements for comparison (section 2.2.1). A 10 x 30 x 30 cm^3 section of Plastic Water was scanned with the GE Discovery CT scanner and imported to BrainScan TPS. A 3 x 3 cm^2 field was generated in the TPS by manually adjusting the mMLC leaves. The gantry was set to direct the radiation beam perpendicularly towards the phantom surface. Isocenter was set to a depth 4 cm with SSD set to 96 cm. (c.f. Figure A1). The central-axis depth-dose profile was extracted from the TPS using the Dose Export function in BrainScan.

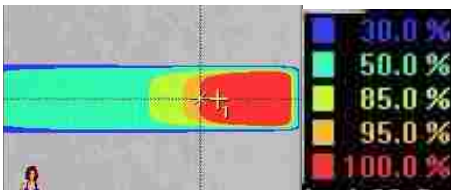

Figure A1.1. BrainScan Depth Dose generation. The crosshair represents isocenter at 4 cm depth.

The calculated depth-dose were compared with film and ion chamber measurements (c.f. Fig A1.2 and A1.3). Film dose values agree to within 3 % of BrainScan TPS dose calculation values. This confirms that the BrainScan dose calculation algorithm is sufficiently accurate that it will have insignificant impact on comparison of spatial accuracy of the delivered dose distribution by comparing measured – calculated relative dose profiles.

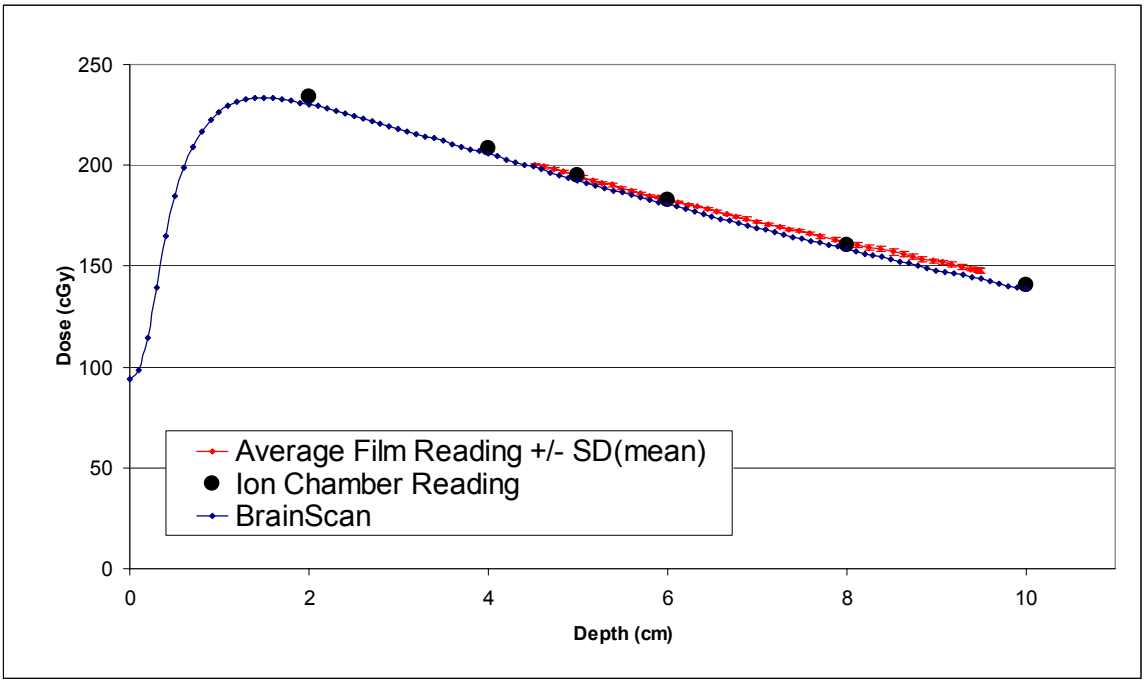

Figure A1.2. Depth-dose measurements in film and ion chamber compared with BrainScan calculation. 3 x 3 cm^2 field size, 6MV, SAD 100, SSD = 96 cm.

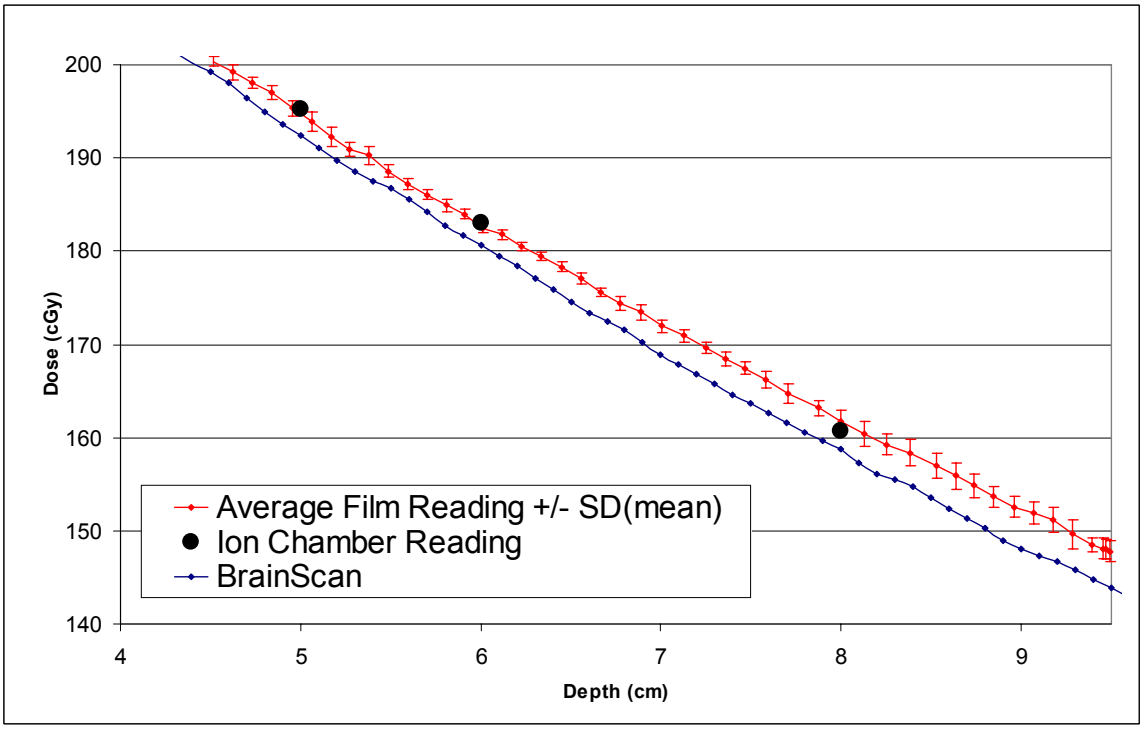

Figure A1.3. Expansion of Figure A1.2 showing the film section only. 3 x 3 cm^2 field size 6MV, SAD =100, SSD = 96

The delivered dose distribution is the result of the dose calculation, which relies on appropriate beam model values in the beam profile editor. Without proper corrections to the beam profile editor, the calculated dose edges were mismatched to the delivered dose. Details are in the following section.

Appendix 2 BrainScan Off-Axis Comparison: Beam Model Adjustments.

Asymmetry in the delivered radiation field from the Novalis was seen in film dose profiles measured at varying depths and field sizes. In the treatment planning system, if the nominal field size is square (i.e. a 2.4 cm x 2.4 cm field created with the mMLC leaves), the beam edges on the calculated dose distribution will define a square field with a 1:1 ratio between the FWHM of the dose profile in the direction of mMLC leaf travel versus the direction of the tongue and groove edge. This ratio was measured on film and in the planning system with the adjusted beam profile, with results in Table A2.1.

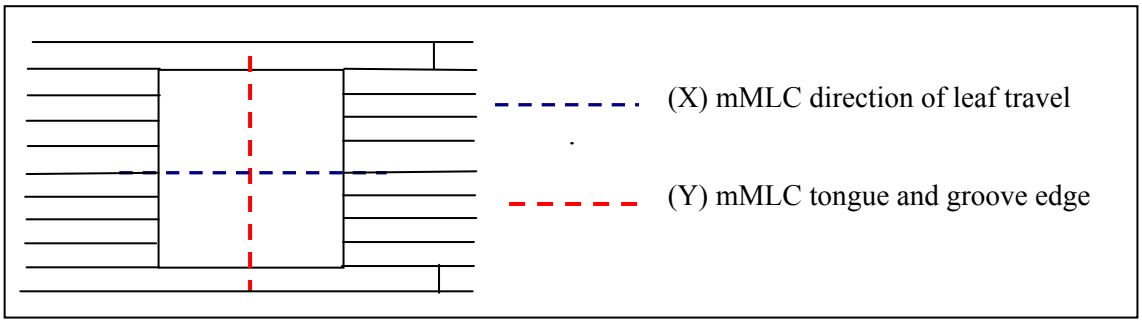

Figure A2.1. Field size diagram depicting the mMLC field definition in BrainScan.

Table A2.1. Ratio (Y/X) of FWHM taken in the mMLC leaf travel dimension versus measurements in the tongue and groove dimension for film and light field, and calculation using adjusted beam model. Without these adjustments the ratio (X/Y) is 1.

Nominal Field Size (cm)	**Film at Surface**	**Film Depth = 5 cm**	**Film Depth = 10 cm**	**Light Field**	**Adjusted Beam Model**
	(Y/X)	(Y/X)	(Y/X)	(Y/X)	(Y/X)
12	0.870	0.887	0.887	0.888	0.895
24	0.927	0.942	0.935	0.963	0.952
36	0.951	0.957	0.952	0.956	0.960

The adjusted beam model changes clinical parameters in the Beam Model Editor under “Radiological Field Correction”. This includes “Leaf Shift Static” (set to 0.4 mm) and “Tongue and Groove” (set to 0.4 mm) correction, both initially set to 0. These factors are a part of the dose calculation which is described in the Appendix 3.

The effect of making these changes was tested by comparing orthogonal profiles measured on film to calculated orthogonal profiles using the original clinical beam model and the adjusted beam model. A single 2.4 cm x 2.4 cm beam was defined in BrainScan to irradiate a film insert in the CIRS head phantom in the coronal measurement plane. Film was loaded into the phantom and oriented to measure the coronal plane and set up to isocenter using ExacTrac image guidance. The planned radiation beam was delivered to the phantom. Figure A2.2 and A2.3 show measured orthogonal profiles compared to calculated dose using both the clinical and adjusted beam model.

Better agreement is seen with the adjusted beam model in each case. For the horizontal profiles the calculated 50% isodose lines are approximately 0.35 mm inside (toward the CAX) the 50 % isodose lines of both the measured and adjusted dose calculation. For vertical profiles the calculated 50% isodose lines are approximately 0.35 mm outside (away from the CAX) the 50% isodose lines of both the measured and adjusted dose calculation. These results prompted use of these beam model adjustments for the dose calculations which were used to test the hypothesis.

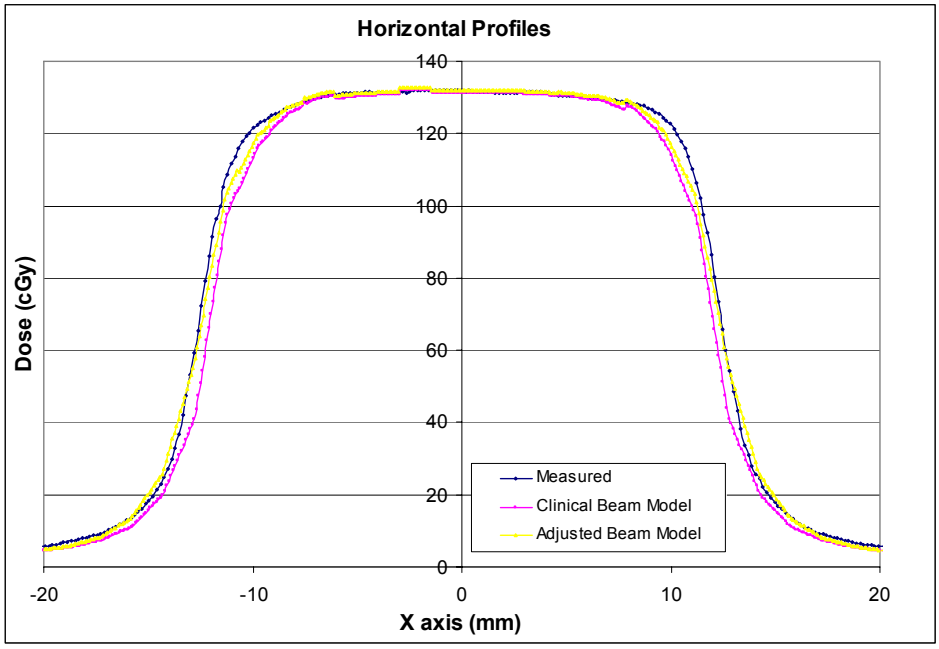

Figure A2.2. Horizontal profile comparison of film measured dose versus calculations using the clinical beam model and the adjusted beam model.

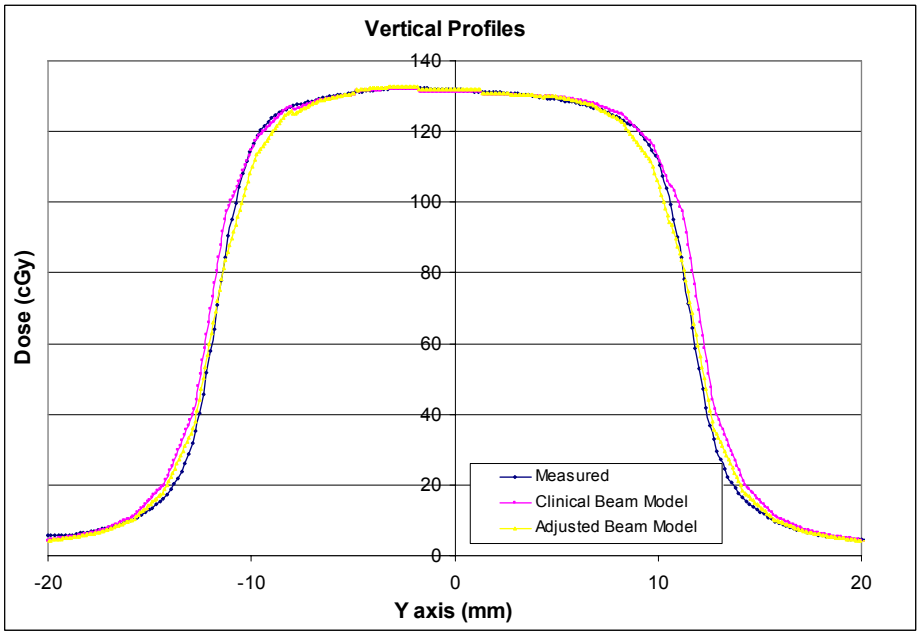

Figure A2.3. Vertical profile comparison of film measured dose versus calculations using the clinical beam model and the adjusted beam model.

Appendix 3 BrainScan Dose Calculation

Comparison between film measurement and planned dose distribution warrants a description of the BrainScan TPS dose calculation and its components. BrainScan version 5.3 provides the option of using either the Clarkson Algorithm or Pencil Beam Algorithm (PBA) for dose calculation. MBPCC uses the PBA exclusively. Implementation of the PBA in BrainScan requires a number of input parameters. First of which is nominal Linac output, which is defined the dose per monitor unit delivered to water at normalization depth. At MBPCC Novalis nominal Linac output is defined at 5 cm depth.

BrainScan Dose Calculation Equation

The dose for a radiation beam is calculated using the following equation (Novalis BrainScan Software Guide Version 5.2x)

$$Dose(x,y,d) = MU \cdot O \cdot S_t(c_{mlc}, c_{jaw}) \cdot \quad (1)$$

$$TMR(\min(c_{mlc}, c_{jaw}), r_{rad}) \cdot \left(\frac{SID}{SSD+d}\right)^2 \cdot IDD(x', y', r_{rad}) \quad \text{, where:}$$

MU	Monitor Units delivered by Linac
O	Linac Output (cGy/MU)
S_t	Total Scatter factor
$c_{jaw/mlc}$	Collimator/mlc square field size
r_{rad}	Radiological path-length
SID	Source Isocenter Distance
SSD	Source Surface Distance
d	depth of observation point in tissue
$IDD(x', y', r_{rad})$	Idealized dose distribution in depth
$x' = x \cdot SID/(SSD+D)$	Horizontal distance from CAX at SID
$y' = y \cdot SID/(SSD+D)$	
$TMR(\min(c_{mlc}, c_{jaw}), r_{rad})$	Tissue Maximum Ratio

Idealized Dose Distribution

The final term in the dose equation (IDD) is the convolution of the beam fluence by the pencil beam kernel. The beam fluence is a function of the fluence matrix in the isocenter plane for the size of the open field, and radial factor at given depth and radial location from the central axis.

$$IDD(x,y,d) = \iint \phi(x',y',d) \cdot p(x'-x, y'-y, d)dx'dy' \tag{2}$$

$$\phi(x,y,d) = \phi_o \cdot RFS(r,d) \tag{3}$$

$$RFS(r,d,SSD) = D(r,d,SSD) / D(0,d,SSD) \tag{4}$$

$$r = \sqrt{x^2 + y^2} \tag{5}$$

Radial factors are determined by BrainLAB based on radial profile measurements taken in the clinic. Radial profiles are horizontal scans taken diagonally across the field at varying depths. These factors are entered into the beam profile editor and correct for off axis inhomogeneities in the beam

Pencil Beam Kernel

$$p(x,y,d) = \iint N_{av}(E) \cdot e^{(-\mu(E)d')} \mu(E) \cdot DPB(\vec{r}(x,y,d) - \vec{r}(0,0,d'))dE \cdot dd' \tag{6}$$

This is the 2D convolution of the monoenergetic pencil beam with the differential pencil beam. ($N_{av}(E) \cdot e^{(-\mu(E)d')} \mu(E)$) is equal to the number of photons undergoing their first collision at d'. N_{av} is the accelerator dependent energy distribution averaged over the open field. The differential pencil beam ,DPB(E,r,θ), describes the dose distribution relative to the first collision of a monoenergetic pencil beam which is pre-calculated with Monte Carlo.

PDD/TMR

Either the percent depth dose (PDD) or tissue maximum ratio (TMR) can be used to establish dose deposition of an incident photon beam as depth in the absorbing medium is increased. PDD measurements are taken along the vertical axis of the beam (i.e. the detector is placed at varying depth positions) with a water equivalent phantom in a fixed position. TMR (used at MBPCC) is measured with the detector at isocenter and measurements are taken with varying buildup material or water placed upstream to vary the depth of measurement.

$$TMR(c,d) = D(c,0,d) / D(c,0,d_{\max}) \tag{7}$$

PDD and TMR values are dependent upon beam energy and field size. Given that the Novalis machine is single energy 6MV linac, measurements for PDD or TMR need only be made for a range of field sizes. Field shapes are created with the BrainLAB m3 mMLC setting equal to the Jaw setting. Resulting PDD/TMR curves are generally normalized to d_{max}, in this case 1.5 cm.

Scatter Factor

The total scatter factor accounts for dose deposition due to scatter effects from the collimator relative to nominal linac output. The scatter factor is defined as the ratio of the central axis dose at the normalization depth (5 cm) to the dose from a 10 x 10 cm^2 beam at the same depth. Scatter factors are measured across a matrix of combinations of jaw settings and mMLC settings, ands are applied to every dose calculation.

$$S_t(c) = D(c,r,d_{\max}) / D(10x10cm^2,0,d_{cal}) \tag{8}$$

Radiological Field Correction

Here a correction can be applied based on the radiological field delivered versus the nominal mMLC field setting. These result from gap settings, rounded leaf ends, and tongue and groove design. Leaf Shift Static is a correction which applies an offset in the direction of leaf travel. Tongue and Groove Size is a correction in the direction perpendicular to leaf travel, defined by the tongue and groove mMLC edge. In this study these parameters were set to 0.4 mm for both the Leaf Shift Static and Tongue and Groove Size. This change was made to the original beam profile which had zero for both parameters because of small deviations in the size of the delivered radiation field versus the mMLC setting in both directions with respect to the mMLC.

Source Function Correction

Source function correction is essentially a Gaussian smearing of the dose distribution. Parameters describing these effects can be entered for two depths and the rest of the depths are linearly interpolated from the two. The purpose of these corrections is to simulate an extended source rather than ideal point source, as well as other effects. The Gaussian curves generated are convolved with the dose calculation.

Leakage

Background Leakage input parameters are dose readings relative to nominal output (with same setup as output measurement) with a closed mMLC field and with both closed and open jaws. These parameters are entered as a percentage of the output and are applied the dose distribution depending on the mMLC and jaw settings for a given beam.

Vita

Justin Vinci was born in Middletown, Connecticut, in October, 1981, son of Keith and Mary Anne Vinci. He graduated from Middletown High School in 2000, where he and went on to attend the University of Connecticut where he studied mechanical engineering. There he was became a member of both, Tau Beta Pi and Pi Tau Sigma, engineering and mechanical engineering honors societies. Upon receiving his bachelor's degree in mechanical engineering in 2004, Justin attended Louisiana State University to study medical physics in the Department of Physics and Astronomy. He received his master's degree in medical physics and health physics in the Department of Physics and Astronomy in 2007 and is a student member of the American Association of Physicists in Medicine.